

Quantum graphs: Applications to quantum chaos and universal spectral statistics

Sven Gnutzmann & Uzy Smilansky

To cite this article: Sven Gnutzmann & Uzy Smilansky (2006) Quantum graphs: Applications to quantum chaos and universal spectral statistics, *Advances in Physics*, 55:5-6, 527-625, DOI: [10.1080/00018730600908042](https://doi.org/10.1080/00018730600908042)

To link to this article: <https://doi.org/10.1080/00018730600908042>



Published online: 28 Nov 2010.



Submit your article to this journal [↗](#)



Article views: 428



View related articles [↗](#)



Citing articles: 107 View citing articles [↗](#)

Quantum graphs: Applications to quantum chaos and universal spectral statistics

SVEN GNUTZMANN*^{†‡¶} and UZY SMILANSKY^{‡§}

[†]Freie Universität Berlin, Germany

[‡]The Weizmann Institute of Science, Rehovot, Israel

[§]School of Mathematics, Bristol University, Bristol BS81TW, England, UK.

(Received 24 April 2006; in final form 13 July 2006)

During the last few years quantum graphs have become a paradigm of quantum chaos with applications from spectral statistics to chaotic scattering and wavefunction statistics. In the first part of this review we give a detailed introduction to the spectral theory of quantum graphs and discuss exact trace formulae for the spectrum and the quantum-to-classical correspondence. The second part of this review is devoted to the spectral statistics of quantum graphs as an application to quantum chaos. In particular, we summarize recent developments on the spectral statistics of generic large quantum graphs based on two approaches: the periodic-orbit approach and the supersymmetry approach. The latter provides a condition and a proof for universal spectral statistics as predicted by random-matrix theory.

Contents

	PAGE
1. Introduction	528
1.1. Graphs and their topology	531
2. The Schrödinger operator on graphs	534
2.1. Vertex boundary conditions – self-adjoint extension	535
2.2. The secular equation	537
3. The quantum evolution map	539
3.1. Vertices as scattering centres	540
3.2. The quantum evolution map	541
3.3. Examples of generalized vertex scattering matrices	543
4. Classical evolution on graphs	546
4.1. Classical phase-space and transition probabilities	546
4.2. The classical evolution operator	548
4.3. The return probability and a classical sum rule	551
5. Spectral theory for quantum graphs	553
5.1. The density of states and the counting function	553
5.1.1. The spectrum of the quantum evolution map	556
5.2. Periodic orbits and the trace formula	557
5.2.1. Trace formulae for the eigenphase spectrum	558
5.3. The length spectrum and the quantum-to-classical duality	559

*Corresponding author. Sven Gnutzmann. Email: gnutz@physik.fu-berlin.de

[¶]Current address: School of Mathematical Sciences, University of Nottingham, United Kingdom.

5.4. The secular function is a ζ -function	560
6. Spectral statistics	562
6.1. Spectral averages	562
6.2. Disorder averages	563
6.3. Phase ergodicity for incommensurate graphs	563
6.4. Spectral correlation functions	564
6.5. Equivalence of spectral correlators and eigenphase correlators in large graphs	565
6.6. The level-spacing distribution for quantum graphs	567
7. Quantum chaos and universal spectral statistics	571
7.1. Universal correlators and random-matrix theory	572
7.2. Analytical approaches to universality	573
8. Periodic orbit theory for spectral statistics	576
8.1. Spectral form factor for star graphs	576
8.2. The diagonal approximation	578
8.3. Off-diagonal contributions	582
8.4. Graphs with spin and their spectral statistics	589
8.5. Andreev graphs and non-standard symmetry classes	591
9. The supersymmetry approach to quantum graphs	598
9.1. An exact supersymmetric model for spectral correlators	599
9.2. The mean-field approximation and universality	604
9.3. Validity of the mean-field approximation and sufficient conditions for universality	606
9.4. Breaking time-reversal invariance	609
9.5. On higher order correlation functions and the gap condition	610
Acknowledgments	610
Appendix A: The symmetry classes of quantum systems	610
A.1. Time-reversal invariance	611
A.2. Kramers' degeneracy	612
A.3. Chiral symmetries and charge conjugation symmetries	612
A.4. The symmetry classes for quantum graphs	614
Appendix B: Some relevant results of random-matrix theory	615
B.1. Universality and universality classes	616
B.2. The Gaussian ensembles of random-matrix theory	616
B.3. Spectral statistics for Gaussian random matrices	617
References	619

1. Introduction

The general mathematical concept of a graph (network) as a set of elements which are connected by some relation has found applications in many branches of science, engineering, and also social science. A street network of a traffic engineer, the network of neurons studied by a neuroscientist, and the structure of databases in computer science, can all be described by graphs.

Recently, the Laplacian on a metric graph has gained a lot of attention in physics and mathematics in terms of the diffusion equation or Schrödinger equation. They have now become known as *quantum graphs* but different aspects are studied under various names such as quantum networks or quantum wires. They have a long history in mathematics and physics.

In physics, the first application has probably been in the context of free electron models for organic molecules, about 70 years ago by Pauling [1], an approach which has been further developed in subsequent years [2–8]. Quantum graphs have also been applied successfully to superconductivity in granular and artificial materials [9], acoustic and electromagnetic waveguide networks [10, 11], the Anderson transition in a disordered wire [12, 13], quantum Hall systems [14–16], fracton excitations in fractal structures [17, 18], and mesoscopic quantum systems [19–23]. Quantum graphs have also been simulated experimentally [24].

The construction of self-adjoint operators, or wave equations with appropriate boundary conditions on graphs, was first addressed by Ruedenberg and Scherr [5] (see also [8]). They considered graphs as an idealization of networks of wires or wave guides of finite cross-section in the limit where the diameter of the wire is much smaller than any other length-scale. Similar approaches to graphs as networks of thin wires with a finite diameter, or *fat quantum graphs* as they are now called, have been a topic in mathematical physics recently [25–30].

Another interesting approach, which has been discussed mainly by Exner and his coworkers, is based on *leaky graphs* [31–39]. Here, a finite attractive potential in the Schrödinger equation is centred on a metric graph. A leaky graph is a generalization of the Schrödinger equation with δ -function potentials. A quantum graph can be realized in the limit of infinitely strong attracting potentials of this type.

Probably the first mathematical approaches to the Laplacian on a metric graph were done by Roth who derived a trace formula for the spectrum of the Laplacian [40, 41] and by von Below [42–44]. The spectral theory of quantum graphs was mainly developed on the basis of the von Neumann theory of self-adjoint extensions for formal differential operators [45–62]. Other recent topics in mathematics and mathematical physics include the spectral theory of infinite periodic graphs [49, 50, 63–66, 255–258], tree graphs [67–73] and Sierpinski graphs [74–76], scattering and bound states in open graphs [77–84], diffusion and localization [23, 85–89], random walks [90, 91], approximations of quantum systems by quantum graphs [92], some inverse problems [41, 42, 54, 58, 93–104], extremal spectral properties [105], and models of dissipative graphs [106–109].

Recent review papers on various mathematical approaches to quantum graphs can be found in [110–112]. Special issues of research journals [113, 114] and recent conference proceedings [115] have been devoted to quantum graphs.

The relevance of quantum graphs to the study of quantum chaos was brought to light by the work of Kottos and Smilansky [116, 117]. They analysed the spectral statistics for simple graphs, and showed that their spectral statistics follow very closely the predictions of random-matrix theory. They proposed an alternative derivation of the trace formula and pointed out its similarity to the famous Gutzwiller trace formula [118, 119] for chaotic Hamiltonian systems. While quantum graphs do not have a deterministic classical limit, they still share a lot of important properties with classically chaotic Hamiltonian systems, e.g. periodic-orbit theory in the semiclassical regime is completely analogous to periodic-orbit theory on a quantum graph. While semiclassical approaches are approximations the analogous approaches for quantum graphs are exact. More importantly, quantum graphs are not as resistant to analytical approaches. Following these pioneering beginnings of

Kottos and Smilansky, quantum graphs have become a new paradigm of quantum chaos and have been applied to various problems, including also disorder and diffusion [120, 121]. All aspects of quantum chaos have been covered: spectral statistics in finite [90, 122–142] and infinite periodic structures [89], localization and wavefunction statistics [120, 143–150], chaotic scattering [151, 152], transport through chaotic devices [153, 154], resonances and decay in open chaotic systems [155–157].

The main purpose of this paper is to review recent approaches to spectral statistics in quantum graphs and discuss the relation to quantum chaos in general. To make the paper self-contained, special effort was made to introduce the necessary concepts in a clear and consistent way.

Recently, important progress has been achieved by Müller *et al.* [158, 159] in the periodic-orbit theory for spectral statistics in chaotic Hamiltonian systems building on the pioneering work of Sieber and Richter [160–162]. A similar approach for quantum graphs has been developed by Berkolaiko, Schanz and Whitney [124, 125, 128]. None of these works captured the low energy sector of spectral statistics. An alternative approach, which so far was successfully applied to quantum graphs [141, 142], was able to close the above mentioned gap, and it will be discussed in detail in the second part of this review.

Several other applications to quantum chaos will not be addressed in this review. Functional integration approaches to statistical properties of wavefunctions and localization are thoroughly reviewed by Comtet, Desbois and Texier [121] (see also [181]). Chaotic scattering and transport in quantum graphs is discussed in [153–157].

This review is arranged in the following way. The first sections provide a detailed introduction to quantum graphs and their spectral theory. Though the choice of material is biased by the application to quantum chaos, the first sections are rather general. In section 1.1 we define graphs and their topological description. In section 2 we quantize graphs in a straightforward way. The reformulation in section 3 in terms of a unitary quantum evolution map will allow us to generalize the quantization procedure. This point of view will be the foundation for the remaining sections. Section 4 gives an account of the classical dynamics that corresponds to a quantum graph and section 5 is devoted to spectral theory with the introduction of the trace formula and its discussion.

The remaining sections are devoted to spectral statistics in quantum graphs. After a general introduction of spectral correlation functions (and other statistical measures of the spectrum) in section 6 we will give some background from quantum chaos and random-matrix theory on universality in the spectral fluctuations of complex quantum systems in section 7. In the last two sections we present two analytical approaches to universal spectral statistics in large quantum graphs. The periodic-orbit approach is presented in section 8 which also includes sections on quantum graphs with spin and quantum graphs which are coupled to superconductors (Andreev graphs). Finally, we summarize the supersymmetry approach with a proof of universality in large quantum graphs in section 9. In Appendix A we add some background on the symmetry classification of quantum systems and in Appendix B we summarize some relevant results from random-matrix theory.

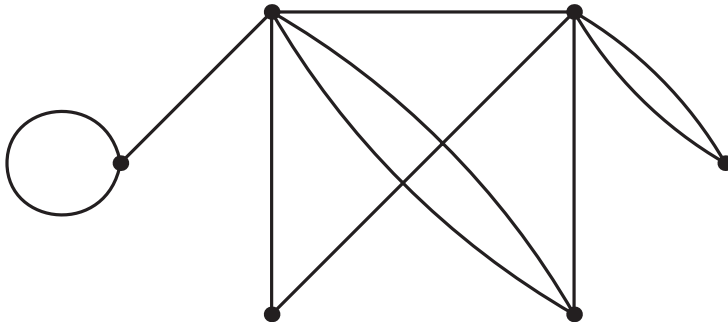


Figure 1. A graph with $V=6$ vertices and $B=10$ bonds.

1.1. Graphs and their topology

A graph $\mathcal{G}(V, B)$ consists of V *vertices* connected by B *bonds* (or *edges*). A graph with six vertices and ten bonds ($V=6$, $B=10$) is shown in figure 1.

The graphs are not necessarily embedded in the plane, and the fact that in the figure bonds cross each other at points which are not vertices is completely immaterial. A physical realization of a graph is a network of coaxial cables (bonds) connected by junctions (vertices). The topology of the graph, that is, the way the vertices and bonds are connected is given in terms of the $V \times V$ *connectivity matrix* $C_{i,j}$ (sometimes referred to as the *adjacency matrix*) which is defined as

$$C_{i,j} = C_{j,i} = \begin{cases} m & \text{if } i \neq j \text{ where } i \text{ and } j \text{ are connected by } m \text{ bonds,} \\ 2m & \text{if } i = j \text{ and there are } m \text{ loops at vertex } i \\ 0 & \text{if } i \text{ and } j \text{ are not connected.} \end{cases} \quad (1)$$

This definition allows for vertices to be connected by several bonds, and also for a vertex to be connected to itself by one or several loops (in which case the corresponding diagonal element of the connectivity matrix equals twice the number of loops).

The *valency* v_i of a vertex i is the number of vertices j connected to i , each weighted by the number of parallel bonds (loops). Thus, m parallel bonds (m parallel loops) contribute m ($2m$) to the valency. In terms of the connectivity matrix,

$$v_i = \sum_{j=1}^V C_{i,j}. \quad (2)$$

The *neighbourhood* Γ_i of the vertex i consists of the vertices j connected to i .

The *boundary* of a subgraph $\hat{\mathcal{G}} \subset \mathcal{G}$, $\Gamma(\hat{\mathcal{G}})$, consists of the vertices which are not in $\hat{\mathcal{G}}$ but which are in the union of the neighbourhoods of the vertices of $\hat{\mathcal{G}}$.

The number of bonds is expressed by

$$B = \frac{1}{2} \sum_{i=1}^V \sum_{j=i}^V C_{i,j}. \quad (3)$$

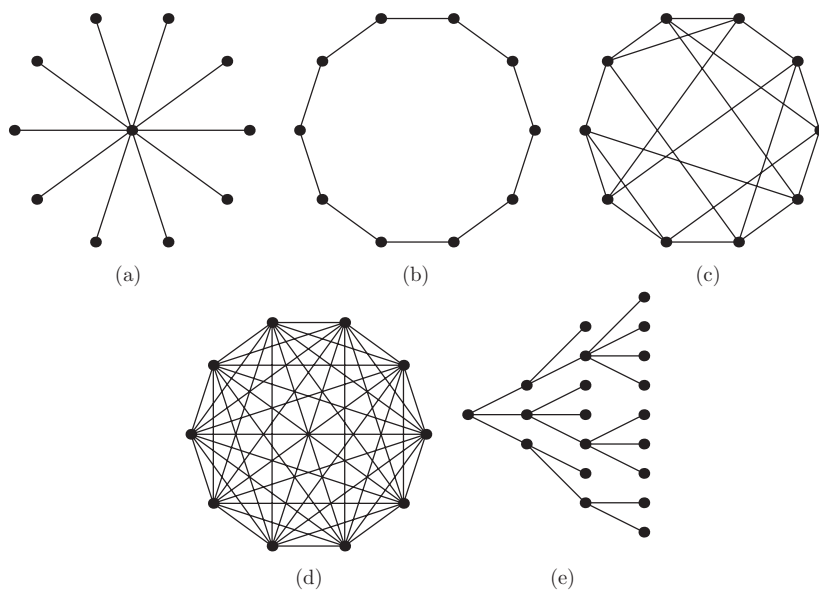


Figure 2. Some examples of graphs: (a) star graph ($B = 10$, $V = 11$), (b) ring graph ($B = 10$, $V = 10$), (c) v -regular graph with $v = 4$ ($B = 20$, $V = 10$), (d) complete graph ($B = 45$, $V = 10$), (e) tree graph ($B = 19$, $V = 20$).

Unless otherwise specified, we shall always consider *connected* graphs, for which the vertices cannot be divided into two non-empty subsets such that there is no bond connecting the two subsets. That is, for a connected graph the connectivity matrix cannot be brought into a block-diagonal form by permuting the vertices.

There are a few classes of graphs which often appear in the literature. They are characterized by their connectivity (see figure 2 for some examples):

- **Simple graphs** are graphs which have no loops and no parallel bonds connecting their vertices (no multiply connected vertices). In this case, for all i and j , $C_{i,j} \in \{0, 1\}$, and in particular all the diagonal elements vanish $C_{i,i} = 0$. For simple graphs, the cardinality of Γ_i is the valency v_i for each vertex. When we define quantum graphs in section 2 we will show that every connected quantum graph can be turned into a graph of simple topology by adding some vertices without changing the spectrum or the wavefunctions. This will allow us to significantly simplify the notation in the remaining sections where a simple topology will be assumed without loss of generality.
- **v -regular graphs** are simple graphs whose vertices have the same valency v . The simplest v regular graphs are the **rings** for which $v = 2$ and $V = B$. A non-trivial ring has at least two vertices. A **v -regular** graph is **complete** when $v = V - 1$.
- **Simply connected graphs** do not contain any non-trivial ring as a subgraph.
- **Tree graphs** are simple, connected and simply connected.
- **Star graphs** are trees that consist of a main (central) vertex with valency v , connected to v peripheral vertices of valency one.

In many applications it is convenient to refer to bonds directly, and we shall use lowercase letters to denote the bonds of the graph. If the graph is simple, we can use

the end points of the bond as its label : $b = (i, j) = (j, i)$. If a graph is not simple (i, j) will denote the set of all bonds that connect the vertices i and j . The round brackets will always be used to denote such a set of undirected bonds unless otherwise stated.

All the bonds which emerge from a vertex i form a *star*,

$$S^{(i)} = \bigcup_{j \in \Gamma(i)} (i, j). \tag{4}$$

If the graph is simple, the bonds in a star $S^{(i)}$ are $\{b = (i, j) : j \in \Gamma(i)\}$.

Directed bonds (also referred to as *arcs* in the literature) are bonds on which a direction is specified. For a simple graph we denote them by the ordered pair of vertex indices enclosed in square brackets $[j, i]$, and the direction is from the right to the left index. Again, for non-simple graphs $[j, i]$ is the set of all directed bonds starting at i and ending at j . Lowercase Greek letters will be used to distinguish them from the undirected bonds. The reverse direction will be denoted by a hat so that e.g., if $\alpha \in [j, i]$ then $\hat{\alpha} \in [i, j]$.

Alternatively, we will denote a directed bond $\alpha \in [j, i]$ as a pair $\alpha = (b, \omega)$ of a bond $b \in (j, i)$ and a direction index $\omega = \pm 1$ where $\omega = +1$ if $j > i$ and $\omega = -1$ if $j < i$. If the bond is a loop ($i = j$) the direction ω has to be assigned to avoid ambiguities. We will use the notation $\omega_\alpha (b_\alpha)$ to refer to the direction index (bond) of the directed bond α . If $\alpha = (b, \omega)$ is a directed bond the reverse direction is $\hat{\alpha} = (b, -\omega)$. All directed bonds that start at a vertex i form an *outgoing star*,

$$S_+^{(i)} = \bigcup_{j \in \Gamma(i)} [j, i]. \tag{5}$$

The *incoming star* $S_-^{(i)}$ is defined analogously as the set of directed bonds that end at i .

The set of directed bonds $[k, l]$ follows the set of directed bonds $[r, s]$ if $r = l$. With $\alpha \in [k, r]$ and $\beta \in [r, s]$ we then write $\alpha \in \mathcal{F}_r(\beta)$ which means that the directed bond α follows β at the vertex r . A *trajectory* $t = (\alpha_1, \dots, \alpha_n)$ from vertex i to j is a sequence of directed bonds $\alpha_l = (b_l, \omega_l)$ such that α_{l+1} follows α_l where α_1 starts at vertex i and α_n ends at vertex j . The *topological length* of the trajectory is the number $n \in \mathbb{N}$ of directed bonds in the path. A *closed trajectory* starts and ends at the same vertex $i = j$ and a *periodic orbit* $p \equiv \overline{\alpha_1, \dots, \alpha_n}$ of *period* n is the equivalence class of closed trajectories that are equal up to cyclic permutation. The *code* of the periodic orbit is the equivalence class $\overline{\alpha_1, \dots, \alpha_n}$ of visited directed bonds. A *primitive periodic orbit* has a code which cannot be written as a repetition of a shorter code. Each trajectory t defines a subgraph \mathcal{G}_t which consists of all bonds and vertices visited by the path. The number of different points on periodic periodic orbits with period n is exactly equal $\text{tr } C^n$. As a consequence, if n is prime the number of periodic orbits $\#(n)$ of period n is exactly

$$\#(n) = \frac{1}{n} \text{tr } C^n = \frac{1}{n} \sum_{j=1}^V \gamma_j^n \tag{6}$$

where γ_j are the eigenvalues of the connectivity matrix. If n is not prime (6) is a good approximation. In the limit of large n , $\#(n)$ is dominated by the maximum eigenvalue which shows that this number grows exponentially with n . In analogy to the theory of dynamical systems we define the *topological entropy* λ_T as the logarithm of the largest eigenvalue. One can easily show that for fully connected graphs $\lambda_T = \log V$ and for star graphs $\lambda_T = 1/2 \log B$.

2. The Schrödinger operator on graphs

In section 1 we defined and discussed the graphs from a topological point of view, where concepts like connectivity and neighbourhood played the main rôles. At this point we would like to endow the graphs with a *metric* which will enable us to define the Schrödinger operator on the graph.

We assign the natural metric to the bonds. The position x of a point on the graph is determined by specifying on which bond b it is, and its distance x_b from the vertex with the *smaller* index such that x_b increases in direction $\omega = +1$ and decreases in direction $\omega = -1$. If the bond b is a loop this defines the starting point for x_b . The length of a bond is denoted by L_b and, $0 \leq x_b \leq L_b$. The length of a path $t = (\alpha_1, \dots, \alpha_n)$ is the sum over all bond lengths $L_t = \sum_{l=1}^n L_{b_l}$ (where $\alpha_l = (b_l, \omega_l)$) along the path. For a bond $b = (i, j)$ we will also use the notation x_b^i and x_b^j for the values of x_b at the vertices. That is, if $i < j$ one has $x_b^i = 0$ and $x_b^j = L_b$. For later use, we define *incommensurable* (or *rationally independent*) bond lengths on the graph. For these the equation

$$\sum_b m_b L_b = 0 \quad (7)$$

where $m_b \in \mathbb{Z}$ only has the trivial solution $m_b = 0$ for all b .

The Schrödinger operator on \mathcal{G} consists of the one-dimensional operators associated with each bond:

$$H_b = \left[\left(\frac{1}{i} \frac{d}{dx_b} + A_b \right)^2 + w_b(x_b) \right] \quad (8)$$

Here, $w_b(x_b)$ is a potential function assumed to be non-negative and smooth on the interval $[0, L_b]$. A_b are real, positive constants. If the graph contains a non-trivial ring as a subgraph (that is, it is not simply connected), and A_b do not vanish on this subgraph, time reversal invariance is broken, as can be seen from the eigenfunctions of (8) with $w_b = 0$ on the line,

$$\left(\frac{1}{i} \frac{d}{dx} + A \right)^2 \psi(x) = k^2 \psi \quad \Rightarrow \quad \psi(x) = e^{-iAx} (c_1 e^{ikx} + c_2 e^{-ikx}) \quad (9)$$

(c_1 and c_2 are arbitrary constants). The complex conjugate of $\psi(x)$ above is not a solution of the same equation, a hallmark of a system which violates time reversal invariance. We shall refer to the constants A_b as *magnetic fluxes* because they play the same rôle as the vector potentials in the Schrödinger operator in higher dimensions. The presence of A implies also that the wavefunctions are intrinsically not symmetric under the reflection $x \rightleftharpoons -x$.

In the physics literature, and in particular in the quantum chaos connection, the bond potentials $w_b(x_b)$ are commonly set to zero. We included them in the general framework for the sake of generality and because they appear in some of the mathematical literature on the topic. Graphs with non-vanishing potentials are sometimes referred to as *dressed graphs* [163–166].

Next, we have to identify the space of wavefunctions and the boundary conditions which renders the operator self-adjoint. In physical terms, this implies

that the evolution induced by the operator conserves probability and the vertices can neither be sinks nor sources. In other words, the boundary conditions at the vertices should be such that the total probability current vanishes when summed over all the bonds which emerge from any of the vertices. This is similar to the well known Kirchhoff rule in the theory of electric networks, and we shall now derive it for quantum graphs.

2.1. Vertex boundary conditions – self-adjoint extension

We consider the set of functions \mathcal{D} which have the following properties: $\Psi(x) \in \mathcal{D}$ are continuous and complex valued functions of $x \in \mathcal{G}$, with $\Psi(x) = \psi_b(x_b)$ for $x \in b$, and $0 \leq x_b \leq L_b$. Continuity is implied here also at the vertices. This means that at each vertex i the limit $\lim_{x_b \rightarrow x_b^i} \psi_b(x_b) = \phi_i$ does not depend on $b \in S^{(i)}$. The functions $\psi_b(x_b)$ are complex valued, bounded with piecewise continuous and square integrable first derivatives. The set \mathcal{D} is the domain of the positive definite quadratic form

$$\begin{aligned} Q_\Lambda[\Psi] &= \int_{\mathcal{G}} dx \left(\left| \left(\frac{1}{i} \nabla + A \right) \Psi(x) \right|^2 + \Psi(x) \cdot W\Psi(x) \right) \\ &\quad + \phi \cdot \Lambda \phi \\ &\equiv \sum_{b=1}^B \int_0^{L_b} dx_b \left(\left| \frac{1}{i} \frac{d\psi_b}{dx_b} + A_b \psi_b(x_b) \right|^2 + w_b(x_b) |\psi_b(x_b)|^2 \right) \\ &\quad + \sum_{j=1}^V \lambda_j |\phi_j|^2 . \end{aligned} \tag{10}$$

Here, ϕ denotes the V dimensional array of ϕ_j . Λ is a positive diagonal matrix with elements $\lambda_j \geq 0$. The rôle of these parameters will become clear in the sequel and their physical significance will be discussed below.

The self-adjoint extension of the Schrödinger operator, H , is determined by the Rayleigh–Ritz extremum principle. For this purpose we compute the variation of the quadratic form $Q_\Lambda[\Psi]$ with respect to Ψ under the condition that $\|\Psi\|^2 \equiv \int_{\mathcal{G}} dx |\Psi(x)|^2 = 1$. This constraint is introduced by considering the variation of the modified quadratic form $\tilde{Q}[\Psi] = Q_\Lambda[\Psi] - k^2 \|\Psi\|$, where k^2 is a positive Lagrange multiplier. The variations of the modified quadratic form with respect to both Ψ and its complex conjugate have to vanish identically. Writing the variation with respect to Ψ^* explicitly, and performing partial integration where necessary, we get

$$\begin{aligned} \delta \tilde{Q}_\Lambda[\Psi] &= \sum_{b=1}^B \int_0^{L_b} dx_b \delta \psi_b^*(x_b) \left(\left(\frac{1}{i} \frac{d}{dx_b} + A_b \right)^2 + w_b(x_b) - k^2 \right) \psi_b(x_b) \\ &\quad + \left[\delta \psi_b^*(x_b) \left(\frac{d}{dx_b} + iA_b \right) \psi_b(x_b) \right]_0^{L_b} + \sum_{j=1}^V \delta \phi_j^* \lambda_j \phi_j . \end{aligned} \tag{11}$$

A similar expression can be obtained for the variation of \tilde{Q} with respect to $\Psi(x)$. Requiring that both variations vanish for every $\delta\Psi(x)$ and $\delta\Psi^*(x)$, we find that the

Downloaded by [Gothenburg University Library] at 13:09 07 December 2017

domain \mathcal{D}_H of the Schrödinger operator consists of functions in \mathcal{D} , with twice differentiable $\psi_b(x_b)$, which satisfy the boundary conditions

$$\forall 1 \leq i \leq V: \sum_{(b, \omega) \in S_+^{(i)}} \omega \left(\frac{d}{dx_b} + iA_b \right) \psi_b \Big|_i = \lambda_i \phi_i. \quad (12)$$

The derivatives in (12) boundary above are computed at the common vertex i . That is at $x_b = x_b^i = 0$ if $\omega = +1$ and $x_b = x_b^i = L_b$ if $\omega = -1$ (if b is a loop, both directions appear in the sum). These conditions are obtained by reorganizing the second line in (11) according to the vertices and their associated (outgoing) stars.

The eigenfunction are solutions of the bond Schrödinger equations

$$\forall 1 \leq b \leq B: H_b \psi_b = k^2 \psi_b, \quad (13)$$

which satisfy the boundary conditions (12) boundary. The spectrum $\{k_n^2\}_{n=1}^\infty$ is discrete, non-negative and unbound. It consists of the values of the Lagrange multiplier k^2 for which a non-trivial solution is found. The sequence of eigenvalues is conveniently arranged by increasing order, so that $k_n \leq k_m$ if $n < m$.

The eigenfunctions (ordered by increasing eigenvalues) have the following property. Let \mathcal{D}_n denote the subspace of functions in \mathcal{D} which are orthogonal to the first $n-1$ eigenfunctions of H . Then, for any non-zero $\Phi \in \mathcal{D}_n$

$$Q[\Phi] \geq k_n^2 \|\Phi\|^2. \quad (14)$$

Equality holds if and only if Φ is the n 'th eigenfunction of H .

At this point it will be good to familiarize oneself with the general formalism above by considering a few examples.

The boundary conditions (12) take a very simple form for vertices with valency $v=2$, when the magnetic fluxes on the two bonds are the same and the potentials on the two bonds take the same value at the vertex. We can now think of the two bonds as two adjacent intervals on the line with a common boundary which we choose as the point $x=0$. Writing (12) explicitly we get

$$\lim_{\epsilon \rightarrow 0^+} \left\{ \frac{d\psi}{dx} \Big|_{0+\epsilon} - \frac{d\psi}{dx} \Big|_{0-\epsilon} \right\} = \lambda \psi(0). \quad (15)$$

This is the well known boundary condition one obtains from a 'δ-potential' of strength λ . In physics textbooks this boundary condition is derived by integrating the Schrödinger equation along an interval of size 2ϵ centred at $x=0$, and the self-adjoint extension of the operator is obtained automatically. This is not the case when we are dealing with a more complex vertex, and the road we chose to derive the boundary conditions must be taken.

Even though the parameters λ_i can take arbitrary values, the limiting values $\lambda_i = 0$ (**Neumann** boundary conditions) or $1/\lambda_i = 0$ (**Dirichlet** boundary conditions) are of special interest.

The importance of Neumann boundary conditions (also known as **Kirchhoff** boundary conditions in mathematical literature) comes from the fact (to be proven shortly) that the spectra of systems with finite (but not vanishing) λ_i approach to the Neumann spectrum as one looks higher up in the spectrum. A similar situation is well known for the spectra of Schrödinger operators on domains with boundaries,

where the boundary conditions intermediate between Dirichlet and Neumann are studied [167]. Note that the case studied in the example above of a vertex with $\nu=2$ is trivial under the Neumann condition. Indeed, (15) implies that the wavefunction and its first derivative are continuous so that the point $x=0$ becomes an ordinary point on the interval. Thus, a Neumann vertex with $\nu=2$ can simply be erased from the graph, without any effect on the spectrum or wavefunctions. This property can be used in the reverse direction as well. In particular, every non-simple quantum graph can be turned into an equivalent (with respect to spectra and wavefunctions) quantum graph of simple topology (no loops, no multiple connections) by adding two Neumann vertices on each loop and one Neumann vertex on each bond which is responsible for multiple connectivity. Because of this reason, and unless stated otherwise, we shall henceforth *consider only graphs with simple topology*:

$$C_{i,j} \in \{0, 1\} \quad \text{and} \quad C_{i,i} = 0. \quad (16)$$

This significantly simplifies the notation while the transition back to the original connectivity is straightforward.

The Dirichlet boundary conditions imply that the value of the wavefunction vanishes at all the vertices. This isolates the various bonds and the spectrum of the Schrödinger of the graph reduces to the union of the bond spectra, with Dirichlet boundary conditions on each of the ends of the bonds. The wavefunction corresponding to a non-degenerate eigenvalue k_n^2 is identically zero on all bonds but one and the spectrum is given by the union of the independent spectra on the bonds

$$\sigma_{\text{Dirichlet}} = \bigcup_{b=1}^B \bigcup_{n=1}^{\infty} \left\{ \left(\frac{\pi n}{L_b} \right)^2 \right\}. \quad (17)$$

2.2. The secular equation

In the previous section the Schrödinger operator and the accompanying boundary conditions were defined and discussed. Here, we shall derive the secular function – the real valued function whose zeros (the values of the argument where the function vanishes) stand in one to one correspondence with the spectrum of the graph. The spectrum of Dirichlet graphs was computed previously and we shall exclude this case in the following.

We shall first assume that the bond potentials vanish, $w_b(x_b) = 0$. We will comment on non-vanishing bond potentials at the end of this section.

The starting point is the potential-free solution (9). On a bond $b = (i, j)$ with $i \leq j$, the general solution of the bond Schrödinger equation is a superposition of the two solutions (9), which can be written as

$$\psi_b(x_b; k) = \frac{e^{-iA_b x_b}}{\sin k L_b} \left(\phi_j e^{iA_b L_b} \sin k x_b + \phi_i \sin k(L_b - x_b) \right). \quad (18)$$

At the two endpoints $x_b=0$ and $x_b=L_b$, the wavefunction $\psi_b(x_b; k)$ assumes the values ϕ_i and ϕ_j , respectively. These same values appear in the wavefunctions on bonds which connect i or j to other vertices, and therefore, the resulting graph wavefunction is continuous. Thus, the most general form of $\Psi \in \mathcal{D}_H$ is completely determined (up to a scalar factor) by V complex parameters $\phi = (\phi_1, \dots, \phi_V)$.

The appearance in the denominator of $\sin kL_b$ for all b will eventually lead to poles of the secular function at the Dirichlet spectrum.

The eigenfunctions and eigenvalues of the Schrödinger operator are found by demanding that the B functions (18) satisfy the boundary conditions (12). Upon substitution, we obtain a set of V homogeneous and linear equations for the vertex wavefunctions ϕ ,

$$\sum_{j=1}^V \phi_j h_{j,i}(k) = 0 \quad \forall i = 1, \dots, V, \quad (19)$$

where,

$$h_{i,i}(k) = \frac{\lambda_i}{k} + \sum_{(b, \omega) \in S_+^{(i)}} \cot kL_b$$

$$h_{j,i}(k) = -C_{j,i} \frac{e^{i\omega A_b L_b}}{\sin kL_b}, \quad (b, \omega) = [j, i]. \quad (20)$$

Note that the matrix h is Hermitian because the indicators ω change their sign when i and j are interchanged. Equations (19) have a non-trivial solution if and only if

$$\zeta_h(k) \equiv \det h(k) = 0. \quad (21)$$

The function $\zeta_h(k)$ is the *secular function*. Because of the symmetry $\psi_b(x; k) = -\psi_b(x, -k)$, the zeros of the secular function appear symmetrically on the negative and positive k half-lines at $\pm k_n$. The Schrödinger spectrum is k_n^2 . In section 3, an alternative secular function will be derived. The suffix h in $\zeta_h(k)$ is added to distinguish between this and the other secular function.

In the previous section we commented (without proof) that in the limit of large eigenvalues, the spectra of the Schrödinger operators with $\lambda_b \neq 0$ converge to the Neumann spectrum. This is immediately apparent from (20), since the parameters λ_b appear in the combination λ_b/k which vanishes in the limit of large k .

Finally, it will be instructive to write explicitly the secular function for a simple example. We do it for a star graph which was defined in section 1.1. We denote the central vertex by the index 0, and label the emanating bonds as well as their exterior vertices by i , $i = 1, \dots, B$. The only non-vanishing matrix elements of h are

$$h_{0,0} = \frac{\lambda_0}{k} + \sum_{i=1}^B \cot kL_i$$

$$h_{j,j} = \frac{\lambda_j}{k} + \cot kL_j$$

$$h_{0,j} = -\frac{e^{-iA_j L_j}}{\sin kL_j}. \quad (22)$$

The secular function can be computed directly,

$$\zeta_h(k) = \left(h_{0,0} - \sum_{i=1}^B \frac{|h_{0,i}|^2}{h_{i,i}} \right) \prod_{j=1}^B h_{j,j}. \quad (23)$$

It is worthwhile noting that the magnetic fluxes A_j do not appear in the secular function. The reason for this is that the star graph is simply connected. Moreover, ζ_h can only vanish if the first factor on the right hand side of equation (23) vanishes. The secular equation reduces to

$$\zeta_{h_*} = \frac{\lambda_0}{k} + \sum_{i=1}^B \cot kL_i - \sum_{i=1}^B \frac{1}{\sin^2 kL_i((\lambda_i/k) + \cot kL_i)} = 0. \quad (24)$$

To end this section we shall indicate how the computation of the secular equation can be generalized to include non-vanishing potentials $w_b(x_b)$ on the bonds. In the general case one cannot write an explicit solution of the bond wave equation as in (18). However, since it is of the Sturm–Liouville type, it is possible to find two independent solutions, which satisfy independent *initial conditions*. One function vanishes at the vertex i and its derivative is set to 1, and the other vanishes at the vertex j and its derivative is 1. The most general solution which takes the values ϕ_i and ϕ_j at both ends of the bond can be written as a linear combination of the two solutions, and from here on one can proceed as in the potential free case. Use should be made of the Wronskian relation, which in the presence of the magnetic flux takes the form

$$W(f, g) \equiv f \left(\frac{dg^*}{dx_b} - iA_b g^* \right) - g^* \left(\frac{df}{dx_b} + iA_b f \right) = \text{Const}. \quad (25)$$

3. The quantum evolution map

It is quite common in theoretical physics that a given subject can be formulated and studied from several points of view which use different concepts and tools. Consider for instance, the Lagrangian and Hamiltonian approaches to classical mechanics. The phase-space description reveals the symplectic structure of classical dynamics in a natural way, which is only implicit in the configuration-space description. Following this example, we shall present in this section another formulation of the spectral theory of graphs which uses other concepts and structures than those used in the previous section. The main observation and intuition which underlays the new formulation is that a wavefunction on the graph can be written as a superposition of waves travelling in opposite directions on the bonds. The waves which propagate towards a given vertex are scattered from the vertex and emerge as outgoing waves, which scatter again and again. A wavefunction is an eigenfunction if it is *stationary* under the multiple scattering scenario described above, and this, in turn can happen only if the wavenumber k of the propagating wave is correctly selected. Thus, a new form of the secular equation can be obtained, based on this multiple scattering approach [117]. The advantages gained by developing the alternative theory are both conceptual and technical, and they will be revealed as the theory is systematically unfolded in the following sections. These advantages are gained at a price: the number of parameters necessary to represent a wavefunction increases from V to $2B$, which is the number of amplitudes of waves which propagate back and forth on the bonds.

Note: In the present section we consider the ‘bare’ graphs so that on all the bonds $w_b=0$. We also want to recall that we assume a simple topology *without loss of generality* (see section 2.1).

3.1. Vertices as scattering centres

Given a graph \mathcal{G} , the bond lengths L_b , magnetic fluxes A_b and the boundary condition parameters λ_b , one can write a general solution of the Schrödinger equation (18) (for $i < j$)

$$\begin{aligned} \psi_b(x_b; k) &= \frac{e^{-iA_b x_b}}{\sin k L_b} \left(\phi_j e^{iA_b L_b} \sin k x_b + \phi_i \sin k(L_b - x_b) \right) \\ &= e^{-iA_b x_b + i k x_b} a_{[i, i]}^{\text{out}} + e^{-iA_b x_b - i k x_b} a_{[i, j]}^{\text{in}} \end{aligned} \quad (26)$$

where, $a_{[i, j]}^{\text{in}} \equiv a_\beta^{\text{in}}$ and $a_{[i, i]}^{\text{out}} \equiv a_\beta^{\text{out}}$ are the (complex valued) amplitudes of the counter-propagating waves (incoming and outgoing at vertex i) along the bond b , and they can be readily written in terms of the parameters ϕ_i and ϕ_j . In section 1.1 we defined the outgoing (incoming) stars $S_+^{(i)}$ ($S_-^{(i)}$) as the set of directed bonds which point away (point at) the vertex i which are convenient for the following discussion. Consider now a single vertex i and the bonds $b \in S^{(i)}$. For the present discussion we also use the convention that the vertex i corresponds to the point $x_b=0$ for all the bonds in the star $S^{(i)}$. From (26) we see that ϕ_i can be expressed as

$$\phi_i = a_{b, \omega}^{\text{out}} + a_{b, -\omega}^{\text{in}}, \quad (27)$$

on all the bonds $b \in S^{(i)}$. These v_i relations provide $v_i - 1$ homogeneous equations

$$a_{b, \omega}^{\text{out}} + a_{b, -\omega}^{\text{in}} = a_{b', \omega}^{\text{out}} + a_{b', -\omega}^{\text{in}} \quad \text{for } b, b' \in S^{(i)}. \quad (28)$$

Another homogeneous expression is derived by substituting both (26) and (27) in the boundary condition at vertex i (12),

$$\sum_{\beta \in S_-^{(i)}} \left(1 - \frac{\lambda_i}{i v_i k} \right) a_\beta^{\text{in}} = \sum_{\alpha \in S_+^{(i)}} \left(1 + \frac{\lambda_i}{i v_i k} \right) a_\alpha^{\text{out}} \quad (29)$$

These v_i relations enable us to write the *outgoing* amplitudes a_α^{out} , $\alpha \in S_+^{(i)}$ in terms of the *incoming* amplitudes a_β^{in} , $\beta \in S_-^{(i)}$ in the form

$$\forall \alpha \in S_+^{(i)} : a_\alpha^{\text{out}} = \sum_{\beta \in S_-^{(i)}} \sigma_{\alpha, \beta}^{(i)} a_\beta^{\text{in}}, \quad (30)$$

where,

$$\sigma_{\alpha, \beta}^{(i)} = \frac{1 + e^{i \rho_i(k)}}{v_i} - \delta_{\hat{\alpha}, \beta} \quad (31)$$

and,

$$e^{i \rho_i(k)} = \frac{1 - i(\lambda_i / v_i k)}{1 + i(\lambda_i / v_i k)}. \quad (32)$$

This can be written shortly as $\sigma^{(i)} = 2k / (v_i k + i \lambda_i) \mathbb{E} - \mathbb{1}$ where \mathbb{E} is a full matrix with unit entries.

It is not difficult to prove that the $v_i \times v_i$ symmetric matrix $\sigma^{(i)}$ is *unitary*, which implies that the total outgoing probability current equals the total incoming probability current, as stated (without proof) in a previous section. The matrices σ^j will be referred to as the **vertex scattering matrices**. The simple topology allows us to use the previous and the next vertex as indices of the vertex scattering matrix instead of the corresponding directed bonds,

$$\sigma_{[j,i],[i,j]}^{(i)} \equiv \sigma_{j'j}^{(i)} \tag{33}$$

for all j, j' in the neighbourhood of i . We shall use both notations at convenience.

Consider as an example a Neumann vertex with $v = 2$ and $S_i^+ = \{\alpha, \beta\}$. It follows from (31) that $\sigma_{\alpha, \hat{\alpha}} = \sigma_{\beta, \hat{\beta}} = 0$, but $\sigma_{\alpha, \hat{\beta}} = \sigma_{\beta, \hat{\alpha}} = 1$. In other words, a $v = 2$ Neumann vertex transmits waves without any reflection. This is consistent with a previous remark that such vertices have no effect on the quantum dynamics on graphs, and can be added or removed at will.

The vertex scattering matrices are the building blocks of much of the subsequent theory, and they deserve some further discussion. The vertex scattering matrices presented above are but one of many possible examples, and they can be constructed to model various physical systems. For example, an engineer considers the graph as a model of a network of wave-guides connected by junctions. In the ideal situation, there is no dissipation at the junctions, and therefore the transmission and reflection at the junctions are characterized by unitary scattering matrices. Their details (such as their dependence on the frequency), reflect the particular way by which the junction is designed and constructed. Also, the quantization procedure of section 2 can be generalized in several ways. We shall dedicate the special section 3.3 to present and discuss the most commonly used classes of vertex matrices beyond the present quantization scheme. We place this section at the end of the section not to interrupt the flow of the exposition.

3.2. The quantum evolution map

The graph is a network of connected vertices, and the waves are scattered between them along the connecting bonds. When the graph is assembled from all its vertices and bonds, it is important to remember that given two connected vertices i and j , a directed bond $\alpha = [i, j]$ is *outgoing* from j , $\alpha \in S_+^{(j)}$ but it is *incoming* to i , $\alpha \in S_-^{(i)}$. That is, when $C_{i,j} = 1$

$$[i, j] = S_+^{(j)} \cap S_-^{(i)} \quad \text{and} \quad [j, i] = S_-^{(j)} \cap S_+^{(i)}. \tag{34}$$

The wavefunction (26) on the bond $b = (i, j)$ was written down by adopting the convention that $x_b = 0$ at the vertex i – this choice emphasizes the vertex i as the scattering centre. However, we can write the same wavefunction in terms of the coordinate $x_{\hat{b}} = L_b - x_b$, so that $x_{\hat{b}} = 0$ marks the vertex j ,

$$\psi_{\hat{b}}(x_{\hat{b}}; k) = e^{+iA_b x_{\hat{b}} + ikx_{\hat{b}}} a_{[i,j]}^{\text{out}} + e^{+iA_b x_{\hat{b}} - ikx_{\hat{b}}} \hat{a}_{[j,i]}^{\text{in}}. \tag{35}$$

Again, the wavefunction is expressed in terms of counter-propagating waves with incoming and outgoing amplitudes with respect to vertex j . However, the magnetic flux appears now with a different sign, as befits its rôle in the theory as the element which breaks time reversal invariance. It is therefore only natural to consider the

magnetic flux as a quantity which is associated with a directed bond, with $A_\alpha = -A_{\bar{\alpha}}$, in contrast with the bond length which does not depend on orientation. Comparing the two expressions (26) and (35) for the wavefunction on the bond b one can read off that the outgoing amplitude at the starting vertex of a directed bond $\alpha = (b, \omega)$ and the incoming amplitude at the next vertex differ by a phase factor

$$a_{b,\omega}^{\text{in}} = e^{ikL_b + i\omega A_b L_b} a_{b,\omega}^{\text{out}} \quad (36)$$

which the wave acquires from one end to the other of the bond.

Equipped with all the above notations and remarks, we can now demand that the bond wavefunctions (26) or (35) satisfy the continuity and the boundary conditions (12) at all the vertices. This results in $2B$ homogeneous linear equations for the $2B$ coefficients a_α which can be written explicitly as

$$\forall \alpha : a_\alpha^{\text{in}} = \sum_{\beta} \mathcal{U}_B(k)_{\alpha,\beta} a_\beta^{\text{in}}, \quad (37)$$

where the sum over β is over all $2B$ directed bonds and the matrix $\mathcal{U}_B(k)$ is written as

$$\mathcal{U}_B(k) = T(k)S(k), \quad (38)$$

with $T(k)$, the **bond propagation matrix**, which is the diagonal $2B \times 2B$ matrix

$$T(k)_{(b,\omega),(b',\omega')} = \delta_{bb'} \delta_{\omega\omega'} e^{i(k+\omega A_b)L_b}. \quad (39)$$

The $2B \times 2B$ -matrix $S(k)$ contains the vertex scattering coefficients

$$S_{\alpha',\alpha}(k) = \begin{cases} \sigma_{\alpha',\alpha}^{(i)} & \text{if } \alpha' \text{ follows } \alpha \text{ at vertex } i, \alpha' \in \mathcal{F}_i \\ 0 & \text{else.} \end{cases} \quad (40)$$

We will refer to S as the **graph scattering matrix**. A non-trivial solution of (37) exists for the wavenumber $k > 0$ for which

$$\zeta_B(k) \equiv \det(\mathbb{1} - \mathcal{U}_B(k)) = 0. \quad (41)$$

$\zeta_B(k)$ is another secular function, whose zeros define the spectrum of the graph. In contrast with $\zeta_h(k)$, it involves a determinant of a matrix of larger dimension, yet it has many advantages, the most outstanding is that $\zeta_B(k)$ has no poles on the real k axis, in contrast to $\zeta_h(k)$ which has poles at the Dirichlet spectrum of the graph. The ζ_B -function can be thought of as the characteristic polynomial $\det(\lambda \mathbb{1} - \mathcal{U}_B(k)) = \sum_{j=0}^{2B} a_j \lambda^j$. A consequence of the unitarity of $\mathcal{U}_B(k)$ is

$$\det(\lambda \mathbb{1} - \mathcal{U}_B(k)) = \det\left(\frac{1}{\lambda} \mathbb{1} - \mathcal{U}_B^\dagger(k)\right) \det(-\mathcal{U}_B(k)) \lambda^{2B} \quad (42)$$

which implies

$$a_j = a_{2B-j}^* \det(-\mathcal{U}_B(k)). \quad (43)$$

This identity is the analogue of the Riemann–Siegel ‘look-alike’ symmetry which holds only approximately for spectral ζ -functions of chaotic quantum systems. Other properties of $\zeta_B(k)$ will be discussed as the theory is developed.

The matrix $\mathcal{U}_B(k)$ will be referred to as *the quantum evolution map* because of the following reasons. Being an involution of two unitary matrices, it is unitary – which is a basic requirement for a quantum map. The action of the map is a composition of two successive operations: scattering followed by a propagation along the bonds: The scattering map operates on *incoming* amplitudes at all the vertices and produces the corresponding *outgoing* amplitudes. For finite $\lambda_i > 0$ the graph scattering matrix depends on the wavenumber – for $\lambda_i = 0$ and for some of the generalizations to discuss later it becomes independent. The matrix $T(k)$ propagates the outgoing waves along the bonds and provides the correct phase for the next scattering event. Starting with an arbitrary distribution of amplitudes a_α^{in} of waves with a wavenumber k , one can examine the evolution of the wave pattern as a function of the number n of scattering events by applying $\mathcal{U}_B^n(k)$ to the initial distribution. The consistency condition (37) can be interpreted as a requirement that at an eigenvalue of the graph, the wavefunction is *stationary* with respect to the quantum evolution map – a very natural requirement. More care has to be taken for vanishing wavenumber $k=0$ where $e^{\pm ikL_b} \rightarrow 1$ is not propagating. That is, only the strictly positive part of the spectrum $k_n > 0$ is equivalent to positive zeros of the secular function while this one-to-one correspondence may fail at $k=0$. The simplest example for such a failure is the line of length L with Dirichlet boundary conditions, for which $\zeta_B(k) = 1 - e^{i2kL}$. Obviously $\zeta_B(0) = 0$ in this case, but $k=0$ is not in the spectrum. Note that for Neumann boundary conditions $\zeta_B(k)$ is not changed but now $k=0$ is in the spectrum. Such ‘false zeros’ of the secular function at $k=0$ appear quite often. For instance, quantum graphs with Neumann boundary conditions have a non-degenerate ground state at $k=0$ which is just the constant function on the graph and the secular function vanishes $\zeta_B(k=0) = 0$. In most topologies this is, however, a highly degenerate zero of the secular function (for instance in all cases, where all valencies are larger than two). In spite of this possible failure of the secular function at $k=0$ the graph scattering matrix S completely determines the boundary conditions at all vertices of the graph and the complete evolution operator $\mathcal{U}_B(k)$ determines the complete spectrum if the limit $k \rightarrow 0$ is considered correctly.†

So far we have shown that the condition (41) is equivalent to the boundary conditions (12). However, with the above interpretation, we can obtain the spectrum of a wider class of graphs, whose vertex scattering matrices are unitary matrices derived or postulated in other ways, as discussed in the next section.

3.3. Examples of generalized vertex scattering matrices

In the quantization procedure of section 2 we have considered only boundary conditions for which the wavefunction is continuous through each vertex and we have given the most general account of them. The continuity condition may however be relaxed, and more general boundary conditions corresponding to a self-adjoint

†This limit has to take into account that for $k=0$ the general solution of the one-dimensional Schrödinger equation (without magnetic field) is a linear function $a + bx$. The rest is straightforward. In the following we will always imply a full knowledge of the quantum map when referring to the condition (41) such that the oddities at $k=0$ can always be removed by the correct limit. We will only come back to this point if it has some non-trivial consequences.

operator on a metric graph have been derived for this case by Kostykin and Schrader [57]. Generalized boundary conditions at the vertex i can be written in the form

$$\sum_j C_{jj}^{(i)} \phi_{(i,j)}(x_{(i,j)}^j) + D_{jj}^{(i)} \frac{d}{dx_{(i,j)}} \phi_{(i,j)}(x_{(i,j)}^j) = 0 \quad (44)$$

where the sum runs over all vertices j in the neighbourhood of i . The (k independent) $v_i \times v_i$ matrices $C^{(i)}$ and $D^{(i)}$ can be chosen arbitrarily for each vertex, restricted only by the conditions that (i) the $v_i \times 2v_i$ matrix $(C^{(i)}, D^{(i)})$ has maximal rank and (ii) $C^{(i)} D^{(i)\dagger}$ is Hermitian. It then follows that the Schrödinger operator on the graph with these boundary conditions is self-adjoint. A small exercise gives the corresponding vertex scattering matrices.

$$\sigma^{(i)}(k) = (ikD^{(i)} + C^{(i)})^{-1}(ikD^{(i)} - C^{(i)}). \quad (45)$$

The vertex scattering matrices defined in this way are unitary and generally k -dependent. With the given restrictions on $C^{(i)}$ and $D^{(i)}$ the matrices $ikD^{(i)} \pm C^{(i)}$ are always invertible [57]. However, the matrices $D^{(i)}$ and $C^{(i)}$ are in general not invertible and the limits $k \rightarrow 0$ and $k \rightarrow \infty$ in (45) are non-trivial.

As an example, let us show that the boundary conditions from section 2 are a subset of this generalized approach. Choosing the $v_i \times v_i$ matrices

$$C^{(i)} = -\lambda_i \mathbb{1} \quad D^{(i)} = \mathbb{E} \quad (46)$$

where $\mathbb{E}_{jj} = 1$ for each matrix element is equivalent to the boundary conditions (12) and satisfies the conditions on $C^{(i)}$ and $D^{(i)}$. The vertex scattering matrix $\sigma^{(i)} = -\mathbb{1} + 2k/(v_i k + i\lambda_i) \mathbb{E}$ given by (31) is easily seen to satisfy $(ikD^{(i)} + C^{(i)})\sigma^{(i)} = ikD^{(i)} - C^{(i)}$ using the property $\mathbb{E}^2 = v_i \mathbb{E}$. In the limit $\lambda_i \rightarrow 0$ our choice of $C^{(i)}$ and $D^{(i)}$ does not satisfy the required condition that $(C^{(i)}, D^{(i)})$ has maximal rank. However, the choice of $C^{(i)}$ and $D^{(i)}$ is not unique and it is easy to find a choice that works for $\lambda_i = 0$. To be explicit, for $v_i = 3$ choose

$$C^{(i)} = \begin{Bmatrix} 1 & -1 & 0 \\ 0 & 1 & -1 \\ 0 & 0 & 0 \end{Bmatrix} \quad D^{(i)} = \begin{Bmatrix} 0 & 0 & 0 \\ 0 & 0 & 0 \\ 1 & 1 & 1 \end{Bmatrix}. \quad (47)$$

Here $C^{(i)} D^{(i)\dagger} = 0$ which is self-adjoint and it is obvious how to extend it to higher valencies $v_i > 3$.

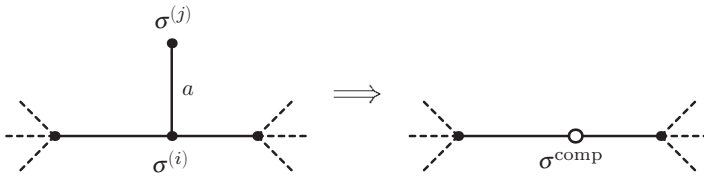
Instead of defining a self-adjoint Schrödinger operator one may as well quantize a metric graph by requiring that a unitary quantum evolution operator of the form $\mathcal{U}_B(k) = T(k)S(k)$ exists. This is equivalent to assigning an arbitrary unitary vertex scattering matrix $\sigma^{(i)}(k)$ to each vertex i . Such an arbitrary choice is in general not equivalent to a self-adjoint Schrödinger operator on a metric graph with boundary conditions specified by (44). With a little abuse of language physicists nonetheless speak of boundary conditions which are defined by such arbitrary vertex scattering matrices – and so will we in the sequel. While mathematically less satisfactory this is a physically well motivated and well defined generalization. Physically, a vertex is some scattering centre which may have some internal structure. While the details of this internal structure are not relevant one just describes it through its unitary

scattering matrix which ensures probability conservation (unitarity of the quantum evolution map). The scattering at the vertex may or may not depend on the wavenumber k depending on the internal structure of the vertex. In most physical applications they are just chosen to be constant. In the remaining sections we will stick to an arbitrary but k -independent choice just for simplicity. Note that a k -independent choice is also mathematically satisfying. It has been shown by Carlson [54] that such a choice defines a self-adjoint Schrödinger operator on a (directed) metric graph. An example of a widely used vertex scattering matrix is the Discrete Fourier Transform (DFT) matrix for which

$$\sigma_{j'j}^{(i), \text{DFT}} = \frac{1}{\sqrt{v_i}} e^{2\pi i (n(j)n(j'))/v_i} \tag{48}$$

where $n(j)$ is a one-to-one mapping of the v_i neighbouring vertices j to the numbers $0, 1, \dots, v_i - 1$. In contrast to a vertex with Neumann boundary conditions where backscattering is favoured for large valency $v > 4$ the scattering amplitudes of a vertex with a DFT vertex scattering matrix has equal absolute value for all incoming and outgoing bonds.

In other applications one may have a specific scattering system in mind (e.g. the bonds that are connected to a vertex are really channels that couple to a quantum billiard). Quite general vertex scattering matrices may also arise starting from a quantum graph with Neumann boundary conditions. In that case one may define a **composite vertex** which combines some subset of the vertices of the graph and combines them to a single one. This may simplify the topology (or calculations) considerably. For the new composite vertex one may derive a vertex scattering matrix by eliminating all bonds that now belong to the internal structure. As a simple example let us look at a composite vertex defined by replacing



where one bond of length a is eliminated. For Neumann boundary conditions $\sigma^{(j)} = 1$ and $\sigma^{(i)} = \frac{2}{3}\mathbb{E}_3 - \mathbb{1}_3$ one gets the k -dependent composite vertex scattering matrix

$$\begin{aligned} \sigma^{\text{comp}} &= \frac{1}{3 + e^{i2ak}} \begin{Bmatrix} e^{i2ak} - 1 & 2(e^{i2ak} + 1) \\ 2(e^{i2ak} + 1) & e^{i2ak} - 1 \end{Bmatrix} \\ &= -\mathbb{1}_2 + \mathbb{E}_2 \left(\frac{2}{3} + \frac{2}{3} \frac{e^{i2ak}}{1 + (1/3)e^{i2ak}} \frac{2}{3} \right). \end{aligned} \tag{49}$$

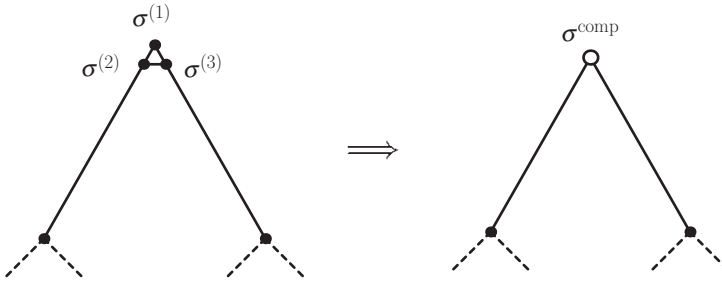
Here, we have written the last line in such a way that an interpretation in terms of trajectories is apparent. The first two terms $-\mathbb{1}_2 + \frac{2}{3}\mathbb{E}_2$ describe direct processes for which the particle does not visit the eliminated bond. In the third term the two

factors $2/3$ are the amplitudes for entering and exiting the eliminated bond and the factor

$$\frac{e^{i2ak}}{1 + \frac{1}{3}e^{i2ak}} = e^{i2ak} \sum_{n=0}^{\infty} \left(-\frac{1}{3}e^{i2ak}\right)^n \quad (50)$$

is a geometric sum over trajectories for which the particle is scattered back to the eliminated bond n times.

Eliminating bonds by defining composite vertices is very useful in numerical calculations (it reduces the matrix dimension), and also in analytical approaches. For instance, if there is a length-scale separation between small bond lengths inside the composite vertex and large bond lengths in the rest of the graph like in



the vertex scattering matrix of the composite vertex will weakly depend on the wavenumber k .

4. Classical evolution on graphs

So far we discussed graph dynamics from a quantum mechanical point of view. At the present stage, we would like to study graphs from a different point of view, which provides the classical counterpart of the quantum theory [117, 132, 168]. Usually, the connection between the quantum and the classical description is provided by *quantizing* a classical system. Here, we take the process in the reverse direction, for reasons which will be explained below.

4.1. Classical phase-space and transition probabilities

Given a graph, we consider a classical particle which moves freely as long as it is on any of the bonds. The vertices are singular points, and it is not possible to write down the analogue of the Newton equations at the vertices. To circumvent this intrinsic difficulty we employ a Liouvillian approach, based on the study of the evolution of phase-space densities. The phase space evolution operator assigns transition probabilities between phase space points, and it is the classical analogue of the quantum evolution operator. We shall employ this analogy to construct the classical dynamics. For this purpose, we should first establish what is the graph classical phase-space, and second, construct the classical analogue of the quantum evolution operator.

The phase-space description will be constructed on a Poincaré section which is defined in the following way. Crossing of the section is registered as the particle encounters a vertex, thus the ‘coordinate’ on the section is the vertex label. The corresponding ‘momentum’ is the direction at which the particle emerges from the vertex. This is completely specified by the label of the next vertex to be encountered. In other words,

$$\left\{ \begin{array}{c} \text{position} \\ \text{momentum} \end{array} \right\} \iff \left\{ \begin{array}{c} \text{vertex index} \\ \text{next index} \end{array} \right\} \equiv (b, \omega). \tag{51}$$

The set of all possible vertices and directions is equivalent to the set of $2B$ directed bonds. Thus, the classical phase space densities are defined on the same space as the corresponding quantum evolution map.

The evolution on the Poincaré section is described in discrete time steps (topological time) and is well defined once we postulate the transition probabilities $P_{\alpha' \leftarrow \alpha}^{(i)} \geq 0$ between the directed bonds α and α' where α' follows α at the vertex i , $\alpha' \in \mathcal{F}_i \alpha$. Probability conservation then requires

$$\sum_{\alpha': \alpha' \in \mathcal{F}_i \alpha} P_{\alpha' \leftarrow \alpha}^{(i)} = 1 \tag{52}$$

for all α .

For a general classical dynamics (Markov process) on a graph one may postulate any transition probabilities $P_{\alpha' \leftarrow \alpha}^{(i)} \geq 0$ that satisfies (52). To construct the classical analogue of the quantum graphs, we choose the classical transition probabilities to be equal to the quantum transition probabilities, expressed as the absolute squares of the \mathcal{U}_B matrix elements

$$P_{\alpha' \leftarrow \alpha}^{(i)} = \left| \sigma_{\alpha', \alpha}^{(i)}(k) \right|^2. \tag{53}$$

In addition to the general condition (52) the transition probabilities on a quantum graph also satisfy

$$\sum_{\alpha: \hat{\alpha} \in \mathcal{F}_i \alpha'} P_{\alpha' \leftarrow \alpha}^{(i)} = 1 \tag{54}$$

for all α' because the $\sigma^{(i)}$ are unitary.

As examples, we quote explicitly the transition probability which correspond to a DFT, Neumann and Dirichlet vertex scattering matrices.

$$P_{\alpha' \leftarrow \alpha}^{(i)} = \begin{cases} \frac{1}{v_i} & \text{for a DFT vertex scattering matrix,} \\ \left(1 - \frac{4}{v_i}\right) \delta_{\hat{\alpha}, \alpha'} + \frac{4}{v_i^2} & \text{for Neumann boundary conditions,} \\ \delta_{\hat{\alpha}, \alpha'} & \text{for Dirichlet boundary conditions.} \end{cases} \tag{55}$$

In the DFT case a particle on a directed bond $\alpha \in S_-^{(i)}$ is scattered with equal probability to all outgoing bond $\alpha' \in S_+^{(i)}$. In contrast, for Neumann boundary conditions at a vertex of high valency $v_i > 4$ backscattering $\alpha' = \hat{\alpha}$ is strongly favoured. One may thus expect that the classical decay of correlations is much faster

in a graph with DFT vertex scattering matrices compared to a Neumann graph. The transition probability for the Dirichlet case admits the following physical interpretation. The particle is confined to the bond where it started and thus the phase space is partitioned to non-overlapping components ('tori', since the dynamics on each bond is periodic). Thus, the Dirichlet boundary conditions correspond to an integrable classical analogue.

In general, a graph is *dynamically connected* if the directed bonds cannot be split into two non-empty subsets such that all transition probabilities to go from one set to the other vanish. Dynamical connectivity for quantum graphs may equivalently be defined via the scattering amplitudes $\sigma_{\alpha, \alpha'}^{(i)}$.

4.2. The classical evolution operator

The transition probabilities $P_{\alpha' \leftarrow \alpha}^{(i)}$ can be combined into a $2B \times 2B$ matrix in the same way that the vertex scattering matrices have been used to construct the graph scattering matrix. This defines the *classical evolution operator* (also called *Frobenius–Perron operator*)

$$\mathcal{M}_{\alpha', \alpha} = |S_{\alpha', \alpha}|^2 = |\mathcal{U}_{B\alpha', \alpha}(k)|^2 = \begin{cases} |\sigma_{\alpha', \alpha}^{(i)}|^2 & \text{if } \alpha' \in \mathcal{F}_i\alpha, \\ 0 & \text{else.} \end{cases} \quad (56)$$

\mathcal{M} does not involve any metric information on the graph, and for Dirichlet or Neumann boundary conditions it is independent of k . The evolution is a discrete Markov process with transition probabilities $\mathcal{M}_{\alpha', \alpha}$. The unitarity of the quantum evolution map $\mathcal{U}_B(k)$ guarantees that \mathcal{M} is a *bistochastic matrix* (also known as *doubly stochastic matrix*) which means

$$\sum_{\alpha} \mathcal{M}_{\alpha', \alpha} = \sum_{\alpha'} \mathcal{M}_{\alpha', \alpha} = 1 \quad \text{and} \quad 0 \leq \mathcal{M}_{\alpha', \alpha} \leq 1. \quad (57)$$

Bistochastic matrices that are defined by a unitary matrix in the form (56) are also called *unistochastic* matrices.† These properties of the classical evolution map are equivalent to the conditions (52) and (54) which ensure probability conservation.

If $\rho_{\alpha}(n) \geq 0$ denotes the probability to occupy the directed bond α at the (topological) time n , then we can write down a Markovian Master equation for the classical density:

$$\rho(n+1) = \mathcal{M}\rho(n), \quad (58)$$

with the $2B$ -dimensional vector $\rho = (\rho_1, \dots, \rho_{2B})$. The total probability to be anywhere on the graph is unity thus

$$\|\rho\| \equiv \sum_{\alpha} \rho_{\alpha} = 1. \quad (59)$$

†In general unistochastic matrices are a subset of bistochastic matrices. A unistochastic matrix defines a Markov process which, can be quantized (though not uniquely) [169–171].

From the bistochastic property of \mathcal{M} follows that the uniformly distributed density on the directed bonds

$$\rho_\alpha^{\text{inv}} = \frac{1}{2B} \tag{60}$$

is invariant under the classical evolution

$$\rho^{\text{inv}} = \mathcal{M}\rho^{\text{inv}}. \tag{61}$$

In most cases there exists only one invariant probability distribution. It then follows that the Markov process is *ergodic* which means that the time average of any *classical observable* $f \in \mathbb{R}^{2B}$ (that is, f_α is the value of the observable on the directed bond α) is equal to an average over the invariant uniform probability distribution

$$\lim_{N \rightarrow \infty} \frac{1}{N+1} \sum_{n=0}^N f \cdot \mathcal{M}^n \rho(0) = f \cdot \rho^{\text{inv}} \equiv \sum_{\alpha} \frac{f_\alpha}{2B} \tag{62}$$

for every initial distribution $\rho(0)$. This is equivalent to the statement that the time averaged occupation probability on a directed bond α is uniformly distributed over α

$$\lim_{N \rightarrow \infty} \frac{1}{N+1} \sum_{n=0}^N \rho_\alpha(n) = \frac{1}{2B}. \tag{63}$$

This is not a very strong statement on the classical dynamics of a graph. It is known that the classical dynamics for every dynamically connected graph is ergodic [168]. A Markov process may have the stronger dynamical property of being *mixing* which is defined by

$$\lim_{n \rightarrow \infty} \mathcal{M}^n \rho(0) = \rho^{\text{inv}} \tag{64}$$

for any initial probability distribution $\rho(0)$.

The properties of the graph which determine whether it is ergodic or mixing are encoded in the classical spectrum v_ℓ , $\ell = 1, \dots, 2B$ which is defined by

$$\mathcal{M}\chi_\ell = v_\ell \chi_\ell. \tag{65}$$

The classical spectrum is restricted to the interior of the unit circle $|v_\ell| \leq 1$ and $v_1 = 1$ corresponds to the uniform distribution $\chi_1 = \rho^{\text{inv}}$. Any probability distribution can be written in the form

$$\rho = \sum_{\ell=1}^{2B} a_\ell \chi_\ell \tag{66}$$

and $a_1 = 1$. For $v_\ell \neq 1$ one has $\|\chi_\ell\| = \sum_{\alpha} \chi_{\alpha,\ell} = 0$ due to the probability conservation of the dynamics.

Ergodicity implies that $v_1 = 1$ is the only unit eigenvector. Thus, there is a *spectral gap*

$$\Delta_g = \min_{\ell=2, \dots, 2B} |1 - v_\ell| \equiv \frac{1}{n^{\text{erg}}} \tag{67}$$

which determines the time-scale n^{erg} on which the left-hand side of (63) decays to the uniform distribution. Thus, ergodicity allows for eigenvalues on the unit circle $\nu_\ell = e^{i\theta}$ which are damped by the time average. In practice, such eigenvalues are non-generic – however there are some examples, such as star graphs which have an eigenvalue $\nu = -1$.[†]

If there is no eigenvalue on the unit circle apart from $\nu_1 = 1$ all non-uniform modes of the probability distribution decay

$$\mathcal{M}^n \rho(0) = \rho^{\text{inv}} + \sum_{\ell=2}^{2B} \nu_\ell^n a_\ell \chi_\ell \xrightarrow{n \rightarrow \infty} \rho^{\text{inv}} \quad (68)$$

and the dynamics is mixing. The rate at which equilibrium is approached is determined by the gap

$$\tilde{\Delta}_g = \min_{\ell=2, \dots, 2B} 1 - |\nu_\ell| \equiv \frac{1}{n^{\text{mix}}} \quad (69)$$

between the next largest eigenvalue and 1. In general ergodic sets in faster than mixing $n^{\text{erg}} < n^{\text{mix}}$.

We shall end this section by showing how the trajectories which we defined formally in section 1.1 acquire a dynamical significance, and emerge naturally in the classical framework developed above.

The classical probability to make a transition from a directed bond α to a directed bond β after n steps equals

$$(\mathcal{M}^n)_{\beta, \alpha} = \sum_{t \in \mathcal{T}_n(\beta, \alpha)} V_{\beta, \alpha}(t) \quad (70)$$

where the sum extends over the set $\mathcal{T}_n(\beta, \alpha)$ of trajectories which start at α and get to β in n steps, and

$$V_{\beta, \alpha}(t) = \prod_{s=1}^{n-1} \mathcal{M}_{\alpha_{s+1}, \alpha_s} \quad (71)$$

are the classical *weights* or probabilities contributed by the trajectory t to the transition probability. This form of the transition probability emphasizes the similarity between the classical dynamics on a graph and the evolution under Hamiltonian maps.

One of the characteristic features of chaotic (mixing) classical dynamics is the exponential proliferation of the number of classical trajectories which connect the same initial and final points as the transition time increases. This property is also shared by the trajectories on the graphs. This follows immediately from the fact that we have a natural code – the sequence of directed bonds – which associates a string of

[†]Star graphs are an example of *bipartite* graphs for which the directed bonds can be split into two non-empty sets and the transition probabilities within each of the two sets vanish. For star graphs due to its topology there is no transition from any outgoing (incoming) bond to another outgoing (incoming) bond. One may easily construct other examples which rely on the dynamical connectivity as well. Dynamically connected star graphs are generally mixing if the classical dynamics is defined on bonds instead of directed bonds as in sections 8 and 9.

numbers with a trajectory $t = (\alpha_1, \dots, \alpha_n)$ (by numbering the directed bonds from 1 to $2B$), and a connectivity matrix which established a Markovian grammar on the codes. In the language used in the theory of dynamical systems this is a Bernoulli code, which in Hamiltonian systems guarantees chaotic dynamics (see [172, 173] for more details). On a simple graph, the sequence of vertices is often used to define an alternative (equivalent) Bernoulli code.

4.3 The return probability and a classical sum rule

Of prime importance in the discussion of the relation between the classical and the quantum dynamics are the traces

$$u_n = \text{tr } \mathcal{M}^n = \sum_{\alpha=1}^{2B} (\mathcal{M}^n)_{\alpha, \alpha}. \quad (72)$$

This is the **return probability** – the classical probability to perform n -periodic motion. The mean probability to return is $u_n/2B$. For mixing dynamics where only one eigenvalue ν is on the unit circle, one has

$$u_n = \sum_{\ell=1}^{2B} \nu_{\ell}^n \xrightarrow{n \rightarrow \infty} 1. \quad (73)$$

Following the discussion at the end of the previous section, u_n can also be written as a classical sum over closed trajectories of length n . The classical weight of a closed trajectory t_c with a code $(\alpha_1, \dots, \alpha_n, \alpha_1)$ is the product

$$V_{t_c} = \prod_{s=1}^n \mathcal{M}_{\alpha_{s+1}, \alpha_s}, \quad (74)$$

where $\alpha_{n+1} \equiv \alpha_1$. The weight can be interpreted as the probability to remain on the trajectory. Any cyclic permutation of the bond indices in the code of a closed trajectory is also a closed trajectory with identical classical weight. Hence, instead of summing over closed trajectories, we may express the return probability as a sum over *periodic orbits*. A code of an n -periodic orbit can be written as a repetition of primitive codes whose lengths n_p divides n . The set of all the primitive orbits which build n periodic orbits will be denoted by $\mathcal{P}(n)$. Denote the weight of a primitive orbit p by W_p . Then, each primitive orbit contributes to the return probability a term which consists of its weight taken to its r power, multiplied by $n_p = n/r$,

$$u_n = \sum_{p \in \mathcal{P}(n)} n_p (W_p)^r \quad (75)$$

This is a basic formula in all our subsequent discussion and it deserves a few comments.

The weights W_p can also be defined for codes which violate the dynamical connectivity, by assigning them the value $W_p = 0$. Sums over periodic orbits that involve the weight as a factor can immediately be replaced by sums over all arbitrary cyclic codes for this reason.

The code gives rise to a variety of classifications of periodic orbits. For instance, a periodic orbit is either **reducible** or **irreducible**. An irreducible periodic orbit visits

each directed bond at most once. All directed bonds appearing in its code are different $\alpha_i \neq \alpha_j$. The maximal period of an irreducible periodic orbit is $n_{\max} = 2B$. All other periodic orbits are reducible, that is at least one directed bond is visited more than once. All periodic orbits of period larger $2B$ are reducible.† Reducible orbits have the remarkable property that their weights can be written as products of weight of shorter orbits $W_p = W_{p_1} W_{p_2}$.

We are now equipped with the background to obtain a classical sum-rule for mixing dynamics by substituting a periodic-orbit expansion of u_n . Combining (73) and (75) we get‡

$$u_n = \sum_{p \in \mathcal{P}(n)} n_p (W_p)^r \xrightarrow{n \rightarrow \infty} 1. \tag{77}$$

This sum rule is analogous to the *Sinai–Bowen–Ruelle* [174–176] sum rule for classically chaotic dynamics (in the physics literature also known as the Hannay–Ozorio de Almeida sum rule [177]). The weights W_p are the counterparts of the stability weights $|\det(I - M_p)|^{-1}$ for hyperbolic periodic orbits in Hamiltonian systems, where M_p is the monodromy matrix. Graphs, however, are one dimensional and the motion on the bonds is simple and stable. Ergodic or mixing dynamics is generated, because at each vertex a (Markovian) choice of one out of v directions is made. Thus, chaos on graphs originates from the multiple connectivity of the (otherwise linear) system.

Using the expression (77) for u_n one can easily write down the complete thermodynamic formalism for the graph. Here, we shall only quote the periodic orbit expression for the Ruelle ζ -function

$$\begin{aligned} \zeta_R(z) &\equiv \det(1 - z\mathcal{M})^{-1} = e^{-\text{tr} \ln(1 - z\mathcal{M})} = e^{\sum_n (z^n/n) u_n} \\ &= \prod_p \frac{1}{(1 - z^{n_p} \exp(-n_p \gamma_p))} \end{aligned} \tag{78}$$

†The definition of reducible and irreducible periodic orbits depends on the code which is used to define a periodic orbit unambiguously. For a simple graph one may use the the sequence of vertices $p = \overline{i_1 i_2 \dots i_n}$ as a code (symbolic dynamics) which uniquely defines a periodic orbit. In the directed bond code the same orbit is given by $p = \overline{[i_2, i_1], [i_3, i_2], \dots, [i_1, i_n]}$. Irreducible periodic orbits with respect to the vertex code (*vertex-irreducible periodic orbits*), do not intersect at any vertex such that all i_j are different. Our definition which is based on the directed bond code is *not equivalent* to the one based on the vertex code. In general, there are bond-irreducible orbits of period $n > V$ and the latter cannot be vertex-irreducible. Both codes have their advantages and disadvantages. The vertex code has the advantage of a smaller number of symbols and a grammar which is readily encoded in the connectivity matrix. In the present context the grammar is less relevant since a code which does not correspond to a periodic orbit has zero weight. The advantage of using the bond code to define reducible orbits, is that weights of reducible orbits are products of weights of non-irreducible orbits.

‡In the non-mixing case a dynamically connected graph is ergodic. With an additional time average over an interval $\Delta n \ll n$ one then gets the sum rule

$$\frac{1}{\Delta n} \sum_{n'=n}^{n+\Delta n-1} u_{n'} = \frac{1}{\Delta n} \sum_{p: n \leq r_p n_p < n+\Delta n} n_p W_p^{r_p} \xrightarrow{n, \Delta n \rightarrow \infty} 1. \tag{76}$$

where the product extends over all primitive periodic orbits p and we have set $W_p = e^{-n_p \gamma_p}$. The Ruelle ζ -function is an important tool to analyse dynamical systems [172, 173].

5. Spectral theory for quantum graphs

Trace formulae are an important tool in spectral theory. They express spectral sums in terms of sums over periodic orbits of the underlying classical dynamics. In this section our main goal is to introduce the trace formula for the density of states of a quantum graph. The first trace formula for a quantum graph was derived by Roth [40, 41] who showed that a spectral determinant (which can be interpreted as a variant of the secular function $\zeta_B(k)$) can be written as a sum over periodic orbits. The trace formula for the density of states goes back to Kottos and Smilansky [116, 117] and is formulated in analogy to the semiclassical Gutzwiller trace formula [118, 119] for chaotic (hyperbolic) Hamiltonian quantum systems. In contrast to the latter, the trace formula for quantum graphs is exact. Apart from the density of states we will also discuss how other spectral functions are related to sums over periodic orbits.

The starting point for the derivation is the secular function $\zeta_B(k)$ which is expressed in terms of the quantum evolution map $\mathcal{U}_B(k)$ (see section 3). Thus, the boundary conditions at the vertices are defined by a given set of vertex scattering matrices and the wavefunctions are not necessarily continuous across a vertex. Without loss of generality we will restrict the discussion to dynamically connected quantum graphs of simple topology. If the graph is not dynamically connected (e.g. a graph with Dirichlet boundary conditions) the graph can be divided into subgraphs which have independent spectra and wavefunctions – that is, the complete spectrum is the superposition of the independent spectra. For simplicity, we will also assume throughout this section that the vertex scattering matrices do not depend on the wavenumber k (the generalization to k dependent scattering matrices follows in a straightforward way).

5.1. The density of states and the counting function

If $\{k_n\}$ ($n \in \mathbb{N}$) is the spectrum of a quantum graph (degenerate eigenvalues appear according to their multiplicity) we define the *density of states* as

$$d(k) = \sum_{n=1}^{\infty} \delta(k - k_n). \quad (79)$$

The *spectral counting function* which provides the number of eigenvalues k_n which are smaller than k is given by the integral

$$N(k) = \theta(k)N_0 + \lim_{\delta \rightarrow 0^+} \int_{\delta}^k dk' d(k') = \sum_{n=1}^{\infty} \theta(k - k_n), \quad (80)$$

where N_0 is the number of eigenvalues at $k=0$ and

$$\theta(k) = \begin{cases} 0 & \text{for } k < 0 \\ 1/2 & \text{for } k = 0 \\ 1 & \text{for } k > 0 \end{cases} \quad (81)$$

is the Heaviside step function. The limit $\delta \rightarrow 0^+$ is needed only when $N(k)$ is computed at $k \rightarrow 0$, and it ensures that $\lim_{k \rightarrow 0} N(k) = N_0$. When the secular function $\zeta_B(k)$ does not have a zero at $k=0$ and $N_0=0$ one can set $\delta=0$ from the start in the following discussion.

We will now express the counting functions $N(k)$ in terms of the secular function $\zeta_B(k) = \det(\mathbb{1} - \mathcal{U}_B(k))$. To this end, we introduce the eigenvalues $\{e^{i\phi_\ell(k)}\}$ ($\ell = 1, 2, \dots, 2B$) of the quantum evolution map $\mathcal{U}_B(k)$ at fixed wavenumber k and first discuss some of their properties. The phases $\phi_\ell(k)$ are important in the present context since the quantization condition $\zeta_B(k) = 0$ is equivalent to the requirement

$$\phi_\ell(k) = 2\pi z \quad \text{with } z = 0, 1, 2, \dots \quad (82)$$

for one of the $\phi_\ell(k)$. Each of the quantization conditions (82) yields a discrete subset $\{k_n^{(\ell)}\} \subset \{k_n\}$ of the complete spectrum and this subset is free of degeneracies since $d\phi_\ell/dk > 0$. Indeed, a direct computation reveals that

$$\frac{d\phi_\ell}{dk} = \sum_{b=1}^B L_b \left(|a_{(b,\omega)}^{(\ell)}(k)|^2 + |a_{(b,-\omega)}^{(\ell)}(k)|^2 \right) > 0, \quad (83)$$

where $a_{(b,\omega)}^{(\ell)}$ are the components of the ℓ eigenvector. This proof of the monotonic increase of the eigenphases depends crucially on the assumption that the vertex scattering matrices are independent of k . It follows immediately that the maximal degeneracy in a quantum graph is $2B$. Direct inspection shows $L_{\min} \leq d\phi_\ell/dk \leq L_{\max}$ where L_{\min} (L_{\max}) is the smallest (largest) bond length, and $\sum_{\ell=1}^{2B} d\phi_\ell/dk = 2B\bar{L}$ where $\bar{L} = \frac{1}{B} \sum_{b=1}^B L_b$ is the mean bond length. For Neumann graphs with rationally independent bond lengths a much stronger statement has been proven: their spectra are generically devoid of degeneracies [178].

We also note that $\mathcal{U}_B(k+i\epsilon)$ is *subunitarity* for any finite $\epsilon > 0$. That is, $|e^{i\phi_\ell(k+i\epsilon)}| < 1$. This is an immediate consequence of the obvious subunitarity of the bond propagator $T(k+i\epsilon)$.

A counting function for the subspectrum $\{k_n^{(\ell)}\}$ is obtained through the correspondence to the zeros of the real function $\sin(\phi_\ell(k)/2)$. A sum over step functions at the (strictly positive part of the) subspectrum can thus be written as

$$\sum_n \theta(k - k_n^{(\ell)}) = -\frac{1}{\pi} \operatorname{Im} \left(\ln \sin \frac{\phi_\ell(k+i\epsilon)}{2} - \ln \sin \frac{\phi_\ell(\delta)}{2} \right) \quad (84)$$

where the limit $\epsilon \rightarrow 0^+$ is always implied. The ϵ -shift ensures that the complex number $\sin(\phi_n(k+i\epsilon)/2)$ rotates counterclockwise around the origin of the complex plane. The term $\ln \sin(\phi_n(\delta)/2)$ ensures that one starts to count at zero and ϵ has been set to zero to indicate that the limit $\epsilon \rightarrow 0^+$ has to be performed before the limit $\delta \rightarrow 0^+$.

The full counting function is obtained by summing over all $2B$ subspectra. Using $\sin(\phi_\epsilon(k)/2) = \frac{1}{2}e^{(-i\phi_\epsilon(k)/2)}(1 - e^{(i\phi_\epsilon(k)/2)})$ we get,

$$\begin{aligned} N(k) &= N_0 + \frac{1}{2\pi} \operatorname{Im} \ln \det \frac{\mathcal{U}_B(k + i\epsilon)}{\mathcal{U}_B(\delta)} - \frac{1}{\pi} \operatorname{Im} \ln \frac{\zeta_B(k + i\epsilon)}{\zeta_B(\delta)} \\ &= N_0 + \frac{B\bar{L}}{\pi} k + \frac{1}{\pi} \operatorname{Im} \ln \zeta_B(\delta) - \frac{1}{\pi} \operatorname{Im} \ln \zeta_B(k + i\epsilon). \end{aligned} \tag{85}$$

We have used the assumption that the vertex scattering matrices do not depend on k in the second line.

The counting function can be decomposed into a smooth term (the so-called **Weyl term**) and an oscillatory term

$$N(k) = N^{\text{Weyl}}(k) + N^{\text{osc}}(k). \tag{86}$$

The smooth term is given by

$$N^{\text{Weyl}}(k) = \frac{B\bar{L}}{\pi} k + N^{\text{Weyl}}(0) \tag{87}$$

where the first term $B\bar{L}/\pi k$ describes the linear increase of the counting function and

$$N^{\text{Weyl}}(0) = N_0 + \frac{1}{\pi} \operatorname{Im} \ln \zeta_B(\delta). \tag{88}$$

is a constant that depends on the boundary conditions at the vertices. This constant ensures that the complete counting reduces to N_0 at $k = \delta$. When one wants to calculate $N^{\text{Weyl}}(0)$ from (88) one should be aware that the logarithm is a multivalued function and it is not always obvious which is the correct sheet. The correct sheet can be identified by the condition $1/K \int_0^K dk (N^{\text{Weyl}}(k) - N(k)) \rightarrow 0$ which just means that the difference is oscillating around zero with a bounded amplitude. For general $\mathcal{U}_B(0)$ the shift $N^{\text{Weyl}}(0)$ can take real values. In many cases (e.g. for Neumann boundary conditions) $\mathcal{U}_B(0) = S$ is a real unitary matrix. Then, $N^{\text{Weyl}}(0)$ is some half-integer number. This can be calculated directly by observing that all eigenvalues of S with non-vanishing imaginary part appear in complex conjugated pairs such that their contributions cancel each other. Real eigenvalues take the values ± 1 . -1 does not contribute since the imaginary part of $\ln 1 - (-e^{i\delta})$ vanishes for $\delta \rightarrow 0$. Only eigenvalues $+1$ contribute $(1/\pi) \operatorname{Im} (\ln 1 - e^{i\delta}) \sim (1/\pi) \operatorname{Im} \ln e^{-i\pi/2} \delta = -1/2$ and $N^{\text{Weyl}}(0) = N_0 - z/2$ where z is the number of unit eigenvalues.

The linear dependence of $N^{\text{Weyl}}(k)$ on k is a consequence of the fact that the graph is a one-dimensional object. The fact that it is not simply connected appears only in the oscillatory part of the counting function – the second term in (86)

$$N^{\text{osc}}(k) = -\frac{1}{\pi} \operatorname{Im} \ln \zeta_B(k + i\epsilon). \tag{89}$$

The oscillations are bounded by the number of bonds $|N^{\text{osc}}(k + i\epsilon)| \leq B$. Equation (89) will be the starting point for our derivation of the trace formula in section 5.2.

It is now straightforward to derive the density of states by differentiation with respect to k as a sum

$$d(k) = d^{\text{Weyl}}(k) + d^{\text{osc}}(k) \quad (90)$$

of a smooth Weyl term

$$d^{\text{Weyl}}(k) = \frac{B\bar{L}}{\pi} \quad (91)$$

and an oscillatory part

$$d^{\text{osc}}(k) = -\frac{1}{\pi} \frac{d}{dk} \text{Im} \ln \zeta_B(k + i\epsilon). \quad (92)$$

5.1.1. The spectrum of the quantum evolution map. The $2B$ eigenvalues $e^{i\phi_\ell(k)}$ of the quantum evolution map $\mathcal{U}_B(k)$ at fixed k can also be used to define a density and a corresponding counting function which will turn out to be interesting objects in their own right. We define the *density of eigenphases* as

$$\tilde{d}(\phi; k) = \sum_{\ell=1}^{2B} \delta_{2\pi}(\phi - \phi_\ell(k)) \quad (93)$$

and the *eigenphase counting function* as

$$\tilde{N}(\phi; k) = \tilde{N}_0 \theta(\phi) + \int_{\delta}^{\phi} d\phi' \tilde{d}(\phi'; k) = \sum_{n=1}^N \sum_{\nu=0}^{\infty} \theta(\phi - \phi_n(k) + 2\pi\nu). \quad (94)$$

In (93) $\delta_{2\pi}(\phi) = \sum_{\nu=-\infty}^{\infty} \delta(\phi + 2\pi\nu)$ denotes the 2π -periodic δ -function.

In complete analogy to the derivation for the spectral counting function above one may write

$$\tilde{N}(\phi; k) = \tilde{N}^{\text{Weyl}}(\phi; k) + \tilde{N}^{\text{osc}}(\phi; k) \quad (95)$$

and express the smooth and oscillatory parts in terms of the ϕ -dependent secular function

$$\zeta_B(\phi; k) = \det(\mathbb{1} - e^{-i\phi} \mathcal{U}_B(k)). \quad (96)$$

As a result one obtains

$$\tilde{N}^{\text{Weyl}}(\phi; k) = \frac{B}{\pi} \phi + \tilde{N}_0 - \frac{1}{\pi} \text{Im} \ln \zeta_B(\delta, k) \quad (97)$$

for the smooth part, and

$$\tilde{N}^{\text{osc}}(\phi; k) = \frac{1}{\pi} \text{Im} \ln \zeta_B(\phi - i\epsilon, k) \quad (98)$$

for the oscillating part. These expressions for the eigenphase counting function can alternatively be derived using Poisson's formula. Note that the second term of the Weyl part $-\frac{1}{\pi} \text{Im} \ln \zeta_B(\delta, k)$ is independent of ϕ , however, as a function of k it can oscillate with a maximal amplitude of B .

The smooth Weyl part of the density of eigenphases

$$\tilde{d}^{\text{Weyl}}(\phi; k) = \frac{B}{\pi} \quad (99)$$

is consistent with having $2B$ eigenvalues distributed in an interval of length 2π . Finally, the oscillating part of the density of eigenphases is given by

$$\tilde{d}^{\text{osc}}(\phi; k) = \frac{1}{\pi} \frac{d}{d\phi} \text{Im} \ln \zeta_B(\phi - i\epsilon, k). \tag{100}$$

5.2. Periodic orbits and the trace formula

We will now consider the oscillating parts of the spectral functions $N(k)$ and $d(k)$ from a periodic-orbit perspective. One of the reasons for the interest in quantum graphs in the quantum chaos community is the analogy of an exact trace formula for quantum graphs to Gutzwiller’s semiclassical trace formula for the density of states of chaotic Hamiltonian systems. While there is no underlying *deterministic* classical dynamics for graphs they still display the generic behaviour of chaotic Hamiltonian systems. At the same time they are less resistant to either rigorous or numerical approaches.

The logarithm of the secular equation appearing in (89) can directly be written in terms of traces of powers of the quantum evolution map

$$\ln \det(1 - \mathcal{U}_B(k)) = \text{tr} \ln(1 - \mathcal{U}_B(k)) = - \sum_{n=1}^{\infty} \frac{1}{n} \text{tr} \mathcal{U}_B^n(k). \tag{101}$$

We can now follow the path we used in section 4.3 to compute the classical return probability $u_n = \text{tr} \mathcal{M}^n$ in terms of periodic orbits. The result is again a sum over primitive periodic orbits [117]

$$\begin{aligned} N^{\text{osc}}(k) &= \frac{1}{\pi} \text{Im} \sum_{n=1}^{\infty} \frac{1}{n} \text{tr} \mathcal{U}_B^n(k + i\epsilon) \\ &= \text{Im} \sum_p \sum_{r=1}^{\infty} \frac{1}{\pi r} \mathcal{A}_p^r e^{irL_p(k+i\epsilon)+ir\Phi_p} \\ &= \sum_p \sum_{r=1}^{\infty} \frac{1}{\pi r} |\mathcal{A}_p|^r \sin r(L_p k + \Phi_p + \mu_p) e^{-L_p \epsilon}. \end{aligned} \tag{102}$$

In the second line we have introduced the sum over all primitive periodic orbits p of the graph and their repetitions r . Here, $L_p \equiv \sum_{l=1}^{n_p} L_{b_l}$ is the length of the primitive periodic orbit $p = \overline{\alpha_1, \dots, \alpha_{n_p}}$,

$$\mathcal{A}_p = |\mathcal{A}_p| e^{i\sigma_p} \equiv S_{\alpha_1 \alpha_{n_p}} S_{\alpha_{n_p} \alpha_{n_p-1}} \dots S_{\alpha_2 \alpha_1} \tag{103}$$

is the quantum amplitude of the primitive orbit defined as the product of all scattering amplitudes along the orbit, and

$$\Phi_{\hat{p}} = \sum_{l=1}^{n_{\hat{p}}} A_{\alpha_l} = \sum_{l=1}^{n_{\hat{p}}} \omega_l A_{b_l} \tag{104}$$

is the overall magnetic flux through the periodic orbit. The step from the first line of (102) to the second is performed by collecting all contributions to the n -th trace that stem from the same primitive periodic orbit such that $n = rn_p$. After a

resummation over the repetitions r in the second line of (102) the oscillatory part of the counting function can be expressed as

$$N^{\text{osc}}(k) = \text{Im} \frac{1}{\pi} \sum_p \ln \left(1 - \mathcal{A}_p e^{iL_p(k+i\epsilon)+i\Phi_p} \right). \tag{105}$$

It should be noted that these period-orbit sums are not absolutely convergent due to the exponential proliferation of periodic orbits. That is, the number of periodic orbits of period n grows exponentially in n . Absolute convergence is only obtained for complex k beyond an entropy barrier $\text{Im} k > \epsilon_{\text{crit}}$. For real k the limit $\epsilon \rightarrow 0$ implies that the infinite sum over periodic orbits is ordered with respect to the length rL_p of the periodic orbit.

The derivative of (102) with respect to k leads to the, equally exact, trace formula

$$\begin{aligned} d^{\text{osc}}(k) &= \text{Re} \sum_p \sum_{r=1}^{\infty} \frac{L_p}{\pi} \mathcal{A}_p^r e^{irL_p(k+i\epsilon)+ir\Phi_p} \\ &= \sum_p \sum_{r=1}^{\infty} \frac{L_p}{\pi} |\mathcal{A}_p|^r \cos r(L_p k + \Phi_p + \sigma_p) e^{-L_p \epsilon} \\ &= \text{Re} \sum_p \frac{L_p}{\pi} \frac{\mathcal{A}_p e^{iL_p(k+i\epsilon)+i\Phi_p}}{1 - \mathcal{A}_p e^{iL_p(k+i\epsilon)+i\Phi_p}} \end{aligned} \tag{106}$$

for the oscillatory part of the density of states. Instead of the sum over primitive periodic orbits and its repetitions, one may combine the two sums in a single sum over *all* periodic orbits $d^{\text{osc}}(k) = \text{Re} \sum_p (L_p \mathcal{A}_p / \pi r_p) e^{iL_p k}$. In that case \mathcal{A}_p is the amplitude of the full orbit, and L_p its full length while the primitive length is L_p / r_p where r_p is the repetition number of the periodic orbit. Note that the classical probability to stay on a periodic orbit (74) is just the absolute square of the quantum amplitude

$$W_p = |\mathcal{A}_p|^2. \tag{107}$$

Comparing the trace formula (106) to the Gutzwiller trace formula reveals a complete analogy.

5.2.1. Trace formulae for the eigenphase spectrum. The oscillatory parts of the spectral functions $\tilde{N}(\phi; k)$ and $d(\phi; k)$ for the eigenphase spectrum of quantum evolution map at fixed wavenumber k can be written in terms of primitive periodic orbits in an analogous way. This leads to the trace formulae

$$\tilde{N}^{\text{osc}}(\phi; k) = -\text{Im} \sum_p \sum_{r=1}^{\infty} \frac{1}{\pi r} \mathcal{A}_p^r e^{ir(L_p k + \Phi_p - r n_p(\phi - i\epsilon))} \tag{108}$$

and

$$\tilde{d}^{\text{osc}}(\phi; k) = \text{Re} \sum_p \sum_{r=1}^{\infty} \frac{n_p}{\pi} \mathcal{A}_p^r e^{ir(L_p k + \Phi_p - n_p(\phi - i\epsilon))}. \tag{109}$$

5.3. The length spectrum and the quantum-to-classical duality

The trace formula (106) for the density of states may be written in the form

$$d(k) = \text{Re} \int_{-\delta}^{\infty} dL \mathcal{A}(L) e^{ikL} \quad (110)$$

where $\delta \rightarrow 0$ will always be implied, and

$$\mathcal{A}(L) = \frac{B\bar{L}}{\pi} \delta(L) + \frac{1}{\pi} \sum_p \sum_{r=1}^{\infty} L_p A_p^r e^{ir\Phi_p} \delta(L - rL_p) \quad (111)$$

is a sum over primitive periodic orbits and their repetitions plus a zero length contribution (related to the Weyl term) that is proportional to the length $B\bar{L}$ of the graph. The complex function $\mathcal{A}(L)$ is a weighted sum over δ -functions located at the length spectrum $\{L_p\}$ (and their repetitions). This reveals a quantum-to-classical duality between the length spectrum $\{L_p\}$ and the spectrum $\{k_n\}$ of the quantum graph. The relation may also be inverted

$$\mathcal{A}(L) = \frac{1}{\pi} \int_{-\delta}^{\infty} dk d(k) e^{-ikL} = \frac{1}{\pi} \sum_{k_n} e^{-ik_n L}. \quad (112)$$

The length spectrum is highly degenerate. This follows from the fact that the length of any periodic orbit of period n is an integer combination of the bond lengths

$$L_p = \sum_{b=1}^B q_b L_b \quad q_b = 0, 1, 2, \dots, \quad (113)$$

with $\sum_{b=1}^B q_b = B$. Periodic orbits with the same length differ only in the order by which the bonds are traversed. Note that not every combination of integers q_b is consistent with the connectivity of the graph. The degeneracy class will be denoted by the vector \mathbf{q} where $\mathbf{q} = (q_1, \dots, q_B)$. For star graphs the degeneracies are maximal, only even q_b are allowed by the connectivity without any further restriction.

The presence of the exact ‘quantum-to-classical’ duality imprinted by the relation between the **length spectrum** $\{L_p\}$ and the quantum spectrum $\{k_n\}$ has been used efficiently in the context of isospectrality. In a variant of Kac’ famous question ‘Can one hear the shape of a drum?’ [179] one may ask the question if there are topologically or metrically different quantum graphs which have the same spectrum $\{k_n\}$ [93]. Such graphs are called **isospectral**. Kac’ question can be reformulated as ‘Can one hear the shape of a graph?’. Exploiting the quantum-to-classical duality an affirmative answer has been proven in [97] if the class of graphs is restricted to simple topologies and rationally independent bond lengths. In contrast, if the restriction of rationally independent bond lengths is dropped, a lot of examples of isospectral graphs are known today. Still, isospectrality is not understood in sufficient detail. Recently, it has been asked [180] how one may resolve isospectrality for quantum graphs by adding non-trivial additional information such as nodal counting [146].

5.4 The secular function is a ζ -function

Let us set $t_p = \mathcal{A}_p e^{ikL_p}$ for a primitive orbit p . For a fixed primitive orbit p the sum over repetitions r in the trace formula for the counting function (103) can easily be performed $\sum_{r=1}^{\infty} t_p^r / r = -\ln(1 - t_p)$. Summing over all primitive periodic orbits and comparing to (102) then leads to the exact expression

$$\zeta_B(k + i\epsilon) = \prod_p (1 - t_p) \quad (114)$$

for the secular function, a truly remarkable identity. The expression on the left-hand side is defined as the determinant of $\mathbb{1} - \mathcal{U}_{BB}(k)$. As such, when expanded in periodic orbits it has contributions from irreducible periodic orbits only [181]. A superficial look on the right-hand side could lead to the conclusion that it involves all possible multiples of periodic orbits and their repetitions. This apparent paradox is resolved by observing that there is an exact cancellation mechanism which is responsible for the identity of the left and right-hand sides. From this follows that a truncation of the infinite product or an approximation of any of the terms t_p leads to systematic errors and therefore has no practical advantage for graphs. This contrasts the situation in the analogous semiclassical trace formulae where shadowing of periodic orbits is the analogue of the exact cancellations mentioned above. Nevertheless, for pedagogical reasons mainly, we shall investigate (114) further.

The similarity to the Euler product formula for the Riemann ζ -function $\zeta_{\text{Riemann}}(s) = \prod_{\text{primes: } n} (1 - 1/(1 - n^s))$ justifies the letter ζ by which the secular function is denoted. The product over primitive periodic orbits in the secular function corresponds to a product over primes in the Riemann ζ -function. Like the periodic-orbit sum the infinite product on the right-hand side of (114) is absolutely converging only for complex k beyond the entropy barrier. For real k the product is defined by analytic continuation. Note that a complex k with positive imaginary part, orders the product by the length of the periodic orbit. Thus, this ordering is implied in the analytic continuation. Ordering the contributions by the period n instead of the length is essentially equivalent. Other non-equivalent orderings generally diverge, or worse: they converge to a wrong result (with false zeros [182]). Note that generally $|t_p| < 1$ for a periodic orbit (if we exclude the line, that is the trivial graphs with $B=1$). Thus, the zeros of the secular function which define the spectrum of the graph are *not equivalent* to zeros of the factors $1 - t_p(k)$ (which have zeros only for complex k with negative imaginary part). Instead the zeros of the secular equation for real k are due to the infinite product over primitive periodic orbits.

Let us now come back to the exact cancellations on the right-hand side of (114) which eventually reduce it to the finite polynomial on the left-hand side. One principle behind these cancellations which is known as **shadowing** may be understood from a closer look at the the expression t_p for reducible primitive orbits. Let p_a and p_b be two irreducible primitive orbits with codes $a = \overline{\alpha P_a}$ and $b = \overline{\alpha P_b}$ which have exactly one directed bond in common. Here, P_a and P_b are the codes for two paths that close the periodic orbits such that P_a and P_b never visit the same directed bond. For the reducible primitive periodic orbit p_{ab} with code $ab = \overline{\alpha P_a \alpha P_b}$ one gets the identity $t_{ab} = t_a t_b$ [181]. Longer reducible

primitive orbits may be obtained from p_a and p_b . With an obvious short-hand notation for the codes, aab and abb are the only possibilities to create reducible primitive orbits composed of three irreducible orbits (with four irreducible orbits one has $aaab$, $aabb$, and $abbb$; for five $aaaab$, $aaabb$, $aabab$, $aabbb$, $ababb$, and $abbbb$). Performing the product over the primitive orbits \hat{p} that are composed of p_a and p_b one gets

$$\begin{aligned} \prod_{\hat{p}} (1 - t_{\hat{p}}) &= (1 - t_a)(1 - t_b)(1 - t_{ab})(1 - t_{aab})(1 - t_{abb}) \dots \\ &= (1 - t_a - t_b + t_a t_b)(1 - t_a t_b)(1 - t_a^2 t_b)(1 - t_a t_b^2) \dots \\ &= (1 - t_a - t_b + t_a^2 t_b + t_a t_b^2 + t_a^2 t_b^2)(1 - t_a^2 t_b)(1 - t_a t_b^2) \dots \end{aligned} \quad (115)$$

In the third line all contributions of second order in t_a and t_b have cancelled. It is obvious at this stage that the third order terms will cancel after the next two factors have been multiplied. Eventually all higher order terms cancel and one gets the simple result $\prod_p (1 - t_p) = 1 - t_a - t_b$ which is a finite polynomial that only depends on reducible primitive orbits (and its zeros are not zeros of one factor $1 - t_p$).[†] If more irreducible orbits are taken into account a direct multiplication gets much more involved but the exact shadowing of reducible periodic orbits remains valid. Eventually, when all factors $1 - t_p$ are expanded and the shadowing principle is used to replace reducible orbits by products of irreducible orbits the final result only depends on the *finite* set of irreducible orbits and their amplitudes t_p . Note that all these orbits have a period smaller than (or equal to) the dimension $2B$ of the quantum map.[‡] A more systematic treatment of approximations to the secular function for calculating the spectrum from a finite set of primitive periodic orbits is obtained within the cycle (or curvature) expansion [172, 173]. The cycle expansion also holds for the Ruelle ζ -function $\zeta_R(z)$ (78) that describes the classical dynamics on the graph.

Cycle expansions are also used efficiently for semiclassical expansions of ζ -functions in Hamiltonian quantum systems [183]. As soon as semiclassical approximations are used the analytical properties of the ζ -function are destroyed. Also, replacing long orbits by products of short orbits (also called pseudo-orbits in this context) is a semiclassical approximation in these systems. For quantum graphs the expansion of the secular function into products of irreducible periodic orbits is exact due to the finite dimension of the quantum evolution map – that is, due to the discreteness of phase space.

[†]One may prove that each finite product over factors $1 - t_p$ equals $1 - t_a - t_b + R$ with $R = \mathcal{O}(t^n)$ if all contributions from periodic orbits that are composed of less than n irreducible periodic orbits appear in the finite product. It is a signature of the bad convergence of the infinite product that the modulus of the remainder $|R|$ for real k in generally does not go to zero in the limit of large n .

[‡]The final result can also be obtained with Newton's formulas which express the coefficients a_n of a secular determinant $\det(z - A) = \sum_{n=0}^N a_n z^n$ through the first N traces $\text{tr} A^n$ in a recursive way.

6. Spectral statistics

Any respectable statistical theory starts by specifying the space of variables over which the probability distribution (measure) is defined, and where the statistical tests and conclusions are drawn. Here we would like to study the spectrum of a single graph or of an ensemble of graphs, from a statistical point of view. To remain within the range of acceptable respectability we should at least state what is our space of variables. In other words, what are we averaging over to get a statistical (probabilistic) description? The statistical approach to the spectra of graphs can be developed at several levels. The conceptually simplest level is to consider the ensemble of all the graphs which share the same connectivity but whose bond lengths, and possibly also vertex scattering matrices are drawn randomly according to prescribed probability distribution functions. This approach is very similar to disorder averaging, common, for example, in the study of mesoscopic systems. The less obvious approach is the study of the spectral statistics of a *single* graph. Here, one can consider non-overlapping spectral domains and study the distribution of the spectral intervals within each of the domains, assigning to the domains equal probabilities. This approach, which is referred to as **spectral averaging**, makes sense only if one can prove that the probabilities converge to a well defined *limit distribution* as the spectral domains and their number increase.

6.1. Spectral averages

The spectral average over some interval $k_0 \leq k \leq k_0 + K$ of a spectral function $f(k)$ of a quantum graph is defined by

$$\langle f(k) \rangle_k = \frac{1}{K} \int_{k_0}^{k_0+K} dk f(k). \quad (116)$$

In the simplest case one chooses $f(k) = d(k)$ and calculates the mean density of states

$$\langle d(k) \rangle_k = d^{\text{Weyl}} + \frac{1}{K} (N^{\text{osc}}(k_0 + K) - N^{\text{osc}}(k_0)). \quad (117)$$

Since $|N^{\text{osc}}(k)| \leq B$ one may neglect the second term if $K \gg \pi/\bar{L}$. Thus, the spectral average of the density of states equals the Weyl term if the spectral interval is chosen larger than the inverse mean bond length (equivalently, when the number of states in that interval is large compared to the dimension of the quantum evolution map). In most cases we will take an infinite spectral interval $K \rightarrow \infty$ for averaging. For finite K the result explicitly depends on k_0 . For small $K < 1/d^{\text{Weyl}} \equiv \bar{\Delta}$ where $\bar{\Delta}$ is the **mean level spacing** the δ -peaks are broadened but generally do not overlap. More interesting is the regime $\bar{\Delta} \ll K < \pi/\bar{L}$ where pronounced oscillations modulate the Weyl term. Replacing the periodic orbit sum for N^{osc} one sees that the most pronounced of these oscillations $\sim e^{iL_p k_0}$ stem from the short periodic orbits with length L_p .

Some spectral averages remain very spiky functions even after the spectral averaging. A simple example for this is the correlator

$$\begin{aligned} \langle d(k)d(k+k') \rangle_k &= \left\langle \sum_{m,n} \delta(k-k_n)\delta(k'+k_n-k_m) \right\rangle_k \\ &= d^{\text{Weyl}}\delta(k') + \lim_{K \rightarrow \infty} \frac{1}{K} \sum_{\substack{k_n, k_m < K \\ n \neq m}} \delta(k'+k_n-k_m) \end{aligned} \quad (118)$$

where we have taken the average over the complete spectrum and assumed that there are no degeneracies. In the limit $K \rightarrow \infty$ the second part becomes an infinite sum over δ -functions with a weight $\sim 1/K$ which is often equivalent (in a distributional sense) to some well-behaved function. Both in numerical and in analytical approaches an additional average over a short interval in k' is usually needed to make a well-behaved function apparent. In chaotic systems the interesting features of such correlators occur on the scale of the mean level spacing $\overline{\Delta} = 1/d^{\text{Weyl}} = \pi/B\overline{L}$ and the additional average over k' has to be on a much shorter scale. Equivalently, one may replace the δ -functions by a Lorentzian or Gaussian function of width $\Delta k'$. The Lorentzian is natural when the trace formula is used. The addition of an imaginary part $i\epsilon$ to the wavenumber results in replacing the δ -functions in the density of states by Lorentzians of width ϵ .

In practical (numerical) calculations one can circumvent the difficulties encountered in direct application of equation (118) by dividing the spectrum of length K into M subsequent intervals. For each of the intervals one can use (118) replacing the δ -functions by Lorentzians or Gaussians of finite width. The average over all the intervals is a well-behaved numerical approximation. As a rule of thumb one should use $M \approx \sqrt{Kd^{\text{Weyl}}}$.

6.2. Disorder averages

In the study of spectral statistics averaging over an ensemble of systems, usually referred to as ‘disorder average’, is a useful theoretical tool which is naturally called for in many applications. Disorder averaging for graphs can be implemented in several ways. The most obvious one is to take a family of graphs with the same connectivity but with a random distribution of bond lengths. Other possible variables to average over are the vertex scattering matrices which can be picked at random from some well-defined ensemble. Both methods were used in past works and we illustrate this method in section 8.5. For graphs there is an intimate connection between disorder and spectral averages which will be explained in the next section.

6.3. Phase ergodicity for incommensurate graphs

All spectral functions $f(k)$ that we are going to consider depend on k via the B phase factors e^{ikL_b} in the bond propagator $T(k)$. They are thus quasiperiodic functions of k . Let us again assume that the bond lengths L_b are *incommensurate*. Under this condition the flow

$$k \mapsto \left\{ e^{iL_1k}, e^{iL_2k}, \dots, e^{iL_Bk} \right\} \in T^B \quad (119)$$

covers the B -dimensional torus T^B ergodically. With $\phi_b(k) \equiv kL_b$ and modest conditions on the function $f(k) \equiv f(\mathbf{e}^{i\phi_1(k)}, \dots, \mathbf{e}^{i\phi_B(k)})$ we have thus the *exact* equality [122, 184]

$$\begin{aligned} \langle f(k) \rangle_k &= \lim_{K \rightarrow \infty} \frac{1}{K} \int_0^K dk f(\mathbf{e}^{i\phi_1(k)}, \dots, \mathbf{e}^{i\phi_B(k)}) \\ &= \frac{1}{(2\pi)^B} \int d^B \phi f(\mathbf{e}^{i\phi_1}, \dots, \mathbf{e}^{i\phi_B}) \\ &\equiv \left\langle f(\mathbf{e}^{i\phi_1}, \dots, \mathbf{e}^{i\phi_B}) \right\rangle_\phi. \end{aligned} \quad (120)$$

Thus, the spectral average $\langle \cdot \rangle_k$ is equivalent to a phase (or torus) average $\langle \cdot \rangle_\phi$. We will make extensive use of this equivalence in the following section and in section 9.

If only a subset of bond lengths is incommensurate one may define ergodic flows on tori of smaller dimension and establish an equivalence of the phase average with phase averages over these tori. We refer to the literature [122] for details and the application to quantum graphs.

The equivalence (133) between spectral statistics and eigenphase statistics in large graphs on one hand and the equivalence between a spectral average and a phase average (120) on the other hand also gives a connection between the spectral statistics of an individual quantum system (with the spectrum $\{k_n\}$) and the spectral statistics of an *ensemble* of unitary matrices $\mathcal{U}_B(k) = ST(k) \mapsto ST(\phi)$ parameterized by B parameters ϕ_b . Thus, the spectral statistics of a large graph (with incommensurable bond lengths and moderate bond length fluctuations) is equivalent to that of a (special) ensemble of unitary random matrices.

6.4. Spectral correlation functions

Let us now define spectral correlation functions. We have already shown that the spectral average of the density of states reduces to the Weyl term. Spectral correlations thus appear in the oscillating part. We define the *n -point correlation function* as [185]

$$R_n(s_1, \dots, s_{n-1}) = \overline{\Delta}^n \langle d^{\text{osc}}(k) d^{\text{osc}}(k + s_1 \overline{\Delta}) \dots d^{\text{osc}}(k + s_{n-1} \overline{\Delta}) \rangle_k \quad (121)$$

where the average is over the whole spectrum $0 \leq k < \infty$. In this definition we anticipated that we will be interested mainly in correlations on the scale of the mean level spacing $\overline{\Delta}$. The corresponding length-scale is the *Heisenberg length* $L_H = 2\pi/\overline{\Delta} = 2B\overline{L}$ and the corresponding period, the *Heisenberg period* is $n_H = 2B$ which is just the dimension of the quantum evolution map.

The two-point correlation function $R_2(s)$ and its Fourier transform, the *spectral form factor*

$$K(\tau) = \int_{-\infty}^{\infty} ds R_2(s) e^{-2\pi i s \tau} \quad (122)$$

will be at the centre of much of the discussion in sections 8 and 9. Though τ and s are dimensionless quantities that have been obtained from rescaling a length and a wavenumber we will often follow the convention to call them ‘time’ and ‘energy’ – $\tau = 1$ corresponds to the Heisenberg time and $s = 1$ to the mean level spacing.

As mentioned above, spectral correlation functions (and their Fourier transforms) are not self-averaging quantities. With the original definition of the density of states it is obvious that they are usually a sum over δ -functions. An additional average over a small window $\Delta s \ll 1$ in the correlators or $\Delta \tau \ll 1$ in the form factor has to be performed to smooth the function. A combination of a spectral average and a subsequent average over τ or s will be denoted by $\langle \cdot \rangle_s$ or $\langle \cdot \rangle_\tau$.

Instead of correlations in the spectrum $\{k_n\}$ of the graph one may also be interested in the correlations in the eigenphases of the quantum map $\mathcal{U}_B(k)$ averaged over k . The corresponding correlation functions

$$\tilde{R}_n(s_1, \dots, s_n - 1) = \left(\frac{\pi}{B}\right)^n \times \left\langle \tilde{d}^{\text{osc}}(\phi; k) \tilde{d}^{\text{osc}}\left(\phi + s_1 \frac{\pi}{B}; k\right) \dots \tilde{d}^{\text{osc}}\left(\phi + s_{n-1} \frac{\pi}{B}; k\right) \right\rangle_k \quad (123)$$

are defined analogously.† For the spectral form factor of the quantum map this reduces to

$$\tilde{K}(\tau) = \frac{1}{2B} \sum_{n=1}^{\infty} \delta\left(|\tau| - \frac{n}{2B}\right) \tilde{K}_n \quad (124)$$

where

$$\tilde{K}_n = \frac{1}{2B} \left\langle \left| \text{tr} \mathcal{U}_B(k)^n \right|^2 \right\rangle_k. \quad (125)$$

The δ -functions in (124) can be smoothed by an additional time average over an interval $\Delta \tau > \frac{1}{2B}$

$$\left\langle \tilde{K}\left(\tau = \frac{n}{2B}\right) \right\rangle_\tau \equiv \frac{1}{\Delta \tau} \int_{\tau - \Delta \tau/2}^{\tau + \Delta \tau/2} d\tau' \tilde{K}(\tau') = \frac{1}{2B \Delta \tau} \sum_{n'; |n' - n| < B \Delta \tau} \tilde{K}_{n'} \equiv \langle \tilde{K}_n \rangle_n. \quad (126)$$

6.5. Equivalence of spectral correlators and eigenphase correlators in large graphs

For large graphs with moderate bond length fluctuations spectral and eigenphase correlation functions are equivalent. We will now discuss this statement in a periodic-orbit approach to the two-point correlation function of a quantum graph with incommensurate bond lengths. Replacing d^{osc} by the sum over periodic orbits (106) and performing the spectral average one obtains

$$R_2(s) = \sum_{p, p'} \sum_{r, r'=1}^{\infty} \delta(rL_p, r'L_{p'}) \frac{\overline{\Delta}^2 (r_p L_p)^2 e^{-2r_p L_p \epsilon}}{2\pi^2 r_p r_{p'}} \text{Re} \mathcal{A}_p^r \mathcal{A}_{p'}^{r'*} e^{i\overline{\Delta} r_p L_p s}. \quad (127)$$

Here, the Kronecker $\delta(r_p L_p, r_{p'} L_{p'})$ restricts the sum over pairs of periodic orbits to pairs of the same (full) length $r_p L_p = r_{p'} L_{p'}$. This result does not depend on the assumption of incommensurate bond lengths. The latter has the additional implication that each bond is visited the same number of times by a pair of periodic orbits with the same length (thus the full periods $r_p n_p$ and $r_{p'} n_{p'}$ are also the same).

†The k -average destroys any dependence on the value ϕ which can thus be set to $\phi = 0$ without loss of generality.

Using the notation introduced in section 5.3 the two-point correlator of a quantum graph with incommensurate bond lengths can be written as

$$R_2(s) = \sum_{\{q\}} \frac{\overline{\Delta}^2 L_q^2 e^{-2L_q \epsilon}}{2\pi^2} \sum_{p, p' \in \{q\}} \frac{1}{r_p r_{p'}} \operatorname{Re} \mathcal{A}_p^r \mathcal{A}_{p'}^{r' *} e^{i\overline{\Delta} L_q s} \quad (128)$$

where $\{q\}$ is the degeneracy class of periodic orbits of length $L_q \equiv \sum_{b=1}^B q_b L_b$. Interference only takes place between the amplitudes of periodic orbits in the same degeneracy class.

The spectral form factor (for $\tau > 0$)

$$K(\tau) = \sum_{\{q\}} \tau^2 e^{-2L_q \epsilon} \delta\left(\tau - \frac{\overline{\Delta} L_q}{2\pi}\right) \sum_{p, p' \in \{q\}} \frac{1}{r_p r_{p'}} \mathcal{A}_p^r \mathcal{A}_{p'}^{r' *} \quad (129)$$

is a sum over δ -functions located at the lengths of the periodic orbits – it is thus directly related to the length spectrum discussed in section 5.3.

Finally,

$$\tilde{K}_n = \sum_{\{q\}: \sum_b q_b = n} \frac{n^2 e^{-2L_q \epsilon}}{2B} \sum_{p, p' \in \{q\}} \frac{1}{r_p r_{p'}} \mathcal{A}_p^r \mathcal{A}_{p'}^{r' *} \quad (130)$$

is the periodic orbit expression for the discrete time form factor obtained from the Fourier transform of the two-point eigenphase correlator. Here, the sum includes only pairs of orbits of full period $n = r_p n_p = r_{p'} n_{p'} \equiv \sum_{b=1}^B q_b$.

An additional time average over a small interval reveals the equivalence of the discrete time form factor \tilde{K}_n and the spectral form factor $K(\tau)$ for large graphs. To this end, let us write the spectral form factor as a sum

$$K(\tau) = \sum_{n=1}^{\infty} K_n(\tau) \quad (131)$$

where $K_n(\tau)$ contains only those periodic orbits of full period $n = n_p r = n_{p'} r'$. Next, let us discuss the distribution of the quantity $\tau_p = \overline{\Delta} r_p L_p / 2\pi$ (this is the metric length in units of the Heisenberg length $L_H = 2\pi/\overline{\Delta}$, or the traversal ‘time’) for periodic orbits with period n . If $n \gg 1$ one may invoke the central limit theorem and set $\tau_p = n\overline{\Delta}L/(2\pi) + \delta\tau_p$ where $n\overline{\Delta}L/(2\pi)$ is the mean traversal time. The fluctuations $\delta\tau_p$ vanish in the mean over all periodic orbits and have the variance $\langle \delta\tau_p^2 \rangle_p = n\overline{\Delta}^2 \overline{\Delta L^2} / (2\pi)^2$ where $\overline{\Delta L^2} = (\sum_b (L_b - \overline{L})^2) / B$ is the variance of bond lengths. We consider periodic orbits of large period in a large graph $n, B \rightarrow \infty$ where $n/2B$ is constant. Additionally we assume moderate bond length fluctuations in the sense that $\overline{\Delta L^2} / \overline{L}^2$ remains constant when $B \rightarrow \infty$. Thus $K_n(\tau)$ contributes to $K(\tau)$ in a small time window of width $\sim \sqrt{n}/B \rightarrow 0$ around $\tau = n/2B$. The overall contribution of $K_n(\tau)$ to $K(\tau)$ can be calculated by the integral

$$\begin{aligned} \int_0^{\infty} d\tau K_n(\tau) &= \sum_{\{q\}: \sum_b q_b = n} \tau_p^2 e^{-2L_q \epsilon} \sum_{p, p' \in \{q\}} \frac{1}{r_p r_{p'}} \mathcal{A}_p^r \mathcal{A}_{p'}^{r' *} \\ &= \frac{1}{2B} \tilde{K}_n \left(1 + \mathcal{O}\left(\frac{n}{B^2}\right) \right). \end{aligned} \quad (132)$$

As a consequence, with a suitable time average over an interval $\Delta\tau \sim B^{-1/2}$ the spectral form factor is well approximated by the discrete time form factor (averaged over periods which correspond to the time interval) for large graphs and $\tau \gg 1/2B$

$$\langle K(\tau) \rangle_\tau = \langle \tilde{K}_n \rangle_n. \quad (133)$$

This proves the above statement that the statistics of the spectrum $\{k_n\}$ and of the spectrum of eigenphases of the quantum map are equivalent for large graphs (if bond length fluctuations are moderate). The discrete time form factor \tilde{K}_n does not explicitly depend on the bond lengths. It only depends on the degeneracy classes of periodic orbits which have the same lengths. All incommensurate choices of the bond lengths lead to the same degeneracy classes $\{q\}$ and thus to the same value for \tilde{K}_n . As a consequence the spectral form factors $\langle K(\tau) \rangle_\tau$ for different incommensurate choices of the bond lengths are equivalent for large graphs. This is a first signature of universality: all large graphs with the same vertex scattering matrices but different incommensurate choices of bond lengths share the same spectral statistics.

6.6. The level-spacing distribution for quantum graphs

The level-spacing distribution $P(s)$ is one of the most well-known signatures of quantum chaos. For a graph with the ordered spectrum $\{k_n\}$, $k_{n+1} \geq k_n$, it is defined by

$$P(s) = \lim_{N \rightarrow \infty} \frac{\Delta}{N} \sum_{n=1}^N \delta_\epsilon(\Delta s - (k_{n+1} - k_n)) \quad (134)$$

where $\delta_\epsilon(x)$ is some continuous approximation to a δ -function with width ϵ . The limit $\epsilon \rightarrow 0$ is implied at the end after $N \rightarrow \infty$ and we will omit ϵ in the following.

The level-spacing distribution depends on spectral correlators of all orders. For this reason it is desirable to express the level-spacing distribution of a quantum graph directly. Such an expression has been derived by Barra and Gaspard [122] and we will outline their approach in this section.

The starting point is the observation that the spectrum is given by the (positive) zeros of a quasiperiodic function $f(k)$. For every graph there are many such functions. For example, the secular function $f(k) = \zeta_B(k)$ will do the job but $\zeta_B(k)\alpha(k)$ where $|\alpha(k)| > 0$ will equally be valid. We will not specify the choice of $f(k)$ in the following and the approach can be generalized beyond quantum graphs to any spectrum which is given by such a function. By definition quasiperiodicity implies that there is a function $\tilde{f}(\phi) \equiv f(\phi_1, \dots, \phi_B)$ of B variables $\phi = (\phi_1, \dots, \phi_B)$ which is periodic in each argument

$$\tilde{f}(\phi_1, \dots, \phi_b + 2\pi, \dots, \phi_B) = \tilde{f}(\phi_1, \dots, \phi_b, \dots, \phi_B) \quad (135)$$

such that

$$f(k) = \tilde{f}(\phi_1 = L_1 k, \dots, \phi_B = L_B k) \quad (136)$$

where L_1, \dots, L_B is a set of rationally independent frequencies. In the case of quantum graphs these frequencies are the bond lengths.† For the secular function $\zeta_B(k)$ of a graph quasiperiodicity is easily seen since it depends on k only through the bond propagator $T(k)$. Replacing $L_b k \mapsto \phi_b$ in $T(k) \mapsto T(\phi_1, \dots, \phi_B)$ leads to a periodic function $\tilde{\zeta}_B(\phi_1, \dots, \phi_B)$ which shows that $f(k) = \zeta_B(k)$ is a quasiperiodic function. We have already encountered this in section 6.3. The variables ϕ_b live on a B -dimensional torus \mathbb{T}^B and

$$\Phi^k(\phi) = (\phi_1 + kL_1, \dots, \phi_B + kL_B) \quad (137)$$

defines an ergodic flow in ‘time’ k on this torus. When the initial condition of the flow is set to $\phi_1^{(0)} = \dots = \phi_B^{(0)} = 0$ one has

$$f(k) = \tilde{f}(\Phi^k(\phi^{(0)})). \quad (138)$$

Thus, the intersections of the flow with the hyperplane Σ defined by

$$\tilde{f}(\phi) = 0 \quad (139)$$

give the spectrum. Denoting a point on the $(B-1)$ -dimensional hypersurface Σ by χ the flow defines a Poincaré map

$$\begin{aligned} \chi_{n+1} &= \tilde{\Phi}(\chi_n) \\ k_{n+1} &= k_n + \tau_R(\chi_n) \end{aligned} \quad (140)$$

where χ_n is a point on Σ that is mapped by the flow to χ_{n+1} on Σ . The two points are the successive intersections of the trajectory $\phi_b = kL_b$ with Σ at times k_n and k_{n+1} . The difference $\tau_R(\chi_n) \equiv k_{n+1} - k_n$ is the first return time to the surface of section.

We can now write the level-spacing distribution as

$$\begin{aligned} P(s) &= \lim_{N \rightarrow \infty} \frac{\bar{\Delta}}{N} \sum_{n=1}^N \delta(\bar{\Delta}s - \tau_R(\chi_n)) \\ &= \lim_{N \rightarrow \infty} \frac{\bar{\Delta}}{N} \sum_{n=1}^N \delta(\bar{\Delta}s - \tau_R(\tilde{\Phi}^{n-1}(\chi_1))) \end{aligned} \quad (141)$$

As a consequence of ergodicity this distribution is independent of the initial conditions $\phi_b^{(0)} = 0$ of the flow. Thus, the initial conditions can be taken anywhere on the torus without changing the limiting distribution for $N \rightarrow \infty$. Moreover, ergodicity implies that the initial condition can be taken anywhere on the surface Σ and that there exists an appropriate measure $d^{B-1}x \nu(x)$ such that

$$P(s) = \int_{\Sigma} d^{B-1}x \nu(x) \bar{\Delta} \delta(\bar{\Delta}s - \tau_R(\chi(x))), \quad (142)$$

where $x = (x_1, \dots, x_{B-1})$ is a set of $B-1$ variables that parameterize $\chi(x) \in \Sigma$.

†If not all bond lengths of the quantum graphs are rationally independent the number of variables has to be reduced to some number smaller than B . The generalization of the following argument is straightforward. However, we will keep a notation that implies incommensurability of all bond lengths.

We now turn to the calculation of the function $\nu(x)$ that determines the invariant measure on the hypersurface. A good starting point is the known invariant measure on the complete torus. That is for every (measurable) function $g(\phi_1, \dots, \phi_B)$ on the torus ergodicity implies

$$\lim_{K \rightarrow \infty} \frac{1}{K} \int_0^K dk g(\Phi^k(\phi^{(0)})) = \frac{1}{(2\pi)^B} \int d^B \phi g(\phi). \tag{143}$$

where $(1/(2\pi)^B)d^B \phi$ is the invariant measure on the torus implied by the homogeneous ergodic flow. Defining $\tau[\Phi^k(\phi^{(0)})]$ as the time of flight after the last intersection with the surface of section Σ (thus $\tau[\Phi^k(\phi^{(0)})] = k - k_n$ if the last intersection happened at time k_n) and setting $\phi^{(0)} = \chi_1^\dagger$ to the first point of intersection we replace the function $g(\phi)$ by

$$g[\Phi^{k-k_1}(\chi_1)] = \overline{\Delta} \Theta(\overline{\Delta}s - \tau[\Phi^{k-k_1}(\chi_1)]) \sum_{n=1}^{\infty} \delta(k - k_n). \tag{144}$$

Let us first show that the left-hand side of (143) is the cumulative function of the level-spacing distribution, that is

$$\begin{aligned} I(s) &= \int_0^s ds' P(s') \\ &= \lim_{K \rightarrow \infty} \frac{\overline{\Delta}}{K} \int_0^K dk \Theta(\overline{\Delta}s - \tau[\Phi^{k-k_1}(\chi_1)]) \sum_{n=1}^{\infty} \delta(k - k_n). \end{aligned} \tag{145}$$

We assume that there are N intersections at times k_2, \dots, k_{N+1} of the trajectory $\phi^k(\chi_1)$ with Σ in the interval $0 < k \leq K$. The integral over k then gives

$$\begin{aligned} \int_0^K dk g[\Phi^{k-k_1}(\chi_1)] &= \sum_{n=1}^N \overline{\Delta} \Theta(\overline{\Delta}s - (k_{n+1} - k_n)) \\ &= \sum_{n=1}^N \overline{\Delta} \Theta(\overline{\Delta}s - \tau_R[\tilde{\Phi}^{n-1}(\chi_1)]). \end{aligned} \tag{146}$$

For large values one may replace $K = N\overline{\Delta}$ and arrives at

$$I(s) = \lim_{N \rightarrow \infty} \frac{1}{N} \Theta(\overline{\Delta}s - \tau_R[\tilde{\Phi}^{n-1}(\chi_1)]) \tag{147}$$

which shows that $I(s)$ is indeed the cumulative function of the level-spacing distribution.

For the calculation of the right-hand side of (143) one first needs to rewrite the sum over δ -functions such that it depends explicitly on the point ϕ on the torus. Using that the values k_n are given as the zeros of $f(k)$ and thus

$$\sum_{n=1}^{\infty} \delta(k - k_n) = \left| \frac{df(k)}{dk} \right| \delta(f(k)). \tag{148}$$

†This implies a shift $k \mapsto k - k_1$ without changing the time difference between the last intersection. Thus, $\tau[\Phi^{k-1}(\chi_1)] = k - k_n$.

Now $f(k) = \tilde{f}(\Phi^{k-k_1}(\chi_1))$ and

$$\frac{df}{dk} = \sum_{b=1}^B \frac{\partial \tilde{f}}{\partial \phi_b} L_b$$

lead to

$$g[\Phi^{k-k_1}(\chi_1)] = \bar{\Delta} \Theta(\bar{\Delta}s - \tau[\Phi^{k-k_1}(\chi_1)]) \times \left| \sum_{b=1}^B \frac{\partial \tilde{f}(\Phi^{k-k_1}(\chi_1))}{\partial \phi_b} L_b \right| \delta(\tilde{f}(\Phi^{k-k_1}(\chi_1))). \quad (149)$$

As a next step we change the variables $\phi \mapsto (x, \tau)$ where the $B-1$ variables $x = (x_1, \dots, x_{B-1})$ parameterize the surface of section Σ for $\tau=0$ and τ is the time of flight of the flow since the last intersection with Σ . That is

$$\phi_b = L_b \tau + s_b(x) \quad (150)$$

where the B functions s_b satisfy $\tilde{f}(s_1(x), \dots, s_B(x)) = 0$ such that $\chi(x) \equiv (s_1(x), \dots, s_B(x)) \in \Sigma$. In the new variables we have $\tilde{f}(\Phi^{k-k_1}(\chi_1)) \equiv \tilde{f}(x, \tau)$ and a measure

$$d^B \phi = d^{B-1} x d\tau J(x) \quad (151)$$

with the Jacobian determinant

$$J(x) = \begin{vmatrix} L_1 & \dots & L_B \\ \frac{\partial s_1}{\partial x_1} & \dots & \frac{\partial s_B}{\partial x_1} \\ \dots & \dots & \dots \\ \frac{\partial s_1}{\partial x_{B-1}} & \dots & \frac{\partial s_B}{\partial x_{B-1}} \end{vmatrix}. \quad (152)$$

The cumulative function becomes

$$I(s) = \frac{\bar{\Delta}}{(2\pi)^B} \int_{\Sigma} d^{B-1} x J(x) \int_0^{\tau_R[\chi(x)]} d\tau \Theta(\bar{\Delta}s - \tau) \times \left| \sum_{b=1}^B \frac{\partial \tilde{f}}{\partial \phi_b} L_b \right| \delta(\tilde{f}(x, \tau)). \quad (153)$$

The integral over τ can be performed explicitly by introducing the new variable

$$u(\tau) = \tilde{f}(x, \tau) \quad (154)$$

where x is fixed. With

$$\frac{du}{d\tau} = \sum_{b=1}^B \frac{\partial \tilde{f}}{\partial \phi_b} L_b$$

one arrives at

$$I(s) = \frac{\bar{\Delta}}{(2\pi)^B} \int_{\Sigma} d^{B-1} x J(x) \int du \Theta(\bar{\Delta}s - \tau(u)) \delta(u). \quad (155)$$

The integral over u picks up the value of $\tau(u)$ at $u=0$. This has the two solutions $\tau=0$ and $\tau = \tau_R(\chi(x))$. Since τ is the time of flight since the last intersection only the second solution is valid and we finally arrive at

$$\begin{aligned}
 I(s) &= \frac{\bar{\Delta}}{(2\pi)^B} \int_{\Sigma} \mathbf{d}^{B-1}x J(x)\theta(\bar{\Delta})\Theta(\bar{\Delta}s - \tau_R(\chi(x))) \\
 &= \frac{1}{\int_{\Sigma} \mathbf{d}^{B-1}x J(x)} \int_{\Sigma} \mathbf{d}^{B-1}x J(x)\theta(\bar{\Delta})\Theta(\bar{\Delta}s - \tau_R(\chi(x)))
 \end{aligned}
 \tag{156}$$

where the last line follows from

$$\frac{\bar{\Delta}}{(2\pi)^B} \int_{\Sigma} \mathbf{d}^{B-1}x J(x) = 1.
 \tag{157}$$

Equation (157) is consistent with the normalization of the level-spacing distribution

$$P(s) = \frac{\mathbf{d}I(s)}{\mathbf{d}s} = \frac{\bar{\Delta} \int_{\Sigma} \mathbf{d}^{B-1}x J(x)\delta(\bar{\Delta}s - \tau_R(\chi(x)))}{\int_{\Sigma} \mathbf{d}^{B-1}x J(x)}
 \tag{158}$$

and can be derived from

$$1 = \lim_{K \rightarrow \infty} \frac{\bar{\Delta}}{K} \int_0^K \mathbf{d}k \sum_{n=1}^{\infty} \delta(k - k_n)
 \tag{159}$$

in analogy to the above derivation. The invariant measure on the surface of section can now be read off easily as

$$\mathbf{d}^{B-1}x \nu(x) = \mathbf{d}^{B-1}x \frac{J(x)}{\int_{\Sigma} \mathbf{d}^{B-1}x J(x)}.
 \tag{160}$$

The integral (158) for a large quantum graph is in general too complex to be performed analytically. Barra and Gaspard [122] have used this integral to investigate the level-spacing distribution of small graphs. For large generic graphs approximations have to be used and it is not known how to proceed from this expression to understand the universal behaviour of generic large graphs that we will discuss in the remaining sections.

7. Quantum chaos and universal spectral statistics

More than 20 years ago it was observed that spectral fluctuations in individual complex (chaotic) quantum systems are universal [186]. That is, all the spectral correlators defined in section 6 (and also the level-spacing distribution) of any chaotic quantum system are described by non-trivial system-independent functions. Once rescaled by the (system-dependent) mean level spacing, they only depend on some general symmetry properties that follow the classification scheme of Wigner and Dyson [187–190]. This symmetry classification scheme is based on the behaviour of the system under a time-reversal operation. Systems either violate time-reversal invariance (symmetry class A in the notation of [191]) or they are time-reversal invariant. In the latter case there are two symmetry classes

which, in fermionic systems, are realized by time-reversal invariant dynamics with conserved spin (symmetry class *AI*) or with broken spin rotational invariance (symmetry class *AII*). For a general overview of symmetry classes and their algebraic properties, see Appendix A. The spectral statistics in integrable systems is different from the chaotic case. Spectral statistics in integrable systems with at least two degrees of freedom is generically Poissonian [192]. The above statement of universal spectral statistics is based on an overwhelming basis of experimental and numerical evidence and has been promoted to a conjecture for chaotic (hyperbolic) Hamiltonian systems in the semiclassical regime by Bohigas, Giannoni and Schmit [193] (see also [194, 195]). Since, proving the Bohigas–Giannoni–Schmit conjecture and understanding the physical basis of this type of universality has been one of the major challenges in the field of quantum chaos [119, 196–199]. The dominant method that has been applied is semiclassical periodic orbit theory based on Gutzwiller’s trace formula [118, 119] which expresses (the oscillatory part of) the density of states as a sum over periodic orbits of the corresponding classical Hamiltonian dynamics. In spite of significant recent progress, universal spectral correlations in *individual* Hamiltonian systems are not fully understood. Moreover, some counterexamples of classically chaotic quantum systems have been identified which do not show universal spectral statistics [200–202]. While in these systems the strong deviation from universality is fairly well understood, it raises the question what are the precise conditions to find universality in the spectra of classically chaotic Hamiltonian systems? Today, large quantum graphs are the only class of individual quantum systems for which universality has been proven and precise sufficient conditions can be stated [141, 142]. We will give an outline of this proof later in section 9.

7.1. Universal correlators and random-matrix theory

It has been known for some time that universality can be proven with an (*additional*) average over *ensembles* of systems. The first successful approach was random-matrix theory [185, 203, 204] where a complex quantum system is described by a Hermitian matrix with random entries. Random-matrix theory has become an important tool to predict spectral statistics, wavefunction statistics and transport statistics in complex quantum systems (e.g. disordered mesoscopic systems) [205–207]. Wigner and Dyson [187–190] proposed three Gaussian random-matrix ensembles, one for each symmetry class: the Gaussian Unitary Ensemble (GUE, symmetry class *A*), the Gaussian Orthogonal Ensemble (GOE, symmetry class *AI*) and the Gaussian Symplectic Ensemble (GSE, symmetry class *AII*). The universal spectral correlators for these ensembles have been calculated analytically in the limit of infinite matrix dimension [185]. See Appendix B for a definition of the ensembles and for their correlation functions. The success of random-matrix theory in predicting universal correlators is reflected in the physical literature where ‘universality’ is frequently replaced by ‘random-matrix behaviour’.

If the spectrum of a quantum system is known (either by experimental measurements or by a numerical calculation) a simple way to see if its spectral statistics follows the universal predictions of random-matrix theory, is to plot a histogram of its level-spacing distribution against the Wigner surmises (an energy

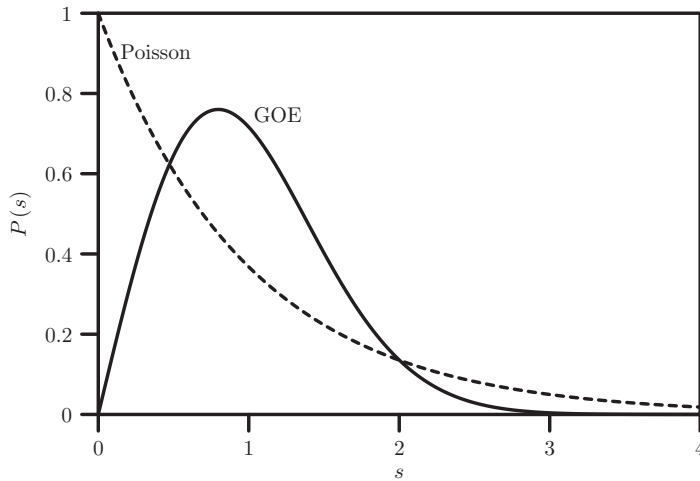


Figure 3. Level-spacing distributions of a complex quantum system (Wigner surmise for the GOE, full line) and of an uncorrelated spectrum (Poisson distribution, dashed line).

interval with a few hundred eigenvalues is usually sufficient). The Wigner surmises (B9) are the random-matrix results for the level-spacing distributions of the Gaussian random-matrix ensembles of dimension 2×2 (GUE and GOE) or 4×4 (GSE). They only deviate very slightly from the exact universal result for infinite matrix dimension [196] and the difference can only be resolved with very large data sets. In figure 3 the level-spacing distribution of a completely uncorrelated spectrum is plotted against the Wigner surmise of the GOE. Uncorrelated spectra are realizations of a Poisson process. Poissonian eigenvalue statistics is generic for integrable systems (with at least two freedoms) [192, 196] and the level-spacing distribution is just an exponential decay

$$P(s) = e^{-s}. \quad (161)$$

The strong deviation of the Wigner surmise from the Poisson distribution is a signature of the non-trivial correlations in complex quantum systems. The most obvious difference of the two distributions is that small values of the level spacing are favoured in a Poisson spectrum (level clustering) but are strongly suppressed in the Wigner surmise. This *level repulsion* in complex quantum systems can be understood using a perturbative approach [196]. Also, large values of the level spacing occur much more frequently in a Poisson spectrum than in a universal complex quantum system. That is universal spectra are much more rigid than Poisson spectra.

7.2. Analytical approaches to universality

Apart from random-matrix theory there have been two other successful attempts to understand universality for *ensembles* of quantum systems: a particle in a random potential (disordered system) [208, 209] and the so-called Pechukas–Yukawa gas

where the parametric dependence of eigenvalues and eigenvectors on a parameter λ in a Hamiltonian of the form $H = H_1 + \lambda H_2$ is investigated [196, 210–212]. In spite of their success and significance these studies (and also random-matrix theory) cannot explain the deep quantum-to-classical correspondence between spectral correlations in a Hamiltonian systems and the dynamic properties of the underlying classical flow.

This correspondence is the main focus in quantum chaos where semiclassical periodic-orbit theory has been used [183, 213–217]. We will not go into the details of the semiclassical periodic orbit approach here but only summarize qualitatively some of the main results and ideas. For an introduction we refer to textbooks on quantum chaos [119, 196–198] and to the cited literature. The periodic-orbit expansions for quantum graphs, which we will present in the next section, are in most parts analogous to semiclassical periodic orbit theory. While periodic-orbit theory on graphs is not always trivially generalized to Hamiltonian systems, its main advantage is that it allows for exact analytical treatments with controlled approximations.

The semiclassical theory distinguishes between several relevant time-scales which have either classical or quantum mechanical origin. The classical scale t_{erg} is determined by the inverse Lyapunov exponent. The shortest quantum time-scale is the Heisenberg time $t_H = 2\pi\hbar/\Delta$. This is the time-scale on which the discreteness of the spectrum is resolved. In the semiclassical limit $t_H \gg t_{\text{erg}}$.

The spectral form factor has been the main focus of semiclassical periodic orbit theory of spectral statistics. The universal spectral form factors for the three Wigner–Dyson classes are shown in figure 4. The non-trivial spectral correlations in the form factor are apparent as deviations from $K^{\text{Poisson}}(\tau) = 1$.

Using Gutzwiller’s trace formula [118, 119] the form factor $K(\tau)$ for a classically chaotic Hamiltonian system can be approximated semiclassically as a sum over pairs

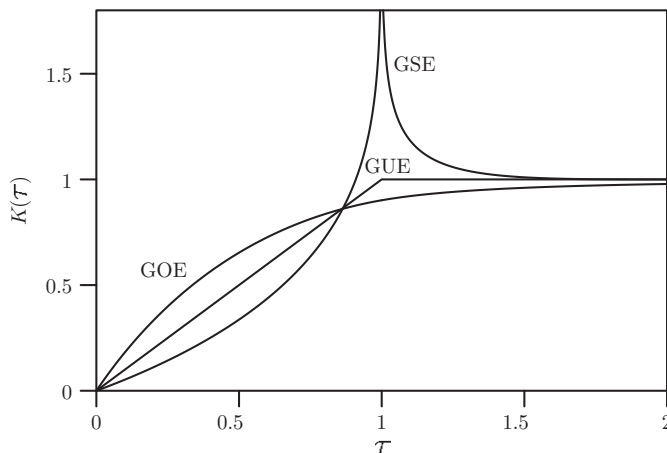


Figure 4. The spectral form factors for the three universality classes described by the GUE, GOE, and GSE.

of periodic orbits with period $t_p = \tau t_H$

$$K(\tau) \sim \sum_{p,p'} \frac{t_p^2}{r_p r_{p'}} \mathcal{A}_p \mathcal{A}_{p'}^* \quad (162)$$

where $\mathcal{A}_{p/p'}$ are amplitudes corresponding to the periodic orbits and $r_{p,p'}$ are repetition numbers. The magnitude of \mathcal{A} depends on the classical stability, and its phase on the classical action of the orbit p .

The contribution of periodic-orbits in the range $t_{\text{erg}} \ll t_p \ll t_H$ to the spectral correlators is quite well understood and it reproduces the universal form factor. In a seminal paper Berry [214] showed that a reduction of the double sum in (162) to pairs which are either the same or time reversed (the *diagonal approximation*) can be performed on the basis of the sum rules [177] and leads to an agreement with the linear universal behaviour of the form factor for short times. Since, it has been a challenge to understand the next-to-leading order in the short time expansion

$$\begin{aligned} K_{\text{GUE}}(\tau) &= \tau \\ K_{\text{GOE}}(\tau) &= 2\tau - 2\tau^2 + \mathcal{O}(\tau^3) \\ K_{\text{GSE}}(\tau) &= \frac{\tau}{2} + \frac{\tau^2}{4} + \mathcal{O}(\tau^3) \end{aligned} \quad (163)$$

of the form factor or to understand the long-time behaviour $\tau > 1$. Many interesting results on action correlations [213, 216, 217] in terms of so-called ‘pseudo-orbit’ expansions have been obtained [183, 215]. Sieber and Richter made a crucial progress by identifying pairs of correlated periodic orbits whose contribution gives the next-to-leading order term in (163) [160–162] (see also [218–220]). This approach has been developed further in a number of recent articles [221–225]. The present status of semiclassical periodic orbit theory singles out in a systematic way the pairs of periodic orbits contribute to progressively higher terms in the short-time expansion of the form factor [158, 159]. However, due to the essential singularity of the form factor at the Heisenberg time $\tau = 1$ this result cannot be extended beyond $\tau > 1$. Another drawback of the present theory is that not all periodic orbits are considered. An estimate of the contribution of the omitted orbits to the form factor is not given.

There exists yet another attempt to explain universality in individual chaotic quantum systems. It relies on a mapping to a supersymmetric field theory. It was hoped that these so-called ‘ballistic σ -models’ would allow a direct access to universality via their mean field approximations [226–229]. However, there are serious problems in regularizing these theories, and so far they could only be established under the protection of an additional average over (very weak) disorder [230].

For *individual* quantum graphs periodic-orbit methods and methods from random-matrix theory and disordered systems like mappings to supersymmetric field theories can all be applied rigorously. The inherent disorder introduced into the quantum graph by a fixed choice of rationally independent bond lengths is sufficient to treat a quantum graph in a similar way as an ensemble of disordered systems or as an ensemble of unitary matrices. In the following sections we will give

a detailed account of the periodic-orbit theory and its supersymmetric counterpart to quantum graphs.

8. Periodic orbit theory for spectral statistics

In this section we describe the periodic-orbit theory for the spectral form factor for large graphs. We will not try to give the most general account but will restrict our discussion to star graphs. While the results can be generalized to other topologies, the main ideas can be explained in a clearer way for star graphs, where one avoids a few technical problems that arise in the general case. For the same reason we will only consider the discrete version of the form factor which corresponds to two-point correlations in the eigenphases of the quantum map. As shown in section 6.5 eigenphase correlations are equivalent to spectral correlations for large graphs with bond lengths which are incommensurate and which are confined to a moderately narrow interval of lengths.

The quantum dynamics on a star graph is not affected by adding a magnetic field (24). The only way to violate time-reversal invariance is by choosing a central vertex scattering matrix in an appropriate way. Similarly, one can add a spin degree of freedom which enables us to study the resulting spectral statistics and compare them with the predictions of random-matrix theory.

One of the important features of random-matrix theory is that the statistics derived for ensembles of $N \times N$ matrices tend to well-defined limiting distributions in the limit $N \rightarrow \infty$, provided that the spectral parameters are properly scaled. In periodic-orbit theory the analogous limit is $t_H \rightarrow \infty$ which is the semiclassical limit for Hamiltonian flows. For graphs the limit $\hbar \rightarrow 0$ has no consequence. However, one can make the Heisenberg time t_H arbitrarily large by increasing the number of bonds B . The disadvantage of graphs with respect to Hamiltonian flows is that there is no way to increase the number of bonds and at the same time preserve the classical dynamics on the graph. As a matter of fact there is no unique way to reach the limit $B \rightarrow \infty$. In the case of star graphs the limit $B \rightarrow \infty$ is topologically straightforward. However, one has to prescribe a sequence of central vertex scattering matrices. For this reason it is more appropriate to consider fixed large graphs and expand the spectral functions as powers series in B^{-1} . In the cases of Neumann or DFT vertex scattering matrices which we study here as examples one can perform the limit $B \rightarrow \infty$ in a consistent way.

8.1. Spectral form factor for star graphs

One of the main technical advantages of star graphs is the fact that one may reduce the dimension of the quantum evolution operator from $2B$ to B . This follows from the observation that a wave which scatters into a bond is totally reflected at the peripheral vertex. This idea can be implemented in the following way. The $2B \times 2B$ graph scattering matrix for star graphs has the form

$$S = \begin{pmatrix} 0 & -S_\star \\ -\mathbb{1}_B & 0 \end{pmatrix} \quad (164)$$

where S_\star is the $B \times B$ *star scattering matrix*. We assume only dynamically connected star graphs for which S_\star cannot be brought into block-diagonal form by a permutation of bond indices. It is equal to the central vertex scattering matrix up to a minus sign which we introduce for convenience. We have chosen Dirichlet boundary conditions at the peripheral vertices. These appear as minus the identity matrix in the graph scattering matrix. The secular function of a star graph can be written as

$$\zeta_B(k) = \det(\mathbb{1}_{2B} - \mathcal{U}_B(k)) = \det(\mathbb{1}_B - \mathcal{U}_{B_\star}(k)) \tag{165}$$

where

$$\mathcal{U}_{B_\star}(k) = T_\star(k)S_\star. \tag{166}$$

with $T_\star(k)_{b,b'} = \delta_{bb'}e^{2ikL_b}$ is the $B \times B$ star quantum evolution map. The star bond propagation matrix $T_\star(k)$ describes the phase accumulated during the propagation from the centre to the peripheral vertices and back. The minus signs picked up during the scattering at the peripheral vertices are cancelled by the minus sign of the central scattering matrix $-S_\star$. Thus, the star quantum evolution map $\mathcal{U}_{B_\star}(k)$ describes the process of scattering at the centre and subsequent propagation along the bonds until coming back to the centre. This way we have removed the direction index ω from the description.

The topological length n of a trajectory in this reduced picture is equal to the number of peripheral vertices (or undirected bonds) visited. This corresponds to a length $2n$ in the general approach based on directed bonds. Thus the Heisenberg period is now $n_H = B$. The discrete form factor at time $\tau = n/B$ is

$$\tilde{K}_{\star,n} = \frac{1}{B} \langle |\text{tr } S_\star^n|^2 \rangle_k = \sum_{p,p' \in \mathcal{P}(n)} \delta(r_p L_p, r_{p'} L_{p'}) \frac{n^2}{B r_p r_{p'}} \mathcal{A}_p^{r_p} \mathcal{A}_{p'}^{r_{p'}*} \tag{167}$$

where a periodic orbit $p = \overline{b_1, b_2, \dots, b_{n_p}}$ is now specified by the sequence of undirected bonds $b = 1, \dots, B$ and its amplitude is the product of the amplitudes of the star scattering matrix $A_p = S_{\star b_1, b_{n_p}} \cdots S_{\star b_3, b_2} S_{\star b_2, b_1}$. Another way of writing the same expression is

$$\tilde{K}_{\star,n} = \sum_{\{q\}: \sum q_b = n} \frac{n^2}{B} \left| \sum_{p \in \{q\}} \frac{1}{r_p} \mathcal{A}_p^{r_p} \right|^2 \tag{168}$$

where $\{q\}$ is the degeneracy class of periodic orbits of length $L = 2 \sum_{b=1}^\infty q_b L_b$.

A sufficient condition for a star graph to be invariant under time-reversal (symmetry class AI) is that the star scattering matrix is symmetric

$$S_\star = S_\star^T. \tag{169}$$

Otherwise, time-reversal symmetry is in general broken (symmetry class A). More precisely, any star graph with a scattering matrix of the form $S_\star = S_0 D$ where S_0 is symmetric $S_0 = S_0^T$ and $D = \text{diag}(e^{i\beta_b})$ is time-reversal invariant. Under this condition every periodic orbit has the same amplitude as its time-reversed partner. Note also that the secular equations for a graph with scattering matrix $S_\star = S_0 D$ and a graph with the scattering matrix $S'_\star = D^{1/2} S_0 D^{1/2}$ are completely equivalent.

Time reversal invariant star graphs of symmetry class AII can be constructed by adding a spin freedom to the wavefunction [139]. This will be implemented in section 8.4.

We will use two examples of scattering matrices for star graphs to illustrate our results: (i) *Neumann star graphs* [123, 126, 127, 147, 149, 150]

$$S_{\text{Neumann}\star bb'} = \delta_{bb'} - \frac{2}{B}, \quad (170)$$

and (ii) *DFT star graphs* [139, 140]

$$S_{\text{DFT}\star bb'} = -\frac{1}{\sqrt{B}} e^{i2\pi bb'/B} \quad (171)$$

for which the the central vertex scattering matrix is taken as the discrete Fourier transform matrix (see section 3.3). Both scattering matrices are symmetric, thus both families of star graphs are time-reversal invariant. The main difference between the two families is revealed by comparing the probability of backscattering $b \rightarrow b$ to the probability to be scattered into any other bond $b \rightarrow b' \neq b$. For DFT star graphs an incoming wave packet is scattered into any bond with the same probability $P_{\text{DFT}\star b \leftarrow b} = P_{\text{DFT}\star b \leftarrow b'} = 1/B$. For Neumann star graphs with large B back scattering $P_{\text{Neumann}\star b \leftarrow b} = (1 - \frac{2}{B})^2$ is favoured, while scattering into any other bond has a small probability $P_{\text{Neumann}\star b \leftarrow b'} = 4/B^2$. In the limit $B \rightarrow \infty$ this difference has a strong impact on spectral statistics. While DFT star graphs have the canonical universal spectral statistics of the GOE the Neumann star graphs belong to a different universality class [123, 127, 147].

8.2. The diagonal approximation

We shall start the discussion of the periodic-orbit theory by considering the first leading term in the short time expansion of the form factor $K(\tau)$. This limit is defined by the requirement that $\tau = n/B$ is much smaller than the Heisenberg time $\tau \ll \tau_H \equiv 1$.

In (168) we have expressed the form factor $\tilde{K}_{\star n}$ as a sum over degeneracy classes $\{q\}$ of periodic orbits which share the same length L_q . Each degeneracy class $\{q\}$ gives a contribution

$$\frac{n^2}{B} \left| \sum_{p \in \{q\}} \frac{\mathcal{A}_p}{r_p} \right|^2 = \frac{n^2}{B} \left(\sum_{p \in \{q\}} \frac{|\mathcal{A}_p|^2}{r_p^2} + \sum_{p, p' \in \{q\}: p \neq p'} \frac{\mathcal{A}_p^* \mathcal{A}_{p'}}{r_p r_{p'}} \right). \quad (172)$$

If the phases of the amplitudes \mathcal{A}_p were completely random one would expect that the purely diagonal term which is the first term on the right-hand side of (172) dominates the form factor. However, the phases of the terms are not random and the extraction of the form factor as a power series in τ amounts to unravelling the phase correlations in a systematic way.

Let us now consider the time-reversal invariant case where $S_{\star} = S_{\star}^T$. In general each periodic orbit has then the same amplitude as its time-reversed partner. Therefore, time-reverse pairs add coherently to the form factor which results in

doubling the contribution of the pure diagonal approximation. This is not exactly true because there always exist *self-retracing orbits*, for which by definition the time-reversed partners are identical.

It is natural to divide the form factor into diagonal and off-diagonal contributions

$$\tilde{K}_{\star n} = \tilde{K}_{\star n}^{\text{diag}} + \tilde{K}_{\star n}^{\text{off-diag}} \tag{173}$$

where the diagonal part

$$\tilde{K}_{\star n}^{\text{diag}} = \frac{2n^2}{B} \sum_{p \in \mathcal{P}(n)} \frac{|\mathcal{A}_p^{r_p}|^2}{r_p^2} - \frac{n^2}{B} \sum_{p \in \mathcal{P}(n); p=\hat{p}} \frac{|\mathcal{A}_p^{r_p}|^2}{r_p^2} \tag{174}$$

consists of all pairs $p, p' \in \mathcal{P}(n)$ of primitive periodic orbits that are either equal $p' = p$ or time-reversed to each other $p' = \hat{p}$. The second term is a sum over *self-retracing* periodic orbits which have been counted twice in the first term.

The off-diagonal contribution

$$\tilde{K}_{\star n}^{\text{off-diag}} = \frac{n^2}{B} \sum_{p, p' \in \mathcal{P}(n); p' \neq p, p' \neq \hat{p}} \delta(r_p L_p, r_{p'} L_{p'}) \frac{\mathcal{A}_p^{r_p} \mathcal{A}_{p'}^{r_{p'}^*}}{r_p r_{p'}} \tag{175}$$

to the form factor amounts to all remaining pairs of periodic orbits. It is responsible for the quantum interference effects which are not present in the diagonal part.

The diagonal approximation [214] consists of writing the form factor in terms of the diagonal part only. This is justified for short times $n \ll B$ because of the following argument. For $n \ll B$ the majority of periodic orbits visit any bond at most once. In that case only the orbits which contribute to the diagonal approximation contribute coherently to the sum irrespectively of the chosen star scattering matrix S_\star and one may expect that the off-diagonal terms are suppressed due to the remaining phase factors.

At larger times the probability to visit a bond twice is non-negligible – this probability grows proportional to the time for $n \ll B$. When a bond is visited twice (or more often) some off-diagonal orbit pairs have correlated phases and add up coherently. Eventually these give higher order corrections in $\tau = n/B$.

We will come back to a discussion of the off-diagonal part later in section 8.3. For the rest of this section we will discuss the diagonal approximation to the form factor in detail. Note that

$$|\mathcal{A}_p|^2 = \prod_{j=1}^{n_p} |S_{\star b_{j+1}, b'_j}|^2 = \prod \mathcal{M}_{\star b_{j+1} b_j} = W_p \tag{176}$$

is just the classical weight of a periodic orbit (74) for the classical evolution map

$$\mathcal{M}_{\star bb'} = |S_{\star bb'}|^2. \tag{177}$$

Replacing $|\mathcal{A}_p|^2 \rightarrow W_p$ in the diagonal part (174) and comparing it to the classical periodic orbit expansion (75) of the return probability $u_n = \text{tr} \mathcal{M}^n$ one obtains the identity

$$\tilde{K}_{*n}^{\text{diag}} = \frac{2n}{B} u_n - \frac{2n^2}{B} \sum_{p \in \mathcal{P}(n): r_p \geq 2} \frac{r_p - 1}{r_p^2} W_p^{r_p} - \frac{n^2}{B} \sum_{p \in \mathcal{P}(n): p = \hat{p}} \frac{1}{r_p^2} W_p^{r_p} \quad (178)$$

in terms of the classical weights. In the classical periodic orbit expansion of the return probability (75) repetition numbers $r_p \geq 2$ have a different factor in front of the weight $W_p^{r_p}$ compared to the form factor. This difference is neglected in the first term but corrected in the second term of (178). Below we will show that only a very small fraction of orbits $p \in \mathcal{P}(n)$ has $r_p \geq 2$. The last summand in (178) is the sum over self-retracing periodic orbits.

The first term in (178) is the graph analogue of a general semiclassical relation which expresses the short-time form factor as the product of 2τ with the classical probability to return [213, 231].

The total number of periodic orbits of period n grows exponentially $\propto B^n/n = e^{\lambda_T n}/n$ with the topological entropy $\lambda_T = \ln B$ for a star graph. The number of periodic orbits $p \in \mathcal{P}(n)$ which are repetitions of shorter periodic orbits, that is $r_p \geq 2$, is only proportional to $B^{n/r_p} r_p/n \propto e^{\lambda_T n/r_p} r_p/n$. Though this number also grows exponentially it is only an exponentially small fraction of all periodic orbits. For self-retracing orbits a similar argumentation is straightforward because one half of the corresponding code is just the (time) reverse of the other half. Altogether the total number of periodic orbits that contribute in the second and third summand of (178) only grows as $e^{\lambda_T n/2}/n$ with half the topological entropy.

Let us now use the classical sum rule (77) to estimate the diagonal approximation. The sum rule states $u_n \rightarrow 1$ for periods $n \gg n_{\text{mix}}$. On the same time-scale the second and third part of (178) which contain the contributions from repetitions of shorter orbits and self-retracing orbits are exponentially small because the number of these periodic orbits cannot compensate the small weight of the repeated orbit, which is $W_p^{r_p} \propto (1/B)^n$ in the mean. The largest contributions to the second and third parts come from the finite number of short primitive orbits p with a period smaller than the mixing time $n_p < n^{\text{mix}}$. Their repetitions have a weight $W_p^{r_p} \lesssim e^{-n/n^{\text{mix}}}$ which can also be neglected. In summary, a mixing classical evolution implies the quantum mechanical sum rule

$$\frac{B}{n} \tilde{K}_n^{\text{diag}} \xrightarrow{n \rightarrow \infty} 2 \quad (179)$$

for the diagonal part of the form factor for time-reversal invariant quantum graphs. The deviations die out on the mixing time-scale n^{mix} . This time-scale can be replaced by the (in general shorter) ergodic time-scale if an additional time average over a small interval Δn is applied.

Since the diagonal approximation is only valid for quantum mechanically short times $n \ll B$ the sum rule (179) can only be used effectively to predict the form factor if there is a time-scale separation such that mixing sets in much faster than the

Heisenberg time $n^{\text{erg}} \ll n_H = B$. In that case there is a time regime, $n^{\text{erg}}/B \ll \tau \ll 1$, where the spectral form factor

$$\left\langle K\left(\tau = \frac{n}{B}\right) \right\rangle_\tau \approx \langle \tilde{K} \rangle_n \approx 2\tau \tag{180}$$

follows the universal prediction from random-matrix theory up to corrections of order $\mathcal{O}(\tau^2)$.

In the limit of large graphs $B \rightarrow \infty$ at a fixed time $\tau = n/B$ a more detailed account is necessary because the number of classical modes (which equals the number of bonds) grows. The spectral gap $\Delta_g = 1/n^{\text{erg}}$ defined in (67) may also depend on B . If the spectral gap is bounded from below by a constant $\Delta_g > \delta > 0$ equation (180) becomes exact for $B \rightarrow \infty$ for every fixed time τ . If the spectral gap approaches zero more care has to be taken for those classical modes with eigenvalues $\nu_\ell \rightarrow 1$ [137]. In that case the corrections

$$u_n - 1 = \sum_{\ell=2}^B \nu_\ell^n \tag{181}$$

to the classical sum rule (77) have to be considered in more detail. One may estimate these corrections by

$$\langle |u_n - 1| \rangle_n \lesssim (B - 1)(1 - \Delta_g)^n \sim B e^{-\Delta_g n} \tag{182}$$

which shows that the corrections in the limit $B \rightarrow \infty$ can only be neglected if $\Delta_g B \rightarrow \infty$. Otherwise deviations from the universal behaviour remain in the diagonal approximation for the short-time form factor. Based on this observation, Tanner conjectured [137] that large quantum graphs have universal spectral statistics (also beyond the diagonal approximation) if the spectral gap either remains finite or decays as

$$\Delta_g \sim B^{-\alpha} \quad \text{with} \quad 0 \leq \alpha < 1 \tag{183}$$

in the limit $B \rightarrow \infty$. We will discuss this condition again in connection with the supersymmetry approach to quantum graphs in section 9. We shall conclude this general discussion with the following remarks.

(i) If the gap condition is violated, the contributions of repetitions and self-retracing orbits (178) to $\tilde{K}_n^{\text{diag}}$ should be examined because there is no a priori reason to neglect them. We shall give an example below.

(ii) The gap condition is consistent with the existence of the time regime $1 \gg \tau \gg n^{\text{erg}}/B$. It has been shown that the gap conditions holds generically for large star graphs [127, 170].

Let us illustrate the general discussion by two examples – the DFT star graph and the Neumann star graph. The DFT star graph is known to show universal spectral statistics [139] – the classical map is simply $M_{\text{DFT}\star bb'} = 1/B$ for which all eigenvalues apart from $\nu_1 = 1$ vanish exactly. Thus the gap condition is fulfilled maximally. The Neumann star graph is an example with spectral statistics which belongs to a universality class that is not described by the GOE [117, 123, 147], here $M_{\text{Neumann}\star bb'} = (4 + \delta_{bb'}(B^2 - 4B))/B^2$ for which all eigenvalues (except for $\nu_1 = 1$) have the same value $\nu_\ell = (B - 4)/B$ such that the gap is $\Delta_g = 4/B$ which does not fulfil the gap condition. Thus we also have to consider repetitions of

short orbits and self-retracing orbits. In the case of Neumann star graph it suffices to consider the repetitions of the shortest periodic orbits with primitive period $n_p = 1$. These are at the same time self-retracing orbits. Altogether one arrives at [117]

$$\begin{aligned} \tilde{K}_{\text{Neumann}\star n}^{\text{diag}} &= 2\frac{n}{B}u_n + \frac{1}{B}(1 - 2n) \sum_{b=1}^B (\mathcal{M}_{\text{Neumann}\star bb})^n \\ &\longrightarrow e^{-4\tau} + 2\tau(1 - e^{-4\tau}) = 1 - 4\tau + \mathcal{O}(\tau^2) \end{aligned} \tag{184}$$

which shows that the contributions from repetitions and self-retracing orbits dominate the short-time behaviour.

We will now study the form factor in the case of a weakly broken time-reversal symmetry such that $S_\star - S_\star^T \neq 0$ is small. The contributions from time reversed pairs to the diagonal part of the form factor acquire phases and they do not add up coherently any more. In that case (178) is replaced by

$$\tilde{K}_{\star n} \approx \tau(\text{tr } \mathcal{M}_\star^n + \text{tr } \mathcal{R}_\star^n) \tag{185}$$

where

$$\mathcal{R}_{\star bb'} = S_{\star b'b}^* S_{\star bb'} \tag{186}$$

and we have neglected the contributions from repetitions and self-retracing orbits. The first term in (185) is the contribution of equal pairs of periodic orbits. For these the above discussion remains valid and we may replace $\text{tr } \mathcal{M}_\star^n \rightarrow 1$ for $n \gg n_{\text{erg}}$ if we assume that the gap condition holds for the classical map \mathcal{M}_\star . The second term in (185) is the contribution from time-reversed pairs of periodic orbits. The matrix \mathcal{R}_\star has generally complex entries. This reflects the fact that broken time-reversal invariance leads to destructive interference of counter-propagating orbits. In the present context only the leading eigenvalue the matrix \mathcal{R}_\star has to be considered. This can be estimated using perturbation theory. As a result the contribution of the time-reversed pairs decays exponentially

$$\text{tr } \mathcal{R}_\star^n \propto e^{-n/n^{\text{crit}}} \tag{187}$$

in n on a time-scale set by

$$1/n^{\text{crit}} \approx \frac{1}{B} |\text{tr } S_\star^*(S_\star - S_\star^T)|. \tag{188}$$

The inverse time-scale $1/n^{\text{crit}}$ is an obvious measure for the violation of time-reversal invariance. For large graphs $B \rightarrow \infty$ and fixed time $\tau = n/B$ the contribution of counter-propagating orbits vanishes if $1/n^{\text{crit}} \propto B^{\alpha'}$ where $0 \leq \alpha' < 1$. This leaves

$$\langle K(\tau)^{\text{diag}} \rangle_\tau = \langle K_{\star n}^{\text{diag}} \rangle_n \rightarrow \tau \tag{189}$$

which is the leading order of the universal result (163) for broken time-reversal invariance.

8.3. Off-diagonal contributions

The diagonal approximation only gives the leading order in the short-time expansion of the form factor. We will now discuss how universality is built up order by

order when more and more off-diagonal pairs of periodic orbits are included in the expansion of the form factor. We will discuss the limit of large star graphs $B \rightarrow \infty$ at a fixed time $\tau = n/B \ll 1$. The leading off-diagonal correction to the diagonal approximation for general large graphs has been given by Berkolaiko, Schanz, and Whitney [128] following the method by Sieber and Richter [161, 162] for Hamiltonian systems.

For simplicity we will assume that the elements of the quantum map of the star graph are all of the same order $|\mathcal{U}_B(k)_{*bb'}| \sim B^{-1/2}$ as for example in the DFT star graph. As a consequence the gap condition (183) holds with $\alpha = 0$. With some extra effort the following discussion can be generalized to graphs where the gap condition holds with $0 \leq \alpha < 1$.

For time-reversal invariant graphs random-matrix theory predicts a leading off-diagonal correction $K(\tau) - K^{\text{diag}}(\tau) = -2\tau^2 + \mathcal{O}(\tau^3)$ to the diagonal approximation of the form factor. For broken time-reversal symmetry random-matrix theory predicts that there are no corrections to the diagonal part for short times $\tau < 1$. We will start with the time-reversal invariant case and come back to broken time-reversal at the end.

A family of pairs of periodic orbits can conveniently be described in terms of diagrams which show the geometry of the two orbits. A diagrammatic language has first been introduced in [124, 128]. We will follow closely [139, 140] where a variant which is suitable for star graph dynamics has been developed. The art of finding the diagrams which contribute to a given order in τ to the form factor is significantly simplified by our assumptions.

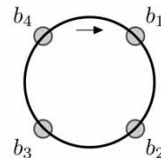
To introduce diagrams let us recall that a pair of periodic orbits p and p' only contributes to the (discrete) form factor \tilde{K}_n if both orbits have the same length $L_p = L_{p'}$. Rationally independent bond lengths imply that the two orbits visit the same bonds with equal multiplicity in a permuted order. That is the code of one orbit is a permutation of the code of the other orbit. All periodic orbit pairs for which this permutation is equal (up to a cyclic permutation) share a similar geometry which can be expressed as a diagram.

The diagrammatic language is most easily introduced by first considering the n -th trace

$$s_n = \text{tr } S_*^n = \sum_{p \in \mathcal{P}(n)} \frac{n}{r_p} \mathcal{A}_p^{r_p} \tag{190}$$

as a sum over periodic orbits of period n . For a fixed period, say $n = 4$, one may write this sum in terms of the following diagram

$$s_4 = \sum_{b_1, b_2, b_3, b_4=1}^B S_{*b_1b_4} S_{*b_4b_3} S_{*b_3b_2} S_{*b_2b_1} = \text{Diagram} \tag{191}$$



The diagram on the right-hand side represents the sum over all periodic orbits of period $n = 4$. The sequence of bonds visited by the periodic orbit in the star graph is represented by a sequence of vertices in the diagram (these should not be confused with the vertices of the graph) which is traversed in the direction indicated by arrow.

Each vertex in the diagram on the right-hand side is translated on the left-hand side as one summation index $b = 1, \dots, B$ which is summed over. Each (directed) line $b \rightarrow b'$ is translated as a factor $S_{\star b'/b}$. A diagram needs not be labelled with the summation indices b_j as above. We will do so sometimes to facilitate the translation. In the diagrams for the traces s_n with higher period n it is useful to define a line element for matrix elements of the n -th power S_{\star}^n by writing the power n explicitly next to the line. This leads to the diagram

$$s_n = \sum_{b=1}^B (S_{\star}^n)_{bb} = \text{Diagram of a circle with a counter-clockwise arrow and a small circle at the bottom} \tag{192}$$

which completes the introduction to diagrams for the trace s_n .

Now we shall introduce diagrams that contribute to the form factor \tilde{K}_n . Instead of immediately giving a full set of rules how to draw and translate diagrams for the off-diagonal part we will first consider the diagonal part where the partner orbits are either the same or time-reversed. Neglecting the overcounting of repetitions of shorter orbits and the double counting of self-retracing orbits the following two diagrams give the dominant contribution to the diagonal approximation of the form factor (here explicitly for $n=4$)

$$\begin{aligned} \tilde{K}_4^{\text{diag}} &= \text{Diagram 1} + \text{Diagram 2} \\ &= \frac{4}{B} \sum_{b_1, b_2, b_3, b_4=1}^B S_{\star b_1 b_4} S_{\star b_1 b_3} S_{\star b_3 b_2} S_{\star b_2 b_1} (S_{\star b_1 b_4} S_{\star b_4 b_3} S_{\star b_3 b_2} S_{\star b_2 b_1})^* + \\ &\quad \frac{4}{B} \sum_{b_1, b_2, b_3, b_4=1}^B S_{\star b_1 b_4} S_{\star b_1 b_3} S_{\star b_3 b_2} S_{\star b_2 b_1} (S_{\star b_4 b_1} S_{\star b_3 b_4} S_{\star b_2 b_3} S_{\star b_1 b_2})^* \\ &= \frac{8}{B} \sum_{b_1, b_2, b_3, b_4=1}^B \mathcal{M}_{\star b_1 b_4} \mathcal{M}_{\star b_1 b_3} \mathcal{M}_{\star b_3 b_2} \mathcal{M}_{\star b_2 b_1} . \end{aligned} \tag{193}$$

The first diagram represents the sum over all equal pairs and the second the sum over time-reversed pairs of periodic orbits. As before each vertex in the diagram is translated as a summation index b_j (the explicit labels in the diagram are not necessary). A full line from vertex b to b' is translated as the corresponding matrix element $S_{\star b'/b}$ and a dashed line as its complex conjugate. If a full and a dashed line are parallel (or antiparallel) one may translate both lines as one matrix element of the classical evolution map $\mathcal{M}_{\star b'/b}$ as in the last line (193). An overall prefactor $4/B$ is added where $1/B$ stems from the definition of the form factor and 4 is the number of cyclic permutations of one orbit with respect to the other.

In general the two diagrams for the diagonal approximation to the form factor $\tilde{K}_n^{\text{diag}}$ has n vertices. The translation rules for lines and vertices are the same as in the example above and the prefactor is n/B . For drawing the diagrams it is useful to replace a long stretch of parallel (antiparallel) full and dashed lines by a

single pair of parallel (antiparallel) lines and put a label next to the line which gives the length of the stretch. For the diagonal approximation this leads to the diagrams

$$\begin{aligned} \tilde{K}_{*n}^{\text{diag}} &= \text{Diagram 1} + \text{Diagram 2} \\ &= \frac{2n}{B} \sum_{b=1}^B (\mathcal{M}_{*}^n)_{bb}^* . \end{aligned} \tag{194}$$

In general a stretch of parallel (antiparallel) lines from vertex b to b' is translated as a matrix element $(\mathcal{M}^n)_{*b'b}$ of the n -th power of the classical map. Ergodicity sets in for $n \gg n^{\text{erg}}$ and one may replace $(\mathcal{M}^n)_{*b'b} \rightarrow 1/B$ in the limit $n, B \rightarrow \infty$. The corrections due to classical decaying modes vanish exactly in that limit and one obtains the form factor $\tilde{K}_n^{\text{diag}} \rightarrow 2\tau$ as predicted by random-matrix theory.

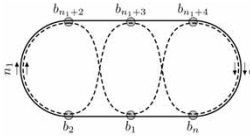
We will now introduce diagrams that contribute to the off-diagonal part of the form factor. The diagrams have to be ordered by the power of τ to which they contribute in the short-time expansion of the form factor. A lot of care has to be taken when more and more diagrams are added to the form factor since certain pairs of periodic orbits occur in more than one diagram. Off-diagonal diagrams and the careful considerations that have to be taken when they are added to the form factor are most easily introduced by considering the diagram

$$\tag{195}$$

as a pedagogical example.

We will first describe how this diagram is translated into a sum over pairs of periodic orbits. Both periodic orbits in the diagram have period $n = n_1 + n_2 + 4$. The full line is a periodic orbit with code $\overline{b_1, \dots, b_n}$. The dashed line is parallel to the full line along the long stretches of length n_1 and n_2 on the left and right. In the code of the partner orbit two indices have interchanged $b_1 \leftrightarrow b_{n_1+3}$ and, for this reason, we will call this diagram a **transposition diagram**. The contribution of this diagram to the discrete form factor \tilde{K}_n is the sum over all pairs of

periodic orbits with the given geometry. For $n_1 \neq n_2$ the diagram is translated as the following sum



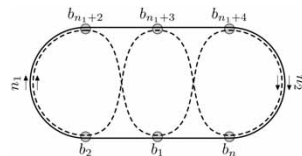
$$= \frac{n^2}{B} \sum_{\substack{b_1, b_2, b_{n_1+2}, \\ b_{n_1+3}, b_{n_1+4}, b_n}} (\mathcal{M}_\star^{n_1})_{b_{n_1+2} b_{n_1+3}} (\mathcal{M}_\star^{n_2})_{b_{n_1+4} b_n} \times \quad (196)$$

$$S_\star b_{n_1+4} b_{n_1+3} S_\star b_{n_1+3} b_{n_1+2} S_\star b_2 b_1 S_\star b_1 b_n \times$$

$$S_\star^* b_{n_1+4} b_1 S_\star^* b_1 b_{n_1+2} S_\star^* b_2 b_{n_1+3} S_\star^* b_{n_1+3} b_n .$$

Apart from an additional factor n in the prefactor the translation follows the same rules as in the diagonal approximation. The additional factor n is explained by the observation that interchanging the indices $b_2 \leftrightarrow b_{n_1+4}$ in the code $\overline{b_1 \cdots b_n}$ describes a different partner orbit than interchanging $b_1 \leftrightarrow b_{n_1+3}$. The diagrams for both transpositions lead to the same diagram – only the labels at the vertices are changed. For $n_1 \neq n_2$ all transpositions $b_j \leftrightarrow b_{j+n_1+2}$ with $j = 1, \dots, n$ lead to different partner orbits with the same contribution which results in the factor n . For $n_1 = n_2$ (thus $n = 2n_1 + 4$ is even) only $b_j \leftrightarrow b_{j+n_1+2}$ with $j = 1, \dots, n/2$ lead to different partner orbits due to the symmetry of the diagram. In that case the additional factor is $n/2$ instead of n . In general the prefactor of any diagram (including the diagonal diagrams) is given by n^2/sB for a diagram with s -fold symmetry (e.g. $s = n$ for the diagonal diagrams).

The total contribution of the transposition diagram is now computed using the unitarity of the graph scattering matrix S_\star and replacing $\mathcal{M}_\star^{n_1}_{bb'}$, $\mathcal{M}_\star^{n_2}_{bb'} \rightarrow 1/B$ for $j = 1, 2$. For fixed lengths $n_1, n_2 = n - n_1 - 4$ of the two loops one gets



$$\cong \frac{n^2}{sB^2} = \frac{1}{s} \tau^2, \quad (197)$$

where $s = 2$ for $n_1 = n_2$ and else $s = 1$.

This shows that a transposition diagram contributes to order τ^2 in the form factor which is the leading correction to the diagonal part. We will now add all diagrams of this type to the two diagonal diagrams. Eventually it will turn out that their total contribution vanishes once pairs of periodic orbits that occur in more than one diagram have been considered correctly. Later we will consider other diagrams that contribute to the same order τ^2 in the form factor and give a non-vanishing contribution which is consistent with the predictions of random-matrix theory.

Taking into account all different transposition diagrams which differ by the size of the loops one gets an overall contribution of $((n - 1)/2)\tau^2$ which diverges as $n, B \rightarrow \infty$.[†] This apparent divergence is resolved due to the fact that certain pairs

[†]Transpositions of an element with its neighbour (formally $n_1 = -1$) or next-neighbour ($n_1 = 0$) leads to diagrams which look a little bit different but have the same value.

of periodic orbits occur in different diagrams and are thus double (or multiply) counted. In particular, each of the transposition diagrams contains diagonal periodic orbit pairs which have to be subtracted before performing the limit of large graphs. In the explicit summation (196) diagonal pairs of periodic orbits appear whenever the two transposed bond indices are the same ($b_1 = b_{n_1+3}$). The subset of pairs of periodic orbits which appears both in the left diagonal diagram in (194) and in the transposition diagram (196) can be expressed by the diagram

$$\begin{aligned}
 &= \frac{n^2}{sB} \sum_{b=1}^B \frac{1}{B^2} \\
 &= \frac{1}{s} \tau^2
 \end{aligned}
 \tag{198}$$

which has the same value as the transposition diagram (197). Each transposition diagram is thus cancelled by subtracting the doubly counted orbit pairs. As a consequence the transposition diagrams do not contribute at all to the form factor in spite of the fact that each diagram is of order τ^2 . A transposition of two indices to the right diagram of the diagonal approximation in (194) (thus changing the direction of the dashed arcs in the transposition diagram) also leads to new diagrams which are cancelled in the same way. This observation can be generalized. Adding a diagram which differs from the transposition diagram by a further interchange of two bonds inside one of the two long stretches of parallel lines gives a contribution n^2/B^3 which is a factor $1/B$ smaller than the transposition diagram. Subtracting all periodic orbits which have been counted twice – once in the transposition diagram and once in the new one – cancels the overall contribution of these orbits.

In the transposition diagrams discussed above the two periodic orbits are parallel in two long stretches on the left and right of the diagram. We will call such long stretches *loops* because they describe a parallel propagation of the two trajectories in phase space. On these the motion is free of interference and described by the classical map. A long loop of length n_1 in a diagram just gives a factor $(\mathcal{M}^{n_1})_{bb'} \rightarrow 1/B$. Interference occurs only in the small region (composed of six bond indices) near the transposed indices. It seems natural to consider diagrams with long parallel stretches of classical motion with a few regions where quantum interference is active in order to find quantum corrections to the diagonal approximation. This leads directly to the so-called loop expansion which orders the diagrams according to the number of classical loops. The diagonal approximation is represented by a single loop. We will show that the universal τ^2 correction to the diagonal approximation is obtained by all diagrams with two loops (including, of course, the correction diagrams for multiply counted pairs). We have already discussed two types of diagrams with two loops: the transposition diagrams where the periodic orbits traverse the loops in the same direction, and the same type of diagram for loops which are traversed in opposite (time-reversed) direction. None of these gave any contribution after the doubly counted orbits have been subtracted. There is a third type of diagram with two loops. For these one loop contains time-reversed

trajectories and the other parallel trajectories. The diagram is easily drawn and calculated

$$\text{Diagram (199)} = \frac{n^2}{B^2} = \tau^2. \tag{199}$$

This eight-shaped diagram is the analog of the semiclassical Sieber–Richter [160–162] pairs for Hamiltonian systems. The left loop has a minimal length $n_1 \geq 2$ since the cases $n_1 = 0, 1$ have already been included as transpositions in the time-reversed diagonal diagram. For the same reason the right loop has a minimal length $n - n_1 - 2 \geq 2$. These minimal lengths of the loops are the graph analog of the minimal length for a classical loop in Hamiltonian flows. Altogether there are $n - 5$ new diagrams of the same value n^2/B^2 . Let us now consider the doubly counted orbit pairs which have diagrams

$$\text{Diagram (200)} = \frac{n^2}{B^2} = \tau^2. \tag{200}$$

with $n_2 = 2, 3, \dots, n - 2$. These pairs have either already been included in diagonal or transposition diagrams or they appear in two new diagrams with different n_1 . As a consequence we have to subtract $n - 3$ correction diagrams with value n^2/B^2 . Altogether the form-factor in the two-loop expansion is

$$\tilde{K}_n = 2\tau + \tau^2(n - 5 - (n - 3)) \rightarrow 2\tau - 2\tau^2. \tag{201}$$

This is equivalent to the short-time expansion of the random-matrix prediction for the form factor in time-reversal invariant systems (symmetry class AI) in the same order.

Breaking time-reversal invariance (symmetry class A) effects all antiparallel loops. Instead of the classical evolution map \mathcal{M} the dynamics along the antiparallel loops is governed by the complex matrix \mathcal{R} (186). A diagram which contains an antiparallel loop is suppressed exponentially and does not contribute in the limit $B \rightarrow \infty$. Thus only the first diagonal diagram remains while all other diagrams in the two-loop expansion are either cancelled by doubly counted pairs or vanish due to antiparallel loops. The two-loop result $\tilde{K}_n = n/B = \tau$ is consistent with the random-matrix prediction.

It takes some effort to write down and calculate all three-loop diagrams for the next order τ^3 [124]. The building blocks of the loop expansion are all known but it has been performed explicitly only for a few orders. For Hamiltonian systems the loop expansion in the semiclassical form factor works analogously and has recently been extended to all orders [158, 159]. One should be aware that the loop expansion is valid only for $\tau \ll 1$. Near the Heisenberg time $\tau = \tau_H = 1$ the probability that a bond is visited more than once is unity and long loops have negligible importance. Similar expansions which work near or beyond the Heisenberg time are not known.

The loop expansion also cannot estimate the error due to all neglected diagrams. For a fixed n the expansion in diagrams is exact and finite, but in the limit $B \rightarrow \infty$, the number of orbit pairs grows exponentially while only a small fraction is included in the loop-expansion.

8.4. Graphs with spin and their spectral statistics

So far we have only discussed two of the three Wigner–Dyson symmetry classes on quantum graphs. The third symmetry class (*AII*) is relevant for fermionic systems with time-reversal invariant dynamics and broken spin-rotational symmetry. The time-reversed path of an electron in such a system travels along the same trajectory in opposite direction $\mathbf{p} \mapsto -\mathbf{p}$, and has, additionally, opposite spin direction $s \mapsto -s$. In quantum mechanics the time-reversal symmetry is described by an anti-unitary operator \mathcal{T} which commutes with the Hamiltonian $[H, \mathcal{T}] = 0$. The two Wigner–Dyson symmetry classes of time-reversal invariant systems are distinguished by $\mathcal{T}^2 = -\mathbb{1}$ in symmetry class *AII* in contrast to $\mathcal{T}^2 = \mathbb{1}$ in symmetry class *AI*.

The spectra of a quantum system in symmetry class *AII* is doubly degenerate due to Kramers' degeneracy. If $|v\rangle$ is an eigenstate of the system $H|v\rangle = E|v\rangle$ the state $\mathcal{T}|v\rangle$ is an orthogonal eigenvector $\langle v|\mathcal{T}v\rangle = 0$ to the same energy $H\mathcal{T}|v\rangle = \mathcal{T}H|v\rangle = E\mathcal{T}|v\rangle$. The different type of time-reversal symmetry has impact on spectral statistics [232]. The spectral fluctuations which are displayed by complex quantum systems in symmetry class *AII* are described by the Gaussian Symplectic Ensemble (GSE). For more details we refer to Appendices A and B and to the literature [196].

For quantum graphs this symmetry class has first been studied by Bolte and Harrison who considered the Dirac operator on the graph with appropriate boundary conditions at the vertices and discussed the spin contribution to spectral statistics. Quantum graphs with a spin degree of freedom have also been discussed in the context of localization induced by spin–orbit coupling [143]. Here, we shall introduce spin degrees of freedom which are only effected by the scattering at the vertices. As in the previous section we shall discuss only star graphs [139, 140]. The spin degree of freedom is added to a graph by considering wavefunctions $\psi_{b\sigma}(x_b)$ on the bond b which have a spin up $\sigma = 1/2$ and a spin down $\sigma = -1/2$ component. Spin rotational invariance is broken by allowing spin flips at the vertices. As in the previous we will limit ourselves to star graphs with spin and allow for spin flips only at the centre.

The construction of the star quantum evolution operator in section 8.1 and spectral theory is completely equivalent to usual star graphs when one replaces the star graph with B bonds and a two-component wavefunction by a star graph with $2B$ bonds and a scalar wavefunction.

Time-reversal symmetry of the star graph with spin requires that the unitary $2B \times 2B$ star graph scattering matrix S_\star has the structure

$$S_\star = \begin{pmatrix} \mathcal{A} & \mathcal{B} \\ \mathcal{C} & \mathcal{A}^T \end{pmatrix} \quad \mathcal{B} = -\mathcal{B}^T \quad \mathcal{C} = -\mathcal{C}^T \quad (202)$$

where the explicit structure is in the spin index such that the $B \times B$ matrix \mathcal{A} (\mathcal{A}^T) describes spin up (down) to spin up (down) scattering from one bond to another

while \mathcal{B} , and \mathcal{C} describe scattering processes where the spin is changed. That is the scattering amplitude $(b', \sigma') \rightarrow (b, \sigma)$ equals the one of the time-reversed process $(b, -\sigma) \rightarrow (b, -\sigma')$ up to a minus sign which occurs when the spin component is flipped

$$S_{\star b\sigma, b'\sigma'} = (-1)^{\sigma-\sigma'} S_{\star b'\sigma', b-\sigma}. \tag{203}$$

Since the number of spin flips along a periodic orbit p is even its amplitude in the trace formula equals the amplitude of the time-reversed periodic-orbit $A_p = A_{\hat{p}}$ where the time-reverse of an orbit with code $p = \overline{(b_1, \sigma_1), (b_2, \sigma_2), \dots, (b_n, \sigma_n)}$ is now defined as $\hat{p} = \overline{(b_n, -\sigma_n), \dots, (b_2, -\sigma_2), (b_1, -\sigma_1)}$.

By convention every pair of degenerate eigenvalues in a spectrum that displays Kramers' degeneracy is only counted once in the density of states. This leads to an overall factor $1/2$ in the trace formula and the mean level spacing between different eigenvalues is $\overline{\Delta} = \pi/B\overline{L}$ as in a scalar graph with the same number of bonds. The equivalence of the spectral form factor with the discrete time form factor of the eigenphases in large graphs leads to the relation

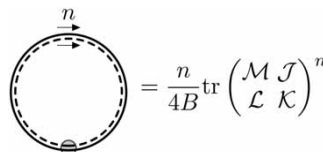
$$\left\langle K\left(\tau = \frac{n}{B}\right) \right\rangle_{\tau} = \langle \tilde{K}_n \rangle_n \tag{204}$$

for time-reversal invariant spin star graphs, where

$$\tilde{K}_n = \frac{1}{4B} \langle |\text{tr} \mathcal{U}_{B\star}(k)^n|^2 \rangle_k. \tag{205}$$

We will discuss the form factor in the diagrammatic language introduced in the previous section and assume that the classical evolution operator $\mathcal{M}_{\star b\sigma, b'\sigma'} = |S_{\star b\sigma, b'\sigma'}|^2$ is strongly mixing such that the decaying classical modes do not contribute to any of the considered diagrams in the limit of large graphs.

The loop expansion follows the same rules as in the previous section. However one needs to add a sum over the $2n$ spin indices along the two orbits. We start with the two diagrams of the diagonal approximation. The first diagram can be written in the form



$$\text{Diagram} = \frac{n}{4B} \text{tr} \begin{pmatrix} \mathcal{M} & \mathcal{J} \\ \mathcal{L} & \mathcal{K} \end{pmatrix}^n \tag{206}$$

where the matrix that appears on the right-hand side describes the propagation of two spins from one bond to another. It contains the classical map \mathcal{M} as a $2B \times 2B$ submatrix which describes the propagation of two parallel spins that remain parallel. Antiparallel spins are propagated by the matrix

$$\mathcal{K}_{b\sigma, b'\sigma'} = S_{\star b\sigma, b'\sigma'} S_{\star b-\sigma, b'-\sigma'}^* \tag{207}$$

while antiparallel spins and parallel spins are coupled by

$$\mathcal{J}_{b\sigma, b'\sigma'} = S_{\star b\sigma, B'\sigma'} S_{\star b\sigma, b'-\sigma'}^* \text{ and } \mathcal{L}_{b\sigma, b'\sigma'} = S_{\star b\sigma, B'\sigma'} S_{\star b-\sigma, b'\sigma'}^*. \tag{208}$$

Being defined in terms of a unitary matrix \mathcal{K} , \mathcal{L} and \mathcal{J} all have eigenvalues inside the unit circle. Their contribution to the trace is thus exponentially suppressed. Only the

ergodic mode of the classical map survives in the n -th trace when n is larger than all decay times. In the limit $B \rightarrow \infty$ the first diagonal diagram gives a contribution $\tau/4$ to the form factor. The second diagonal diagram gives the same contribution – with the only difference that the ergodic modes corresponds to antiparallel spins along the loop. Minus signs occur in addition to the classical propagator whenever both spins flip but since the number of spin flips is even along a periodic orbit they all cancel. We thus have

$$\langle \tilde{K}(\tau = \frac{n}{B})^{\text{diag}} \rangle_\tau = \text{Diagram 1} + \text{Diagram 2} = \frac{\tau}{2} \tag{209}$$

in accordance with the random-matrix result (163).

Loops in other diagrams can be treated in a similar way. Each loop just gives a factor $1/2B$ and only transports parallel spins for a loop that is traversed in the same direction by both orbits and antiparallel spins for loops that are traversed in opposite direction. For time-reversed loops an additional factor -1 appears if the number of spin flips along the loop is odd. The τ^2 corrections to the diagonal approximation are found again in the diagrams with two loops. While the transposition diagrams cancel with the doubly counted orbits in just the same way as for scalar graphs one again gets a non-vanishing contribution from the eight-shaped diagrams of the Sieber–Richter type

$$\text{Diagram} = \sum_{b_1, b_2, b_3, b_4, \sigma_1, \sigma_2, \sigma_3, \sigma_4} \frac{n^2 (-1)^{\sigma_2 - \sigma_3}}{16B^2} \times S_{\star b_2 \sigma_2, b_1 \sigma_1} S_{\star b_4 \sigma_4, b_3 \sigma_3} S_{\star b_3 - \sigma_3, b_1 \sigma_1}^* S_{\star b_4 \sigma_4, b_2 - \sigma_2}^* = -\frac{n^2}{8B^2} \tag{210}$$

The main difference to the scalar case is the different overall sign (the other factors are just due to Kramers’ degeneracy). The different sign also appears in the diagram for the doubly counted orbits which has the same value $-n^2/8B^2$. With $n - 5$ eight-shaped diagrams (not counting the transposition diagrams) and $n - 3$ diagrams accounting for double counting the two loop correction is $n^2/4B^2 = \tau^2/4$ in accordance with the universal result (163).

8.5. Andreev graphs and non-standard symmetry classes

Recently, the threefold symmetry classification of quantum systems by Wigner and Dyson has been extended to a ten-fold classification [191, 233–236]. This has been necessary for certain physical systems, such as a Dirac particle in a random Gauge field, quasiparticles in in a hybrid superconducting–normal-conducting structure or quasiparticles in a disordered superconductor. The new feature in these systems is a electron–hole or particle–antiparticle symmetry. The one-particle excitations are described by a Hamiltonian (for instance, the Dirac operator or the Bogoliubov–de Gennes operator) that have a positive spectrum corresponding to

(quasi-) particle excitations and a negative spectrum corresponding to antiparticle excitations (while the excitation energies of the full many-body field theory remain positive). That is if $|\nu\rangle$ is an eigenstate with energy E , the particle–antiparticle symmetry yields another eigenstate $|\nu'\rangle$ with energy $-E$. There are two types of such particle–antiparticle symmetry operators. They are either unitary or antiunitary. A unitary symmetry operator \mathcal{P} that anticommutes with the Hamiltonian $[\mathcal{P}, H]_{\pm}=0$ is a **chiral symmetry operator** and an anti-unitary operator \mathcal{C} which anticommutes with the Hamiltonian $[\mathcal{C}, H]_{\pm}=0$ is a **charge-conjugation symmetry**. Both types of symmetry have impact on spectral statistics near $E=0$ and lead to new quantum interference effects which are not present in the Wigner–Dyson classes. Sufficiently far away from the symmetry point $E=0$ these systems are usually described well by the standard Wigner–Dyson classes. Combining charge-conjugation and chiral symmetries with time-reversal symmetries one can show that there are seven non-standard symmetry classes beyond the Wigner–Dyson classes [191]. A full account of these is given in Appendix A. In each non-standard symmetry class random-matrix ensembles can be constructed which predict universal statistical properties of their spectra in complex quantum systems.

In this section we will concentrate on two non-standard symmetry classes, which have been called C and CI (see Appendix A), and on chaotic systems with spectral statistics which is dominated by the universal predictions of Gaussian random-matrix ensembles (see Appendix B). The symmetry classes C and CI can be realized by quasiparticles in a hybrid superconducting–normal-conducting structure [235, 236]. The wavefunction obeys the Bogoliubov–de Gennes equation

$$\begin{pmatrix} \left(\frac{\hbar}{i} \nabla + e\mathbf{A}(\mathbf{x}) \right)^2 - E_F & \Delta_s(\mathbf{x}) \\ \Delta_s(\mathbf{x})^* & - \left(\frac{\hbar}{i} \nabla - e\mathbf{A}(\mathbf{x}) \right)^2 + E_F \end{pmatrix} \begin{pmatrix} \Psi_e(\mathbf{x}) \\ \Psi_h(\mathbf{x}) \end{pmatrix} = E \begin{pmatrix} \Psi_e(\mathbf{x}) \\ \Psi_h(\mathbf{x}) \end{pmatrix} \quad (211)$$

where $\Psi_e(\mathbf{x})$ and $\Psi_h(\mathbf{x})$ are the (quasi-) electron and hole components of the wavefunction, $\pm \left(\frac{\hbar}{i} \nabla \pm e\mathbf{A}(\mathbf{x}) \right)^2 / 2m$ is the kinetic energy of the electron or hole in the presence of a magnetic field \mathbf{A} , E_F is the Fermi energy, and $\Delta_s(\mathbf{x})$ is the pair potential of the superconducting condensate which couples electron and hole components. The pair potential vanishes in the normal conducting region. There is an anti-unitary charge conjugation symmetry \mathcal{C}

$$\begin{pmatrix} \Psi_e(\mathbf{x}) \\ \Psi_h(\mathbf{x}) \end{pmatrix} \mapsto \mathcal{C} \begin{pmatrix} \Psi_e(\mathbf{x}) \\ \Psi_h(\mathbf{x}) \end{pmatrix} = \begin{pmatrix} \Psi_h(\mathbf{x})^* \\ -\Psi_e(\mathbf{x})^* \end{pmatrix} \quad \text{with} \quad \mathcal{C}^2 = -\mathbb{1} \quad (212)$$

which transforms an eigenstate with energy E to a different eigenstate with energy $-E$. The Bogoliubov–de Gennes equation is time-reversal invariant with $\mathcal{T}^2 = \mathbb{1}$ (symmetry class CI) if the magnetic field vanishes and the pair potential is real (for broken time-reversal invariance the symmetry class is C).

In a normal conducting region electrons and holes are not coupled. In a hybrid normal-conducting–superconducting system electrons and holes are coupled by Andreev scattering (see figure 5) at a normal-conducting–superconducting interface [237]. An electron (or hole) with energy $|E| \ll |\Delta_s| \ll E_F$ in the normal conducting

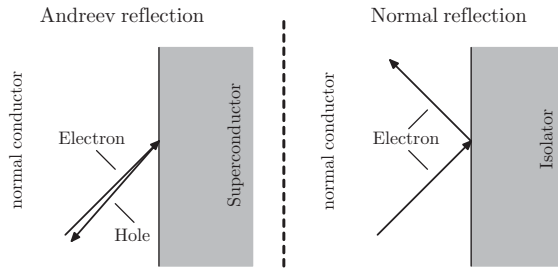


Figure 5. Andreev reflection at a normal-conducting–superconducting interface and normal reflection at a potential wall.

region ($\Delta_s = 0$) hits the interface and is retroflected as a hole (electron) of the same energy in the direction from which the incident quasiparticle came (as opposed to normal specular reflection at a potential wall or normal-conducting–insulating interface). The physical process can be described as an electron which enters the superconductor and recombines with an electron–hole pair such that the two electrons build a new Cooper pair and the hole is ejected out of the superconductor. Up to corrections of order $E/\sqrt{E_F}$ the momentum is conserved in this process, not only in magnitude but also in direction (again in contrast to normal reflection at a potential wall). Note that the velocity of a hole is in opposite direction to its momentum due to the overall minus sign in the kinetic energy (or ‘negative mass’) of the hole.

If a non-magnetic chaotic system is coupled to a superconductor, Andreev reflection will destroy chaos near the Fermi level ($E=0$) since almost every trajectory will hit the superconducting interface and the incident particle travels back along the same trajectory. Exponential divergence of nearby trajectories can only survive on a short time-scale between two Andreev reflections. Still, signatures of chaos in the normal system remain which are a topic of interesting present research. For details we refer to the literature [238–242]. Here we will only be interested in the regime where the *combined* electron–hole dynamics is chaotic[†] – this can be achieved by a magnetic field which bends both electrons and holes in the same direction such that hole trajectories do not travel back along the electron trajectories. In general this breaks time-reversal invariance (symmetry class C) but certain reflection and point symmetries can restore (a non-conventional) time-reversal invariance (symmetry class CI).[‡]

The charge conjugation symmetry in a chaotic system effects all spectral correlation functions near $E=0$ and the deviations from the Wigner–Dyson classes decrease

[†]In the literature on Andreev billiards it has become a convention to call a system chaotic or integrable according to the dynamics of the normal system where electrons and holes are not coupled. We will always refer to the combined electron–hole dynamics in presence of the superconductor.

[‡]Another option to restore chaos is to introduce many point scatterers (disorder). Both symmetry classes can also be realized in a completely different context like two coupled spins where chaos in the semiclassical limit (large spins) is not prevented by Andreev reflections.

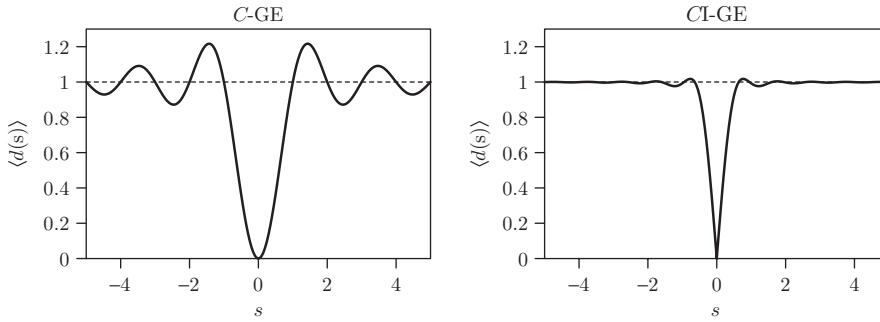


Figure 6. The mean density of states in the random-matrix ensembles C -GE and CI -GE (full lines). The dashed lines give the flat density of states of a system without charge-conjugation symmetry and the same mean level spacing.

on the scale of the mean level spacing $\bar{\Delta}$. That is for $E \gg \bar{\Delta}$ chaotic systems in the symmetry classes C and CI are described by the GUE and GOE (symmetry classes A and AI). The effects can thus not be seen by any type of spectral average in an individual system. Instead the spectral average has to be replaced by an average over some system parameter like the Fermi energy, the magnetic field or the geometry of the system. The deviations from Wigner–Dyson behaviour turn out to be universal and are themselves described by Gaussian random-matrix ensembles which we will call the C -GE and CI -GE.

In contrast to the Wigner–Dyson symmetry classes there are universal interference effects also in the mean density of states for the non-standard symmetry classes (averaged over some system parameter). These will be in the focus of the following discussion.

In figure 6 the mean density of states for the Gaussian random-matrix ensembles C -GE and CI -GE [235, 236] is shown (for explicit formulae see Appendix B) as a function of the energy $s = E/\bar{\Delta}E$ in units of the mean level spacing. Quantum interference leads to a dip in the mean density of states at $s=0$ where $\langle d(s) \rangle = 0$, that is there are no states on the Fermi level. For $s \gg 1$ (or $E \gg \bar{\Delta}$) the mean density of states approaches the value $\langle d(s) \rangle \rightarrow 1$ (or $\langle d(E) \rangle \rightarrow 1/\bar{\Delta}$ which defines the mean level spacing here). With

$$\langle d(s) \rangle = 1 + \int_0^\infty d\tau F(\tau) \cos 2\pi\tau s \quad (213)$$

we introduce the Fourier transform of $\langle d(s) \rangle - 1$ which we will call the **first-order form factor** (or just form factor in this section) because its periodic-orbit treatment is to some extent analogous to the (second-order) form factor in the Wigner–Dyson classes. We will show that the short-time expansion

$$\begin{aligned} F(\tau)^C &= -1 \\ F(\tau)^{CI} &= -1 + \frac{\tau}{2} + \mathcal{O}(\tau^2) \end{aligned} \quad (214)$$

of this form factor for a quantum graph in the corresponding symmetry class is given by a loop expansion analogously to the loop expansion of the second-order form

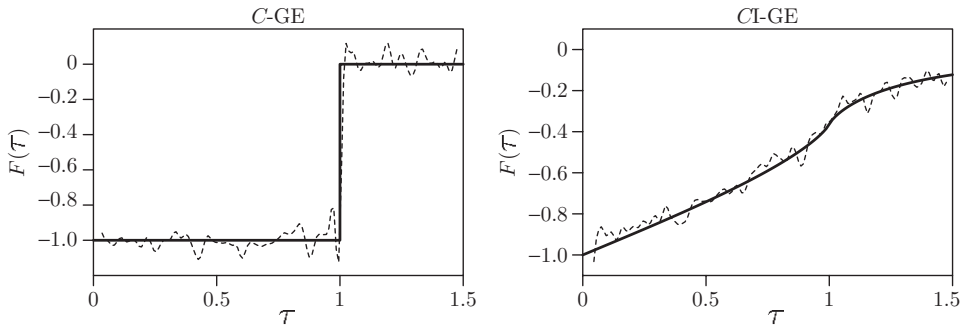


Figure 7. Universal first-order form factor as predicted by the random-matrix ensembles C-GE and CI-GE (full lines). The dashed lines are an average over 10 000 realizations of Andreev star graphs with $B=50$ bonds.

factor in the Wigner–Dyson case. In figure 7 the universal form factors are shown together with a numerical average over Andreev star graphs of the corresponding symmetry classes. The form factor is a strongly oscillating quantity. To compare it to the universal result an additional time average over a small interval $\Delta\tau \ll 1$ is needed to tame the oscillations.

Andreev graphs [139, 140] are quantum graphs which are coupled to a superconductor such that Andreev reflection occurs. Such graphs can be constructed in the symmetry classes C and CI by assigning a two-component wavefunction $\Psi_{b\sigma}(x_b)$ to each bond where $\sigma = e, h$ corresponds to the electron and hole components on the bond b with additional restrictions on the boundary conditions at the vertices. We will not give the most general definition, instead we will look at star graphs. Each bond of the star graph is coupled to a superconductor at the peripheral vertex where Andreev reflection couples the electron and hole components. Along the bonds and at the central vertex the graph is assumed to be normal conducting (electrons are not coupled to holes).

The quantum evolution map of an Andreev star graph with B bonds in symmetry class C (broken time-reversal invariance) has the form

$$U_{B^*}(k) = \begin{pmatrix} S_* & 0 \\ 0 & S_*^* \end{pmatrix} \begin{pmatrix} 0 & T_{eh}(k) \\ T_{he}(k) & 0 \end{pmatrix} \quad (215)$$

where the unitary $B \times B$ matrix S_* is the electron–electron scattering matrix of the central vertex. Charge conjugation symmetry then requires that the hole–hole scattering matrix is the complex conjugate S_*^* . The diagonal $B \times B$ matrices $T_{eh}(k)$ ($T_{he}(k)$) contain the phase factors acquired for a hole propagating from the centre to a peripheral vertex where it is scattered back as an electron which propagates back to the centre. Altogether

$$T_{eh\,bb'}(k) = -i\delta_{bb'}e^{i\theta_b}e^{i2kL_b} \quad T_{he\,bb'}(k) = -i\delta_{bb'}e^{-i\theta_b}e^{i2kL_b}, \quad (216)$$

where e^{i2kL_b} is the phase acquired during the propagating along the bond b from the centre to the periphery and back[†] and $-Ie^{i\theta_b}$ ($-Ie^{-i\theta_b}$) is the phase acquired during the Andreev reflection for a hole (an electron) hitting the superconductor – $e^{-i\theta_b}$ is the phase of the superconductors pair potential. An average over system parameters is easily obtained by taking the phases θ_b as independent random variables which are equidistributed on $0 \leq \theta_b < 2\pi$.

For a time-reversal invariant Andreev star graph (symmetry class CI) there are additional restrictions: the central electron-electron scattering matrix (and thus also the hole-hole scattering matrix) has to be symmetric $S_\star = S_\star^T$ and the pair potential has to be real, thus $e^{i\theta_b} = \pm 1$. For time-reversal invariant Andreev graphs the different signs of the pair potentials will be taken as independent random variables in a system average. Note that it is sufficient to break either the symmetry of the central scattering matrix or the reality of the pair potentials to break time-reversal invariance. Indeed, in the numerical calculations performed in figure 7 we have taken $S_\star = S_{\text{DFT}}$ which is symmetric and one finds very good agreement of the form factor with the universal result.

We will assume that the S_\star is a full matrix and the magnitude of all matrix elements is of order $1/\sqrt{B}$. Since we do not perform any spectral average there is no fundamental difference between rationally dependent and incommensurable bond lengths here. For simplicity we choose all bond lengths equal $L_b = L$. The mean level spacing is $\bar{\Delta} = \pi/2BL$. Setting $k = \bar{\Delta}s$ in the oscillating part of the density of states $d^{\text{osc}}(k)dk = d^{\text{osc}}(s)ds$ we arrive (after a few minor manipulations) at

$$d^{\text{osc}}(s) = \frac{2}{B} \sum_{n=1}^{\infty} (-1)^n \cos\left(2\pi s \frac{n}{B}\right) \text{tr}(S_\star D S_\star^* D^*)^n \quad (217)$$

where $D_{bb'} = \delta_{bb'} e^{i\theta_b}$. One can immediately read off the time averaged form factor

$$\left\langle F\left(\tau = \frac{n}{B}\right) \right\rangle_\tau = \langle F_n \rangle_n \quad (218)$$

where

$$F_n = 2 \langle \text{tr}(S_\star D S_\star^* D^*)^n \rangle_\theta \quad (219)$$

is a discrete variant. The trace appearing in F_n is equivalent to a sum over periodic orbits of period $2n$ which are scattered at the centre of the star alternately as electrons or holes.

Averaging over the phase factors $e^{i\theta_b}$ (for broken time-reversal invariance) only those periodic orbits survive in F_n which visit each bond an even number of times – one half as electrons being Andreev reflected back to the centre as holes the other

[†]At first sight this does not seem to be in accordance with the Bogoliubov–de Gennes equation. Indeed an electron (a hole) propagating along a bond with energy E would acquire a phase $e^{ik_e L_b}$ ($e^{-ik_h L_b}$) according to the Bogoliubov–de Gennes equation where electron (hole) momentum is $k_e = \sqrt{E_F + E}$ ($k_h = \sqrt{E_F - E}$) – the sign in the phase of the hole is different since it propagates in opposite direction to its momentum. Since we are interested in the limit $E_F \gg E$ one may expand the momenta $k_{e,h} = \sqrt{E_F \pm E} = \sqrt{E_F} \pm E/2\sqrt{E_F} + \mathcal{O}(E^2/E_F^{3/2})$. Adding the hole and electron phases $(k_e - k_h)L_b$ the leading part cancels. Keeping $k = E/2\sqrt{E_F}$ fixed in the limit $E_F \rightarrow \infty$ only $2kL_b$ remains.

half as holes being Andreev reflected as electrons. The sum over the remaining orbits is still very complex and cannot be performed in a closed form. It resembles the sum over pairs of periodic orbits in the (second-order) spectral form factor where only those pairs survive the average where both orbits visit the same bonds. Since there is only one orbit there are no diagonal and off-diagonal terms in F_n . However there are *self-dual* periodic orbits which are invariant under electron–hole interchange [243]. That is, a self-dual periodic orbit visits the same sequence of bonds twice with electrons and holes interchanged at the second traversal. The self-dual approximation takes into account only the coherent contribution of self-dual orbits. Since self-dual periodic orbits only exist for odd n one has

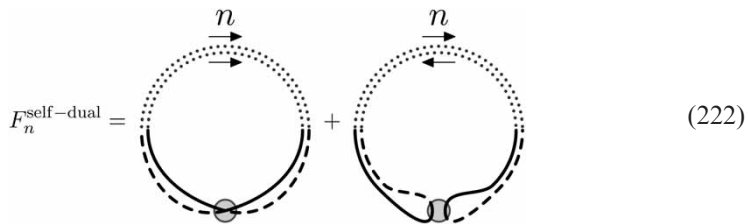
$$F_n^{\text{self-dual}} = \begin{cases} 0 & \text{for odd } n, \\ -2\text{tr}\mathcal{M}^n & \text{for even } n, \end{cases} \quad (220)$$

where $\mathcal{M}_{bb'} = |S_{\star bb'}|^2$ is the corresponding classical map on the graph which does not distinguish between electrons and holes. We can use the classical sum rule (77) and replace $\text{tr}\mathcal{M}^n \rightarrow 1$ and an average over n yields the leading order of the universal term

$$\langle F(\tau)^{\text{self-dual}} \rangle_\tau = \langle F_n^{\text{self-dual}} \rangle_n = -1. \quad (221)$$

The overall minus sign is just a consequence of the $2n$ Andreev reflections each of which gives a factor $-i$. While the diagonal approximation to the second-order form factor \tilde{K}_n is linear in τ the self-dual approximation starts with a constant. The reason for this difference is that the contribution of a pair of periodic orbits in a spectral two-point correlator gets an extra factor n for all cyclic permutations of the second orbit with respect to the first one. In contrast we here deal with a single orbit where such a factor cannot arise.

If time-reversal is broken the contribution of all remaining periodic orbits have to vanish for universal spectral statistics. In contrast time-reversal invariant Andreev graphs in symmetry class CI display corrections to the self-dual approximation – the first order being linear in τ . The average in a time-reversal invariant Andreev graph is just over $e^{i\theta_b} = \pm 1$. The orbits that survive this average outnumber the orbits that contributed at broken time-reversal invariance. Every bond is still visited an even number of times – but there is no restriction that half of them should come from the centre as an electron and the other half as a hole. There are additional orbits already on the level of the self-dual approximation. However their contribution cancels as we will show now. If an orbit first visits a sequence of n bonds and then traverses the same bonds backwards with electrons and holes interchanged it is self-dual with respect to charge-conjugation combined with time-reversal invariance. This is most easily seen by drawing diagrams



where the first diagram contains the self-dual orbits that we have already discussed for broken time-reversal symmetry and the second diagram contains the additional orbits which only survive in the time-reversal invariant case. The first diagram gives a contribution -1 and the second diagram gives $(-)^n 2n$. The additional factor n stems from the reduced symmetry of the diagram with respect to the first self-dual diagram. Averaging over a small time interval the contribution of the second diagram cancels due to its alternating sign.

Higher order corrections in both symmetry classes can be obtained by drawing diagrams with more than one loop [140]. One should be aware that both types of loops parallel and antiparallel are present in the time-reversal invariant case but only the parallel loops survive the ensemble average in the case of broken time-reversal invariance. The linear correction to the self-dual approximation is due to diagrams with two loops. We will not present a full account of these diagrams but refer to the literature. It has been shown that all two-loop diagrams in symmetry class C give a vanishing contribution. In contrast there are two-loop diagrams with a non-vanishing contribution in symmetry class CI – these have one parallel and one antiparallel loop. Subtracting doubly counted orbits they give the value $\tau/2$ which is the linear order of the universal result.

We have shown that periodic-orbit theory in Andreev star graphs can account for universal spectral statistics in non-standard symmetry classes. The remaining five non-standard symmetry classes can equally be treated with star graphs but their treatment does not contain any new ideas and we refer to the literature [140].

9. The supersymmetry approach to quantum graphs

In this section we will come back to universal spectral statistics in the standard Wigner–Dyson symmetry classes and present a proof that the statistics in large well-connected time-reversal invariant quantum graphs follows the predictions of random-matrix theory [141, 142]. This proof involves a field-theoretic description of spectral correlation functions in a specially adapted version of the supersymmetric non-linear σ -model. While the theory can be presented for general simple graphs we restrict again to star graphs which allows for some technical simplifications. Similar methods have been used efficiently in disordered systems [205, 208, 209, 244, 245] where an average over a disorder ensemble leads to supersymmetric σ -models and universal spectral statistics can be proven (for an ensemble of systems). The phases e^{ikL_b} acquired during the propagation through a bond are a source of disorder in an *individual* quantum graph with incommensurate bond lengths. This type of disorder eventually allows for an *exact mapping* to a variant of the non-linear σ -model as an additional powerful tool to analyse their spectral statistics. We will present the theory and the proof of universality for the two-point correlator of the eigenphases of the quantum evolution map of large star graphs. Generalizations to general graphs can be found in the literature [141, 142].

9.1. An exact supersymmetric model for spectral correlators

The starting point of the supersymmetry approach to the two-point correlator of eigenphases of the quantum evolution map is the expression

$$\tilde{R}_2(s) = \frac{1}{8\pi^2} \frac{\partial^2}{\partial j_+ \partial j_-} \Big|_{j_{\pm}=0} \langle \xi(j_+, j_-; s) \rangle_k \tag{223}$$

where

$$\xi(j_+, j_-; s) = \frac{\zeta_B(\theta_{+, \mathbf{F}}; k) \zeta_B(\theta_{-, \mathbf{F}}; k)^*}{\zeta_B(\theta_{+, \mathbf{B}}; k) \zeta_B(\theta_{-, \mathbf{B}}; k)^*} \tag{224}$$

with

$$\begin{aligned} \theta_{\pm, \mathbf{F}} &= \frac{2\pi}{B} \left(j_{\pm} \pm \frac{s}{2} \right) \\ \theta_{\pm, \mathbf{B}} &= \frac{2\pi}{B} \left(-j_{\pm} \pm \frac{s}{2} \right). \end{aligned} \tag{225}$$

$\xi(j_+, j_-; s)$ is a generating function expressed as a quotient of secular functions. A similar expression can be used for the spectral two-point correlator $R_2(s)$ which we will not discuss here (for moderate bond length fluctuations we have shown in section 8 that the two correlators are essentially equivalent for large graphs).

The generating function expressed as a quotient of determinants is an ideal starting point for supersymmetry approaches since it can easily be written as a Gaussian integral over commuting and anticommuting variables. Powerful methods are available to perform averages on Gaussian integrals which renders such an expression a desirable object. We will not give an introduction to the supersymmetry method and the notions of *superdeterminant* $\text{sdet} A$ of a *supermatrix* A or of its *supertrace* $\text{str} A = \text{tr} A_{\mathbf{B}} - \text{tr} A_{\mathbf{F}}$ which is available in many textbooks and reviews [196, 208, 244, 245],[†] but we will give the main steps leading to a convenient Gaussian expression for the generating function.

Defining the supervectors

$$\psi = \begin{pmatrix} z_1 \\ \dots \\ z_N \\ \chi_1 \\ \dots \\ \chi_N \end{pmatrix} \quad \text{and} \quad \tilde{\psi} = (z_1^* \quad \dots \quad z_N^* \quad \tilde{\chi}_1 \quad \dots \quad \tilde{\chi}_N), \tag{226}$$

where z_i are complex commuting (*bosonic*) variables while χ_i and $\tilde{\chi}_i$ are independent anticommuting (*fermionic*) numbers, the quotient of determinants of an $N \times N$

[†]One should be aware that there are different conventions for the definition of a supertrace which might differ by an overall sign and consequently for the superdeterminant which may be defined via $\text{sdet} A = e^{\text{str} \ln A}$. There are also different conventions for the integration over anticommuting numbers which differ by an overall constant.

matrix $A_{\mathbf{F}}$ and a (positive definite) $N \times N$ matrix $A_{\mathbf{B}}$ can be expressed as a Gaussian integral

$$\frac{\det A_{\mathbf{F}}}{\det A_{\mathbf{B}}} \equiv (\text{sdet } A)^{-1} = \int d(\tilde{\psi}, \psi) e^{-\tilde{\psi} A \psi}. \quad (227)$$

Here,

$$A = \begin{pmatrix} A_{\mathbf{B}} & 0 \\ 0 & A_{\mathbf{F}} \end{pmatrix} \quad (228)$$

is a block-matrix in superspace (boson–fermion space) and the measure is given by

$$d(\tilde{\psi}, \psi) = \pi^{-N} \prod_{i=1}^N d\text{Re}(z_i) d\text{Im}(z_i) d\tilde{\chi}_i d\chi_i \quad (229)$$

with $\int d\chi_i \chi_i = 1$ and $\int d\chi_i = 0$.

Before applying this to (224), it will be convenient to double the matrix dimensions using

$$\zeta_B(\theta; k) = \det(\mathbb{1} - e^{-i\theta} \mathcal{U}_{B_{\star}}(k)) = \det(e^{-i\theta} S_{\star}) \det \begin{pmatrix} \mathbb{1} & T_{\star}(k/2) \\ T_{\star}(k/2) & e^{i\theta} S_{\star}^{\dagger} \end{pmatrix}. \quad (230)$$

At this point the doubling of dimension seems arbitrary – it leads to simplifications at a later stage. Now we write the generating function as a Gaussian superintegral

$$\xi(j_+, j_-; s) = \int d(\tilde{\psi}, \psi) e^{-\frac{i\theta s}{2}} e^{-\mathcal{S}[\tilde{\psi}, \psi]} \quad (231)$$

where

$$\begin{aligned} \mathcal{S}[\tilde{\psi}, \psi] &= \tilde{\psi}_+ \begin{pmatrix} \mathbb{1} & T_{\star}(k/2) \\ T_{\star}(k/2) & z_+^* S_{\star}^{\dagger} \end{pmatrix} \psi_+ \\ &+ \tilde{\psi}_- \begin{pmatrix} \mathbb{1} & T_{\star}(k/2)^* \\ T_{\star}(k/2)^* & z_- S_{\star} \end{pmatrix} \psi_-. \end{aligned} \quad (232)$$

Here, $\psi = \{\psi_{a,s,x,b}\}$ is a $8B$ -dimensional supervector where, $a = \pm$ distinguishes between the retarded and the advanced sector of the theory (components coupling to ξ or ξ^* , respectively). The index $s = \mathbf{F}, \mathbf{B}$ refers to complex commuting and anticommuting components (determinants in the denominator and numerator, respectively), and $x = 1, 2$ to the internal structure of the matrix kernel appearing in (232). The 2×2 matrices

$$z_{\pm} \equiv \begin{pmatrix} e^{-i\theta_{\mathbf{B},\pm}} & 0 \\ 0 & e^{-i\theta_{\mathbf{F},\pm}} \end{pmatrix} \quad (233)$$

are diagonal matrices in superspace containing the appropriate phase factors in the boson–boson and fermion–fermion sector.

To account for the (optional) time-reversal invariance of the scattering matrix, we introduce the doublets

$$\begin{aligned} \Psi &= \frac{1}{\sqrt{2}} \begin{pmatrix} \psi \\ \tilde{\psi}^T \end{pmatrix} \\ \tilde{\Psi} &= \frac{1}{\sqrt{2}} (\tilde{\psi}, \psi^T \sigma_3^{\text{bf}}), \end{aligned} \tag{234}$$

where $\sigma_3^{\text{bf}} \equiv \begin{pmatrix} 1 & 0 \\ 0 & -1 \end{pmatrix}$ is the Pauli matrix in superspace. Notice that the lower components of Ψ emanate from the upper component by the time reversal operation (transposition). For later reference, we note that the new fields are related to each other through

$$\Psi = \tau \tilde{\Psi}^T \quad \tilde{\Psi} = \Psi^T \tau. \tag{235}$$

The matrix τ is defined by

$$\tau = E_{\text{B}} \sigma_1^{\text{tr}} - i E_{\text{F}} \sigma_2^{\text{tr}}, \tag{236}$$

where σ_i^{tr} are Pauli matrices in the newly introduced ‘time-reversal’ space and $E_{\text{B/F}}$ are the projectors on the bosonic and fermionic sectors, respectively. All we will need to know to proceed is that τ obeys the conditions

$$\tau^T = \tau^{-1} \quad \text{and} \quad \tau^2 = \sigma_3^{\text{bf}}. \tag{237}$$

The appearance of the matrix τ in (234) suggests to introduce the generalized matrix transposition

$$A^\tau \equiv \tau A^T \tau^{-1}. \tag{238}$$

Using (237) and $(A^T)^T = \sigma_3^{\text{bf}} A \sigma_3^{\text{bf}}$ for a supermatrix [208], one finds that the generalized transposition is an involution,

$$(A^\tau)^\tau = A. \tag{239}$$

For later reference we also note that

$$\tilde{\Psi}_+ A \Psi_- = \Psi_-^T \sigma_3^{\text{bf}} A^T \tilde{\Psi}_+^T = \tilde{\Psi}_- A^\tau \Psi_+. \tag{240}$$

With all these definitions, the action (232) now takes the form

$$\begin{aligned} \mathcal{S}[\tilde{\Psi}, \Psi] &= \tilde{\Psi}_+ \begin{pmatrix} \mathbb{1} & T_\star(k/2) \\ T_\star(k/2) & z_\star^* \mathcal{S}^\dagger \end{pmatrix} \Psi_+ \\ &+ \tilde{\Psi}_- \begin{pmatrix} \mathbb{1} & T_\star(k/2)^* \\ T_\star(k/2)^* & z_- \mathcal{S} \end{pmatrix} \Psi_-. \end{aligned} \tag{241}$$

where the matrix structure is again in the auxiliary index x and we have introduced the matrix

$$\mathcal{S} = \begin{pmatrix} S_\star & 0 \\ 0 & S_\star^T \end{pmatrix} \tag{242}$$

where the matrix structure is in time-reversal space.

We are now in a position to subject the generating functional to the spectral average. We do this by invoking the method discussed in section 6.3, whereby the

average over k is replaced exactly by phase space averaging on the B -torus. The only k -dependence is in $T_*(k/2)$ which is replaced by $T_*(\{\phi_b\}) = \text{diag}(e^{i\phi_b})$. The averaging is written explicitly as

$$\langle \xi(j_+, j_-; s) \rangle_\phi = e^{-i4\pi s/B} \int d(\tilde{\psi}, \psi) e^{-S_0} \prod_{b=1}^B \int \frac{d\phi_b}{2\pi} e^{-S_{1,b}}. \quad (243)$$

Here,

$$\begin{aligned} S_0 = & \tilde{\Psi}_{+,1} \Psi_{+,1} + \tilde{\Psi}_{-,1} \Psi_{-,1} \\ & + \tilde{\Psi}_{+,2} z_+^* S^\dagger \Psi_{+,2} + \tilde{\Psi}_{-,2} z_- S \Psi_{-,2} \end{aligned} \quad (244)$$

is the phase-independent part of the action and

$$S_{1,b} = 2\tilde{\Psi}_{+,1,b} e^{i\phi_b} \Psi_{+,2,b} + 2\tilde{\Psi}_{-,2,b} e^{-i\phi_b} \Psi_{-,1,b}. \quad (245)$$

So far, we have not achieved much other than representing the spectral determinants by a complicated Gaussian integral, averaged over phase degrees of freedom. The most important step in our analysis will now be to subject the generating function to an integral transform known as the colour–flavour transformation [246–248]. The colour–flavour transformation amounts to a replacement of the phase-integral by an integral over a new degree of freedom, Z . Much better than the original degrees of freedom, the Z -field will be suited to describe the long time behaviour of the system, which is equivalent to the low energy sector $s \ll 1$ of the field theory.

In a variant adopted to the present context (a single ‘colour’ and F ‘flavours’) the colour–flavour transformation assumes the form

$$\int \frac{d\phi}{2\pi} e^{\eta_+^T e^{i\phi} v_+ + v_-^T e^{-i\phi} \eta_-} = \int d(\tilde{Z}, Z) \text{sdet}(\mathbb{1} - Z\tilde{Z}) e^{\eta_+^T Z \eta_- + v_-^T \tilde{Z} v_+}, \quad (246)$$

where η_\pm and v_\pm are arbitrary $2F$ dimensional supervectors and Z, \tilde{Z} are $2F$ -dimensional supermatrices. The boson–boson and fermion–fermion block of these supermatrices are related by $\tilde{Z}_{\text{BB}} = Z_{\text{BB}}^\dagger$, and $\tilde{Z}_{\text{FF}} = -Z_{\text{FF}}^\dagger$, while the entries of the fermion–boson and boson–fermion blocks are independent anticommuting integration variables. The integration $d(\tilde{Z}, Z)$ runs over all independent matrix elements of Z and \tilde{Z} such that all eigenvalues of $Z_{\text{BB}} Z_{\text{BB}}^\dagger$ are less than unity and the measure is normalized such that

$$\int d(\tilde{Z}, Z) \text{sdet}(\mathbb{1} - Z\tilde{Z}) = 1. \quad (247)$$

We apply the colour–flavour transformation B times – once for each phase ϕ_b . As a result, we obtain a B -fold integral over supermatrices Z_b . There is one flavour corresponding to the time-reversal index $t=1,2$. We combine all matrices Z_b (\tilde{Z}_b) into a single block-diagonal $4B$ -dimensional supermatrix Z (\tilde{Z}) such that

$$Z_{bts, b't's'} = \delta_{b,b'} Z_{bts, t's'}. \quad (248)$$

The averaged generating function now has the form

$$\langle \xi(j_+, j_-; s) \rangle = e^{i4\pi s/B} \int d(\tilde{\psi}, \psi) \int d(\tilde{Z}, Z) \text{sdet}(\mathbb{1} - \tilde{Z}Z) e^{-S(\tilde{\Psi}, \Psi, \tilde{Z}, Z)} \tag{249}$$

where

$$S(\tilde{\Psi}, \Psi, \tilde{Z}, Z) = \tilde{\Psi}_1 \begin{pmatrix} \mathbb{1} & Z \\ Z^\tau & \mathbb{1} \end{pmatrix} \Psi_1 + \tilde{\Psi}_2 \begin{pmatrix} z_+^* S^\dagger & \tilde{Z}^\tau \\ \tilde{Z} & z_- S \end{pmatrix} \Psi_2, \tag{250}$$

and we used $2\tilde{\Psi}_1 Z \Psi_1 = \tilde{\Psi}_1 Z \Psi_1 + \tilde{\Psi}_1 Z^\tau \Psi_1$, $2\tilde{\Psi}_2 \tilde{Z} \Psi_2 = \tilde{\Psi}_2 \tilde{Z} \Psi_2 + \tilde{\Psi}_2 \tilde{Z}^\tau \Psi_2$. Here, the indices 1, 2 refer to the auxiliary index x , and the matrix structure is in advanced-retarded space. Integrating the Gaussian fields $\tilde{\Psi}$ and Ψ we arrive at the (exact) representation

$$\langle \xi(j_+, j_-; s) \rangle = \int d(\tilde{Z}, Z) e^{-S(\tilde{Z}, Z)} \tag{251}$$

where the action is given by

$$S(\tilde{Z}, Z) = -\text{str} \log(\mathbb{1} - \tilde{Z}Z) + \frac{1}{2} \text{str} \log(\mathbb{1} - Z^\tau Z) + \frac{1}{2} \text{str} \log(\mathbb{1} - S z_+ \tilde{Z}^\tau z_-^* S^\dagger \tilde{Z}), \tag{252}$$

where the prefactor $e^{-i4\pi s/B}$ has cancelled.

What have we gained with expression (252) apart from an exact reformulation of the two-point correlator in terms of a complicated supersymmetric field theory? This question seems quite urgent since instead of an integral over B phase factors $e^{i\phi_b}$ we now have to deal with an integral over B pairs Z_b, \tilde{Z}_b of supermatrices – each of size 4×4 . The main difference of expression (252) with respect to the definition (224) is the direct coupling of the retarded and advanced sectors of the theory. In the defining expression the retarded sector contributes via (products of) periodic orbits of type $\text{tr}(T_*(\phi)S_*)^n$ while the advanced sector contributes further factors involving S_*^* instead. Such periodic orbits gather quasirandom phases. In contrast, after the colour-flavour transformation we obtain a theory which may be expressed as a sum over periodic orbits $\text{str}(\tilde{Z}^\tau S \tilde{Z} S^\dagger)^n$ of a quite different type where forward and backward scattering alternate. The phase of such an orbit can be expected to be less random. We will show in the next section how a saddle-point analysis can be used to extract the universal contribution to spectral statistics together with sufficient conditions for a dominance of universal spectral correlation over small deviations. It is not clear if the supersymmetric method may also be useful for graphs which deviate strongly from universality like the Neumann star graph.

9.2. The mean-field approximation and universality

The expressions (251) and (252) for the generating function of the two-point correlation function of the eigenphases of the quantum map of a quantum graph are an exact identity. While the integral over the modes Z, \tilde{Z} cannot be performed analytically in a closed form this expression is an ideal starting point for saddle-point analysis for large graphs $B \rightarrow \infty$. We will only be interested in the correlator for $s \ll B$ which allows us to expand the sources z_{\pm} defined in (233) as

$$z_{\pm} = \mathbb{1} - i \frac{2\pi}{B} \left(\sigma_3^{\text{bf}} j_{\pm} \mp \frac{s}{2} \right). \quad (253)$$

Higher orders will vanish in the limit $B \rightarrow \infty$. The resulting action can be written as a sum

$$\mathcal{S}(Z, \tilde{Z}) = \mathcal{S}_0(Z, \tilde{Z}) + \mathcal{S}_s(Z, \tilde{Z})s + \mathcal{S}_+(Z, \tilde{Z})j_+ + \mathcal{S}_-(Z, \tilde{Z})j_- \quad (254)$$

where

$$\begin{aligned} \mathcal{S}_0(Z, \tilde{Z}) &= -\text{str} \log(\mathbb{1} - \tilde{Z}Z) \\ &\quad + \frac{1}{2} \text{str} \log(\mathbb{1} - Z^{\tau}Z) + \frac{1}{2} \text{str} \log(\mathbb{1} - S\tilde{Z}^{\tau}S^{\dagger}\tilde{Z}) \\ \mathcal{S}_s(Z, \tilde{Z}) &= -i \frac{\pi}{B} \text{str} \frac{S\tilde{Z}^{\tau}S^{\dagger}\tilde{Z}}{\mathbb{1} - S\tilde{Z}^{\tau}S^{\dagger}\tilde{Z}} \\ \mathcal{S}_+(Z, \tilde{Z}) &= i \frac{\pi}{B} \text{str} \frac{\sigma_3^{\text{bf}}S\tilde{Z}^{\tau}S^{\dagger}\tilde{Z}}{\mathbb{1} - S\tilde{Z}^{\tau}S^{\dagger}\tilde{Z}} \\ \mathcal{S}_-(Z, \tilde{Z}) &= -i \frac{\pi}{B} \text{str} \frac{S\tilde{Z}^{\tau}\sigma_3^{\text{bf}}S^{\dagger}\tilde{Z}}{\mathbb{1} - S\tilde{Z}^{\tau}S^{\dagger}\tilde{Z}}. \end{aligned} \quad (255)$$

The saddle-point manifold (which is also called the zero-mode for reasons to become clear below) is equivalent to a mean-field description in which all system-dependent features (encoded in the matrix S) drop out. We will show that a reduction of the action (255) to the saddle-point manifold yields an exact expression for universal spectral two-point correlators. Later, in section 9.3 we will analyse the validity of this approximation and give sufficient conditions under which deviations from the mean-field can be neglected in the limit $B \rightarrow \infty$. We will assume time-reversal invariance $S_{\star} = S_{\star}^T$ (and thus $\mathcal{S} = S_{\star} \otimes \mathbb{1}^{\text{tr}} \equiv S_{\star}$) throughout – the effect of breaking time-reversal invariance will be discussed in section 9.4.

Let us start with the saddle-point equations for the action (255). Note that the source terms j_{\pm} are the only terms which break the supersymmetry – in other words $\xi(j_+ = 0, j_- = 0; s) = 1$ which can be seen directly from the defining expression (224). The two-point correlator as a derivative of the generating function with respect to the sources is a measure of the response of the supersymmetric action at $j_{\pm} = 0$ to breaking this symmetry. A saddle-point analysis is justified because the largest response can be expected where the supersymmetric action is small. This will be shown explicitly when we analyse the validity of this approximation.

The first saddle point equation at $j_{\pm} = 0$ and $s = 0$ takes the form

$$\frac{\delta \mathcal{S}_0}{\delta \tilde{Z}} = 0 = \text{str} \frac{\tilde{Z}}{\mathbb{1} - \tilde{Z}\tilde{Z}} - \text{str} \frac{Z^{\tau}}{\mathbb{1} - Z^{\tau}Z} \tag{256}$$

and has the solution

$$\tilde{Z} = Z^{\tau}. \tag{257}$$

The second saddle-point equation reads

$$\frac{\delta \mathcal{S}_0}{\delta \tilde{Z}} = 0 = \text{str} \frac{Z}{\mathbb{1} - ZZ^{\tau}} - \text{str} \frac{SZS^{\dagger}}{\mathbb{1} - SZS^{\dagger}Z^{\tau}} \tag{258}$$

where we have used explicitly the solution $Z = \tilde{Z}^{\tau}$ of the first saddle-point equation and the time-reversal invariance of the system via $S^{\tau} = S$. It is solved for field configurations Z that commute with the scattering matrix $[S, Z] = 0$. This implies equidistribution of the field Z over the bond index b . The saddle-point manifold is thus given by the mean-field configurations

$$Z_{0\ b\ ts, t's'} = Y_{ts, t's'} \quad \text{and} \quad \tilde{Z}_{0\ b\ ts, t's'} = \tilde{Y}_{ts, t's'}, \tag{259}$$

where $Y = \tilde{Y}^{\tau}$ is a 4×4 supermatrix. The commuting parts of Y obey $Y_{\text{BB}}^{\tau} = \tilde{Y}_{\text{BB}} = Y_{\text{BB}}^*$ and $Y_{\text{FF}}^{\tau} = \tilde{Y}_{\text{FF}} = -Y_{\text{FF}}^*$ while the non-commuting entries of Y are all independent integration variables. The fermion–fermion part is integrated over $\mathbb{R}^4 \simeq \mathbb{C}^2$ while boson–boson part is restricted to the compact region where all eigenvalues of $Y_{\text{BB}}^{\dagger} Y_{\text{BB}}$ are less than unity.

Reducing the action (255) to the zero-mode the first contribution vanishes exactly $\mathcal{S}_0(Z_0, \tilde{Z}_0) = 0$ while the remaining term becomes†

$$\mathcal{S}^{\text{GOE}}(\tilde{Y}, Y) = -i\pi \text{sstr} \frac{Y\tilde{Y}}{\mathbb{1} - Y\tilde{Y}} + i\pi j_+ \text{str} \frac{\sigma_3^{\text{bf}} Y\tilde{Y}}{\mathbb{1} - Y\tilde{Y}} - i\pi j_- \text{str} \frac{\sigma_3^{\text{bf}} \tilde{Y}Y}{\mathbb{1} - \tilde{Y}Y}. \tag{260}$$

Restricting the integration to the saddle-point manifold, we obtain

$$\langle \xi(j_+, j_-; s) \rangle \simeq \xi^{\text{GOE}}(j_+, j_-; s) \equiv \int d(\tilde{Y}, Y) e^{-\mathcal{S}^{\text{GOE}}(Y, \tilde{Y})}, \tag{261}$$

where the denotation ξ^{GOE} indicates that the matrix integral over Y obtains but an exact representation of the GOE correlation function. The right-hand side can be represented in more widely recognizable form. Let us define the 8×8 supermatrix

$$Q = \begin{pmatrix} \mathbb{1} & Y \\ \tilde{Y} & \mathbb{1} \end{pmatrix} \Sigma_z \begin{pmatrix} \mathbb{1} & Y \\ \tilde{Y} & \mathbb{1} \end{pmatrix}^{-1} = \begin{pmatrix} \mathbb{1} + 2Y\tilde{Y}/(\mathbb{1} - Y\tilde{Y}) & -2Y/(\mathbb{1} - \tilde{Y}Y) \\ 2\tilde{Y}/(\mathbb{1} - Y\tilde{Y}) & -\mathbb{1} - 2\tilde{Y}Y/(\mathbb{1} - \tilde{Y}Y) \end{pmatrix}, \tag{262}$$

†Note that for $s \neq 0$ or $j_{\pm} \neq 0$ the second saddle-point equation is changed which leaves only two saddle points in the reduced action (260). These can serve as starting points for perturbative treatments of the correlator. The loop expansion in the diagrammatic periodic-orbit treatment of the form-factor in section 8 is essentially equivalent to an expansion around the saddle-point $Z = \tilde{Z} = 0$. Keeping the full saddle-point manifold of \mathcal{S}_0 we are able to go beyond such perturbative expansions.

where $\Sigma_z = \begin{pmatrix} 1 & 0 \\ 0 & -1 \end{pmatrix}$. It is then a straightforward matter to show that the action $\mathcal{S}(\tilde{Y}, Y)$ takes the form of Efetov's action [208] for the GOE correlation function

$$\xi^{\text{GOE}}(j_+, j_-; s) = \int dQ e^{i\mathcal{S}(Q)} \quad (263)$$

where the measure is given by $dQ \equiv d(\tilde{Y}, Y)$,

$$\mathcal{S}(Q) = \frac{\pi}{2} \text{str}(Q - \Sigma_z) \hat{\epsilon} \quad (264)$$

and

$$\hat{\epsilon} = - \begin{pmatrix} j_+ \sigma_3^{\text{bf}} + \frac{s}{2} & 0 \\ 0 & j_- \sigma_3^{\text{bf}} - \frac{s}{2} \end{pmatrix}.$$

For a discussion of the integral (263), and the ways random-matrix predictions are obtained by integration over Q , we refer to the textbook [208].

9.3. Validity of the mean-field approximation and sufficient conditions for universality

So far, we have shown that the reduction of the exact supersymmetric field integral for the generating function ξ to an integral over the saddle-point manifold (that is over mean-field configurations) results in the GOE spectral correlations. However, we have not yet shown under which conditions this reduction is actually legitimate. Let us turn to this subject now.

In a full saddle-point analysis one writes the fields as a sum $Z = Z_0 + \delta Z$ where Z_0 parameterizes the saddle-point manifold and δZ describes the fluctuations around the saddle-point manifold. The reduction of the exact field integral to the integral over the saddle-point manifold is obtained by an expansion of the action $\mathcal{S}(Z, \tilde{Z})$ in the fluctuations δZ to second order and a subsequent Gaussian integral over these modes. In general this will lead to deviations from the mean-field result presented above. We will investigate under which conditions these deviations are small and vanish in the limit $B \rightarrow \infty$ of large graphs.

As we will show later it is sufficient for this purpose to consider the expansion of the full action (255) to second order in the fields Z ,

$$\begin{aligned} \mathcal{S}^{(2)}(Z, \tilde{Z}) = & \mathcal{S}_0^{(2)}(Z, \tilde{Z}) - \frac{i\pi s}{B} \text{str}(S \tilde{Z}^\tau S^\dagger \tilde{Z}) \\ & + \frac{i\pi j_+}{B} \text{str}(\sigma_3^{\text{bf}} S \tilde{Z}^\tau S^\dagger \tilde{Z}) - \frac{i\pi j_-}{B} \text{str}(S \tilde{Z}^\tau \sigma_3^{\text{bf}} S^\dagger \tilde{Z}), \end{aligned} \quad (265)$$

where

$$\begin{aligned} \mathcal{S}_0^{(2)}(Z, \tilde{Z}) = & \text{str} \left(\tilde{Z} Z - \frac{1}{2} Z^\tau Z - \frac{1}{2} S \tilde{Z}^\tau S^\dagger \tilde{Z} \right) \\ = & \frac{1}{2} \text{str} \left[(Z - \tilde{Z}^\tau)(\tilde{Z} - Z^\tau) + \tilde{Z}^\tau \tilde{Z} - S \tilde{Z}^\tau S^\dagger \tilde{Z} \right]. \end{aligned} \quad (266)$$

Physically, the quadratic action describes the joint propagation of a retarded and an advanced Feynman amplitude along the same path in configuration space. It thus carries information similar to that obtained from the diagonal approximation in the

periodic orbit approach. More precisely it is equivalent to neglecting deviations from $\tilde{K}_n^{\text{diag}} = 2n \text{tr } \mathcal{M}^n / B$ which come from repetitions and self-retracing orbits. The second order expansion is justified if the fluctuations of the fields Z are massively damped (in the sense that the matrix elements of Z effectively contributing to the integral are much smaller than unity). Under these conditions, the integration over matrix elements of Z may be extended to infinity and we obtain a genuine Gaussian integral. In fact, one is forced to extend the integration to infinity in order to preserve $\xi(j_{\pm}; s) = 1$ at every level of approximation.

The eigenvalues m_{ℓ} of the quadratic form appearing in $\mathcal{S}_0^{(2)}$ determine the damping m_{ℓ} – or the *mass*, in field theoretical jargon – inhibiting fluctuations of an eigenmode. As indicated by its name, the zero-mode Z_0 carries zero mass. With the observation that the quadratic form involves the classical map $\mathcal{M}_{\star bb'} = |S_{\star bb'}|^2$ of the graph via

$$\text{str } S \tilde{Z}^{\tau} S^{\dagger} \tilde{Z} \equiv \text{str} \sum_{bb'} S_{\star bb'} \tilde{Z}_{b'}^{\tau} S_{\star bb'}^* \tilde{Z}_b = \text{str} \sum_{bb'} \tilde{Z}_b M_{\star bb'} \tilde{Z}_{b'} \tag{267}$$

the action is easily diagonalized by an orthogonal transformation $Z_b = \sum_{b'} O_{bb'} Z'_{\ell}$ (we will drop the primes of Z'_{ℓ} in the sequel) and can then be written as a sum over separate contributions

$$\mathcal{S}^{(2)}(Z, \tilde{Z}) = \sum_{\ell=1}^B \mathcal{S}_{\ell}^{(2)}(Z_{\ell}, \tilde{Z}_{\ell}) \tag{268}$$

where $\mathcal{S}_{\ell}^{(2)}$ is the contribution

$$\begin{aligned} \mathcal{S}_{\ell}^{(2)}(Z_{\ell}, \tilde{Z}_{\ell}) &= \frac{1}{2} \text{str} [(Z_{\ell} - \tilde{Z}_{\ell}^{\tau})(\tilde{Z}_{\ell} - Z_{\ell}^{\tau}) + (1 - \nu_{\ell}) \tilde{Z}_{\ell}^{\tau} \tilde{Z}_{\ell}] \\ &\quad - \nu_{\ell} \frac{\pi i}{B} \text{str} [s \tilde{Z}_{\ell}^{\tau} \tilde{Z}_{\ell} - (j_+ \sigma_3^{\text{bf}} \tilde{Z}_{\ell}^{\tau} - j_- \tilde{Z}_{\ell}^{\tau} \sigma_3^{\text{bf}}) \tilde{Z}_{\ell}] \end{aligned} \tag{269}$$

of the eigenmode of the classical map \mathcal{M} with eigenvalue ν_{ℓ} . Let us now focus on the integral over one mode $Z_{\ell}, \tilde{Z}_{\ell}$. We can split the action of a single mode into contributions from a pair fields $Z_{\ell}, \tilde{Z}_{\ell}$ that satisfies the first saddle-point equation $Z = \tilde{Z}^{\tau}$ and contributions violating it. One can show that only the configurations $Z = \tilde{Z}^{\tau}$ contribute non-trivially while the integral over configurations violating this condition just give a factor unity.† We are left with half the number of integration variables and an action $\mathcal{S}_{\ell}^{(2)} = (1 - \nu_{\ell}/2) \text{str } Z \tilde{Z} = (m_{\ell}/2) \text{str } Z \tilde{Z}$ for vanishing sources $j_{\pm} = s = 0$. In this expression we see that the eigenvalues ν_{ℓ} of the classical map are related to the masses $m_{\ell} = 1 - \nu_{\ell}$ of the supersymmetric field theory. Performing the

†For the integral over anticommuting numbers this can easily seen from the action (269) where the shifts $Z_{\ell, \text{BF/FB}} \mapsto Z_{\ell, \text{BF}} - \tilde{Z}_{\ell, \text{BF/FB}}^{\tau}$ decouple the anticommuting parts of Z_{ℓ} from the anticommuting part of \tilde{Z} . For the commuting entries one can write down the integral over all real and imaginary parts of the entries $Z_{\ell, \text{BB/FF}}$ and $\tilde{Z}_{\ell, \text{BB/FF}}$ – shifting the entries and changing the contours of integration leads to a similar decoupling such that the action at $s = j_{\pm} = 0$ is of the form $\mathcal{S}_{\ell} = (1/2) \text{str} [+(1 - \nu_{\ell}) \tilde{Z}_{\ell, \text{even}} Z_{\ell, \text{even}}]$ where $Z_{\ell, \text{even}} = \tilde{Z}_{\ell, \text{even}}^{\tau}$ and $Z_{\ell, \text{odd}} = -\tilde{Z}_{\ell, \text{odd}}^{\tau}$ and the terms at $s \neq 0$ and $j_{\pm} \neq 0$ only involve $Z_{\ell, \text{even}}$.

remaining integral we will see that the mass m_ℓ sets the scale for the response to the sources j_\pm which break the supersymmetry of the model. That is, a large mass m_ℓ corresponds to a strongly damped contribution to the two-point correlator. The remaining Gaussian integral over one mode gives

$$I_\ell = \int \mathbf{d}(Z_\ell, \tilde{Z}_\ell) e^{-S_\ell^{(2)}(Z_\ell, \tilde{Z}_\ell)} \\ = \frac{\left[1 + i \frac{\pi(m_\ell - 1)(s + j_\Sigma)}{m_\ell B}\right]^2 \left[1 + i \frac{\pi(m_\ell - 1)(s - j_\Sigma)}{m_\ell B}\right]^2}{\left[1 + i \frac{\pi(m_\ell - 1)(s + j_\Delta)}{m_\ell B}\right]^2 \left[1 + i \frac{\pi(m_\ell - 1)(s - j_\Delta)}{m_\ell B}\right]^2} \quad (270)$$

where $j_\Delta = j_+ - j_-$ and $j_\Sigma = j_+ + j_-$. The generating function in this approximation is just the product

$$\xi^{(2)}(j_+, j_-; s) = \prod_{\ell=1}^B I_\ell \quad (271)$$

over the contributions from each mode. Differentiating with respect to the sources j_\pm we finally obtain the quadratic approximation to the correlation function,

$$\tilde{R}_2^{(2)}(s) = \sum_{\ell=1}^B \frac{1}{8\pi^2} \operatorname{Re} \left. \frac{\partial^2}{\partial j_+ \partial j_-} I_\ell \right|_{j_\pm=0} \\ = \sum_{\ell=1}^B \frac{(m_\ell - 1)^2 (m_\ell^2 B^2 - \pi^2 (m_\ell - 1)^2 s^2)}{(m_\ell^2 B^2 + \pi^2 (m_\ell - 1)^2 s^2)^2}. \quad (272)$$

The contribution of the zero mode ($m_1 = 0$) is given by $-1/\pi^2 s^2$ and coincides with the diagonal approximation to the GOE correlation function. Later on we shall see that in the case of broken time reversal invariance, one half of the matrix elements of Z_0 become massive implying that the contribution of the zero mode reduces to the GUE expression $-1/2\pi^2 s^2$.

In the limit $B \rightarrow \infty$, the s -dependence of the contribution of massive modes to the correlation function is negligible for our purpose, i.e. individual modes contribute maximally as $\sim (m_\ell - 1)^2 / 2m_\ell^2 B^2 \sim (m_\ell B)^{-2}$. Only modes of mass $m_\ell \sim B^{-\alpha}$, where α is a non-vanishing positive exponent, can survive the limit $B \rightarrow \infty$. The contribution of an individual mode is negligible if the exponent $0 \leq \alpha < 1$. There are at most $\mathcal{O}(B)$ nearly massless modes, and we are led to require that $B^{2\alpha-1}$ must vanish in the limit of large graphs $B \rightarrow \infty$, or that $0 \leq \alpha < 1/2$.

This is a slightly stronger condition than the one discussed within the context of the periodic-orbit analysis of section 8.2, where we have seen that for fixed τ the form factor is universal if $0 \leq \alpha < 1$. The two results are fully consistent as the condition $0 \leq \alpha < 1/2$ implies the stronger statement that deviations to the two-point correlator vanish uniformly in s .

In the intermediate region $1/2 \leq \alpha < 1$ – permissible by Tanner’s criterion – non-universal corrections vanish only if the number r of classical modes with a small mass remains constant (or does not grow too fast) such that $B^2 \Delta_g^2 / r \rightarrow \infty$. If, however, the number of low energy modes is extensive, $r \sim B$, the stricter condition $0 \leq \alpha < 1/2$ has to be imposed. An example of a graph with $\mathcal{O}(B)$ almost massless

modes is the Neumann star graph, for which all the classical modes (apart from the zero-mode $m_1 = 0$) have a mass $m \sim 1/B$. The Neumann star thus strongly violates the condition for universal GOE statistics – as a single mode with mass $m \sim 1/B$ is already sufficient to give non-vanishing corrections.

Above we have shown that in the limit $B \rightarrow \infty$ only the zero mode effectively contributes to the correlation function (provided, of course, the master condition $\Delta_g \sim B^{-\alpha}$ is met). While the zero mode integral must be performed rigorously, all other modes are strongly overdamped and may be treated in a quadratic approximation. This is the a posteriori justification for the quadratic approximation on which our analysis of the mass spectrum was based.

9.4. Breaking time-reversal invariance

The analysis above applies to time reversal invariant graphs. In this section we discuss what happens if time reversal invariance gets gradually broken. We assume full universality, i.e. $B\Delta_g^2 \gg 1$ such that only the zero-mode contributes to $R_2(s)$. Our aim is to derive a condition for the crossover between GOE-statistics in the time-reversal invariant case and GUE-statistics for fully broken time-reversal invariance.

The substructure of the Z -fields with $Z = \tilde{Z}^T$ in time reversal space is given by

$$Z_b = \begin{pmatrix} Z_{\mathbf{D}b} & Z_{\mathbf{C}b} \\ \tilde{Z}_{\mathbf{C}b}^T \sigma_3^{\mathbf{BF}} & \tilde{Z}_{\mathbf{D}b}^T \end{pmatrix}, \quad \tilde{Z}_b = \begin{pmatrix} \tilde{Z}_{\mathbf{D}b} & \sigma_3^{\mathbf{BF}} Z_{\mathbf{C}b}^T \\ \tilde{Z}_{\mathbf{C}b} & Z_{\mathbf{D}b}^T \end{pmatrix}, \quad (273)$$

where $Z_{\mathbf{D}/\mathbf{C}b}$ and $\tilde{Z}_{\mathbf{D}/\mathbf{C}b}$ are 2×2 supermatrices subject to the constraint $\tilde{Z}_{\mathbf{D}/\mathbf{C}b\mathbf{B}} = Z_{\mathbf{C}/\mathbf{D}b\mathbf{B}}^*$ and $Z_{\mathbf{C}/\mathbf{D}b\mathbf{F}} = -Z_{\mathbf{C}/\mathbf{D}b\mathbf{F}}^*$, while the non-commuting entries of these matrices are independent integration variables. The subscripts $\mathbf{D}(\mathbf{C})$ allude to the fact that in disordered fermion systems, the modes $Z_{\mathbf{D}}$ ($Z_{\mathbf{C}}$) generate the so-called diffusion (cooperon) excitations. Physically, the former (latter) describe the interference of two states as they propagate along the same path (the same path yet in opposite direction) in configuration space. Cooperon modes are susceptible to time reversal invariant breaking perturbations.

Substituting this representation into the quadratic action, we obtain

$$\mathcal{S}^{(2)} = \text{str}(\tilde{Z}_{\mathbf{D}}(\mathbb{1} - \mathcal{M}_\star)Z_{\mathbf{D}} + \tilde{Z}_{\mathbf{C}}(\mathbb{1} - \mathcal{R}_\star)Z_{\mathbf{C}}) \quad (274)$$

for the action of the zero mode at $j_\pm = s = 0$. Here, $\mathcal{M}_{\star bb'} = \{|S_{\star b, b'}|^2\}$ is the classical evolution map and $\mathcal{R}_{\star bb'} = S_{\star b, b'} S_{\star b' b}^*$. For broken time-reversal invariance $\mathcal{M}_\star \neq \mathcal{R}_\star$ and the symmetry of the action in time reversal invariance space gets lost.

Noting that $B = \sum_{b, b'} |S_{\star bb'}|^2$, we conclude that the cooperon zero mode $Z_{\mathbf{C}, b} = Y_{\mathbf{C}}$ acquires a mass term $\sim B m_{\mathbf{C}} \text{str}(Y_{\mathbf{C}} \tilde{Y}_{\mathbf{C}})$, where the coefficient

$$\begin{aligned} m_{\mathbf{C}} &= \frac{1}{B} \left| \sum_{bb'} S_{\star bb'} (S_{\star bb'}^* - S_{\star b' b}^*) \right| \\ &= \frac{1}{B} \left| \text{tr} S_\star^\dagger (S - S^T) \right| \end{aligned} \quad (275)$$

measures the degree of the breaking of the symmetry $S = S^T$. We have encountered the cooperon mass before in section 8.2 as the inverse time $n_T = 1/m_{\mathbf{C}}$ on which

a pair of time reversed orbits decays in the diagonal approximation. The cooperon mode may be neglected once $Bm_C \rightarrow \infty$ as $B \rightarrow \infty$.

9.5. On higher order correlation functions and the gap condition

The supersymmetry method described above can be generalized in a straightforward manner to higher order correlation functions with a generating function that contains an appropriate number of spectral determinants ζ_B in its numerator and denominator. A reduction to a saddle-point manifold gives the universal correlations known from random-matrix theory. It all works the same way as for the two-point correlator and the condition that this reduction becomes exact in the limit of large graphs also remains unchanged. For a finite graph this proves universal spectral correlators up to small deviations in correlators of order n where $n \ll B$.

Acknowledgments

We are grateful to Alexander Altland, Gregory Berkolaiko, Peter Braun, Fritz Haake, Jonathan Keating, Tsampikos Kottos, Marek Kuś, Felix von Oppen, Holger Schanz, Michail Solomyak, and Karol Życzkowski for discussions and help through the years. Both authors would like to thank the School of Mathematics at Bristol University for the hospitality extended during the period this manuscript was prepared. Support is acknowledged from the Minerva foundation, the Einstein (Minerva) Center and The Minerva Center for non-linear physics (Weizmann Institute), the Israel Science Foundation, the German-Israeli Foundation, the EPSRC grant GR/T06872/01 and the Institute of Advance Studies, Bristol University.

Appendix A: The symmetry classes of quantum systems

Based on earlier ideas of Wigner [187], Dyson introduced a three-fold classification of quantum systems according to their behaviour under time-reversal, spin and rotational invariance [188–190]. This symmetry classification turned out to be very useful, for instance in semiclassical, disordered and random-matrix approaches to complex quantum systems. In this appendix we give a short summary of this three-fold symmetry classification and a recent extension to a ten-fold classification which is related with the ten classes of Riemannian symmetric spaces. We only present a description of the ten symmetry classes and refer to the literature [191] for a proof that this classification is complete. Table A1 summarizes this appendix.

In the literature the symmetry classes are often denoted by the Gaussian random-matrix ensemble of Hermitian matrices respecting the corresponding symmetry restrictions. Such a notation is misleading and often quite confusing. Here, we stick to the notation introduced by Zirnbauer [191].

According to a theorem by Wigner a symmetry of a physical system is represented in quantum mechanics either by a unitary operator or by an anti-unitary operator that commutes (or anticommutes) with the Hamiltonian operator H . Unitary symmetry operators which commute with H are associated with constants

Table 1. The ten symmetry classes of quantum systems. If a symmetry class obeys time-reversal symmetry or a spectral mirror symmetry the entry ± 1 in the corresponding column indicates if the symmetry operator squares to $\pm \mathbb{1}$. The entry 0 indicates that the corresponding symmetry is broken. The last column gives the corresponding Riemannian symmetric space (of compact type).

symmetry class	\mathcal{T}	\mathcal{P}	\mathcal{C}	symmetric space
A	0	0	0	$U(N)$
AI	+1	0	0	$U(N)/O(N)$
AII	-1	0	0	$U(2N)/Sp(N)$
$AIII$	0	+1	0	$U(p+q)/U(p) \times U(q)$
BDI	+1	+1	+1	$SO(p+q)/SO(p) \times SO(q)$
CII	-1	+1	-1	$Sp(p+q)/Sp(p) \times Sp(q)$
C	0	0	-1	$Sp(N)$
CI	+1	-1	-1	$Sp(N)/U(N)$
$BD(D)$	0	0	+1	$SO(N)$
$DIII$	-1	-1	+1	$SO(2N)/U(N)$

of the motion. In the eigenbasis of such a unitary symmetry operator the Hamiltonian operator is represented by a block diagonal matrix – each block connected to one eigenvalue of the symmetry operator which serves as a quantum number of the state. In the following we will always assume that any unitary symmetry has been used to reduce the Hilbert space.

Anti-unitary symmetry operators which commute with H do not lead to a constant of motion, yet they affect the form of the representation of the Hamiltonian operator in a suitable basis. More importantly, they have an effect on statistical properties of the spectrum and of the wavefunctions in complex quantum systems. The same is true for (unitary and anti-unitary) symmetry operators that anticommute with H .

Though every symmetry of a physical system is represented by a unitary or anti-unitary operator in quantum mechanics the reverse is not true. An arbitrary unitary or anti-unitary operator \mathcal{U} in general does not qualify as a symmetry of the system. E.g. for any Hamiltonian operator H one may uniquely define a anti-unitary operator \mathcal{A} by its action $\mathcal{A} \sum_n a_n |n\rangle = \sum_n a_n^* |n\rangle$ in the eigenbasis $H|n\rangle = E_n|n\rangle$ of the Hamiltonian operator. Trivially, \mathcal{A} commutes with the Hamiltonian operator $[\mathcal{A}, H] = 0$ without being connected to any symmetry of the system. In contrast a symmetry operator can be defined representation independent which includes that it can be defined independent of the value one formally assigns to \hbar . This immediately rules out the trivial operator \mathcal{A} since the eigenbasis will generally depend on the value of \hbar .

A.1. Time-reversal invariance

Consider a physical system represented by the Hamiltonian operator H . The system is **time-reversal invariant** if an anti-unitary symmetry operator \mathcal{T} , the (*generalized*) **time-reversal operator**, exists which commutes with the Hamiltonian operator

$$[\mathcal{H}, \mathcal{T}] = 0. \quad (\text{A1})$$

It can be shown [139, 196] that such an operator obeys either

$$\mathcal{T}^2 = \mathbb{1} \quad \text{or} \quad \mathcal{T}^2 = -\mathbb{1}. \quad (\text{A2})$$

and \mathcal{T} reverses the direction of time in the Schrödinger equation.

It follows that there are three symmetry classes, the *Wigner–Dyson classes* connected to time-reversal invariance:

Class *A*: Systems with broken time–reversal invariance.

Class *AI*: Time-reversal invariant systems and $\mathcal{T}^2 = \mathbb{1}$.

Class *AII*: Time-reversal invariant systems and $\mathcal{T}^2 = -\mathbb{1}$.

A particle in a potential described by the Hamiltonian operator $H = (\mathbf{p}^2/2m) + V(x)$ is time-reversal invariant. The corresponding time-reversal operator \mathcal{T}_{AI} is defined to be the anti-unitary operator obeying $\mathcal{T}_{AI} \mathbf{x} \mathcal{T}_{AI}^{-1} = \mathbf{x}$ and $\mathcal{T}_{AI} \mathbf{p} \mathcal{T}_{AI}^{-1} = -\mathbf{p}$. In the coordinate representation \mathcal{T}_{AI} is represented as complex conjugation of the wavefunction $\langle \mathbf{x} | \mathcal{T}_{AI} | \psi \rangle = \langle \mathbf{x} | \psi \rangle^*$. Obviously, $\mathcal{T}_{AI}^2 = \mathbb{1}$ and such systems belong to class *AI*.

For particles with spin $s = 1/2$ and broken spin rotation invariance one may define the time-reversal operator \mathcal{T}_{AII} , which acts as \mathcal{T}_{AI} on \mathbf{x} and \mathbf{p} and additionally obeys $\mathcal{T}_{AII} s \mathcal{T}_{AII}^{-1} = -s$. For this operator $\mathcal{T}_{AII}^2 = -\mathbb{1}$ and the system is in class *AII* if $[H, \mathcal{T}_{AII}] = 0$.

In both cases time-reversal is broken by the presence of a magnetic field. Thus a particle in a magnetic field generally belongs to class *A*. Note however that we made a special choice of the time-reversal operator in our examples.

A.2. *Kramers' degeneracy*

The energy spectrum of any physical system which is time-reversal invariant with $\mathcal{T}^2 = -\mathbb{1}$ is (at least) two-fold degenerate. If $|n\rangle$ (normalized such that $\langle n|n\rangle = 1$) solves the stationary Schrödinger equation $H|n\rangle = E_n|n\rangle$ so does $\mathcal{T}|n\rangle$. Since $\langle \mathcal{T}n | \mathcal{T}n \rangle = \langle n | n \rangle^* = 1$ the state $\mathcal{T}|n\rangle$ does not vanish. At the same time $|n\rangle$ and $\mathcal{T}|n\rangle$ are orthogonal $\langle n | \mathcal{T}n \rangle = \langle \mathcal{T}n | \mathcal{T}^2 n \rangle^* = -\langle n | \mathcal{T}n \rangle = 0$ such that E_n is two-fold degenerate.

A.3. *Chiral symmetries and charge conjugation symmetries*

We will now consider certain unitary symmetry operators \mathcal{P} and anti-unitary operators \mathcal{C} which anticommute with the Hamiltonian operator,

$$[H, \mathcal{P}]_+ = 0 \quad \text{or} \quad [H, \mathcal{C}]_+ = 0. \quad (\text{A3})$$

One may have to shift the Hamiltonian operator by a constant to reveal such a kind of symmetry which is tacitly assumed in the following. Equation (A3) leads to an energy spectrum which is symmetric. If E is in the spectrum, so is $-E$. Since the Hamiltonian operator of a proper quantum mechanical system should be bounded from below such symmetries either occur in systems with finite-dimensional Hilbert space (e.g. a finite number of coupled spins) or in the framework of one-particle

equations of a field theory. Examples are the Dirac and Bogoliubov–de-Gennes equations which are formally equivalent to the Schrödinger equation, that is they can be written in the form $i\hbar(\partial/\partial t)|\Psi(t)\rangle = H|\Psi(t)\rangle$. The negative part of spectrum of these operators is related to positive energy excitations of the corresponding field theory. Since we will not consider the complete field theory here we will call the one-particle operator H the Hamiltonian operator of the system.

A **chiral symmetry operator** \mathcal{P} is unitary and obeys $\mathcal{P}^2 = \mathbb{1}$. A physical system with a chiral symmetry can have an additional time-reversal invariance. In that case the time-reversal operator \mathcal{T} and the chiral symmetry operator \mathcal{P} are required to commute $[\mathcal{T}, \mathcal{P}] = 0$. Thus there are three **chiral symmetry classes**:

Class AIII: Systems with a chiral symmetry and broken time–reversal invariance.

Class BDI: Time-reversal invariant systems with a chiral symmetry and $\mathcal{T}^2 = \mathbb{1}$.

Class CII: Time-reversal invariant systems with a chiral symmetry and $\mathcal{T}^2 = -\mathbb{1}$.

The chiral symmetry classes have first been considered in quantum chromodynamics as Dirac particles in a random gauge potential [233, 234]. They also occur for Bogoliubov–de-Gennes quasiparticle excitations in the certain types of disordered superconductors [249].

Finally, a **charge conjugation symmetry** is described by an anti-unitary operator \mathcal{C} that anticommutes with the system Hamiltonian operator and which obeys either $\mathcal{C}^2 = \mathbb{1}$ or $\mathcal{C}^2 = -\mathbb{1}$. Accounting for the possibility of additional time-reversal invariance there are six symmetry classes which have a charge conjugation symmetry all of which can be found in certain types of disordered superconductors. Two of them have been presented as the time-reversal invariant chiral symmetry classes. Indeed, if \mathcal{P} is a chiral symmetry operator and \mathcal{T} with $[\mathcal{P}, \mathcal{T}] = 0$ a time-reversal operator $\mathcal{C} = \mathcal{P}\mathcal{T}$ is a charge conjugation operator with $[\mathcal{C}, \mathcal{T}] = 0$ and $\mathcal{C}^2 = \mathcal{T}^2$. The remaining four symmetry classes have not been given any satisfactory and consistent name. We will call them **charge conjugation symmetry classes** though the symmetry operator \mathcal{C} may not be related to any physical charge conjugation (see below). In any case the distinction between the three chiral symmetry classes and the four charge conjugation classes has historical origins and should not be taken as a mathematical or physical relevant distinction. The four charge conjugation symmetry classes are:

Class C: Systems with broken time-reversal invariance and a charge conjugation symmetry obeying $\mathcal{C}^2 = -\mathbb{1}$.

Class CI: Time-reversal invariant systems with a charge conjugation symmetry obeying both $\mathcal{T}^2 = \mathbb{1}$ and $\mathcal{C}^2 = -\mathbb{1}$.

Class BD: Systems with broken time–reversal invariance and a charge conjugation symmetry obeying $\mathcal{C}^2 = \mathbb{1}$. This symmetry class is denoted as class D if the Hilbert space has even dimension.

Class DIII: Time-reversal invariant systems with a charge conjugation symmetry obeying both $\mathcal{T}^2 = -\mathbb{1}$ and $\mathcal{C}^2 = \mathbb{1}$.

They have first been discussed in connection to hybrid normal-conducting–superconducting structures and disordered superconductors [235, 236].

Note that the notation for these symmetries stems from the systems for which they have first been discussed in detail where they were connected to the charge conjugation of a quasiparticle or to the chirality of a Dirac particle. In general these symmetries need not have this physical interpretation: any of the seven symmetry classes can be realized by a Hamiltonian operator for two coupled spins $\mathbf{S}_{1,2}$ with spin quantum numbers $s_{1,2}$ where the (generalized) chiral symmetry operator or (generalized) charge conjugation operator are not related to the chirality or electric charge of a particle.

A.4. The symmetry classes for quantum graphs

The symmetries of the Hamiltonian operator H of a physical system can be translated to symmetries for the quantum evolution map [140] $\mathcal{U}_B(k) = T(k)S(k)$. It will be more convenient to define an equivalent quantum evolution map by

$$\mathcal{U}_{B_{1/2}}(k) = T(k/2)S(k)T(k/2) \quad (\text{A4})$$

and discuss this symmetrized variant. Here, the right factor $T(k/2)$ propagates the wavefunction from the centre of a directed bond to the next vertex where it is scattered by $S(k)$ to the next directed bond. Finally, the left factor $T(k/2)$ propagates the wavefunction along the next directed bond to its centre. Some symmetry classes are more naturally discussed for graphs with a multicomponent wavefunction (spin or particle-hole components).

A time-reversal operator \mathcal{T} acts on the evolution map as

$$\mathcal{U}_{B_{1/2}}(k) \mapsto \mathcal{T}[\mathcal{U}_{B_{1/2}}(k)] = \hat{\mathcal{T}}\mathcal{U}_{B_{1/2}}(k)^*\hat{\mathcal{T}}^\dagger \quad (\text{A5})$$

where $\hat{\mathcal{T}}$ is a unitary matrix with the additional property $\hat{\mathcal{T}}^*\hat{\mathcal{T}} = \pm\mathbb{1}$. Time-reversal invariance of a graph means that the evolution map is equal to its time-reversed under the action of \mathcal{T}

$$\mathcal{U}_B(k) = \mathcal{T}[\mathcal{U}_B(k)^\dagger] = \hat{\mathcal{T}}\mathcal{U}_B(k)^T\hat{\mathcal{T}}^{-1}. \quad (\text{A6})$$

For symmetry class *AI* one requires $\hat{\mathcal{T}}^*\hat{\mathcal{T}} = \mathbb{1}$ whereas symmetry class *AII* requires $\hat{\mathcal{T}}^*\hat{\mathcal{T}} = -\mathbb{1}$. The natural choice for the time-reversal symmetry operator in symmetry class *AI* is given by

$$\hat{\mathcal{T}} = \sigma_1^{\text{dir}} \quad (\text{A7})$$

which acts like the corresponding Pauli-matrix on the direction indices ω while bond indices b remain unaffected. Equivalently, the evolution map of a time-reversal invariant graph in class *AI* has the property

$$\mathcal{U}_B(k)_{1/2\alpha\beta} = \mathcal{U}_B(k)_{1/2\hat{\beta}\hat{\alpha}}. \quad (\text{A8})$$

Time-reversal invariant graphs with $\mathcal{T}^2 = -\mathbb{1}$ (class *AII*) can be realized as graphs with spin $s = 1/2$ and

$$\hat{\mathcal{T}} = \sigma_1^{\text{dir}} \otimes \sigma_2^{\text{spin}}. \quad (\text{A9})$$

Thus time-reversal involves a change in direction and in spin.

The chiral and charge conjugation symmetry classes on graphs can all be realized by either putting the Bogoliubov–de-Gennes or Dirac equations on the graph.

Thus, they always involve electron and hole components of a wavefunction (one needs an additional spin $\sigma = \pm 1/2$ in some classes). We will not give a complete construction of the symmetries for all seven classes, for the classes *C* and *CI* an example for a star graph is given in section 8.5.

A chiral symmetry operator \mathcal{P} acts on the evolution map as

$$\mathcal{U}_{B_{1/2}}(E) \mapsto \mathcal{P}[\mathcal{U}_{B_{1/2}}(E)] = \hat{\mathcal{P}}\mathcal{U}_{B_{1/2}}(-E)\hat{\mathcal{P}}^{-1} \quad (\text{A10})$$

where $\hat{\mathcal{P}}$ is a unitary matrix with $\hat{\mathcal{P}}^2 = \mathbb{1}$ and E is the energy. A quantum graph has a chiral symmetry if

$$\mathcal{U}_{B_{1/2}}(E) = \mathcal{P}[\mathcal{U}_{B_{1/2}}(E)^\dagger] = \hat{\mathcal{P}}\mathcal{U}_B(-E)^\dagger\hat{\mathcal{P}}^{-1} \quad (\text{A11})$$

where taking $\mathcal{U}_B(-E)^\dagger$ reflects the anticommuting character of the Hamiltonian operator. It is easy to see from equation (A11) that the corresponding energy spectrum is symmetric. If $\mathcal{U}_{B_{1/2}}(E)$ has an eigenvalue unity and there is a chiral symmetry $\mathcal{U}_{B_{1/2}}(-E)$ also has an eigenvalue unity.

Finally, a charge conjugation symmetry operator \mathcal{C} acts on the evolution map as

$$\mathcal{U}_{B_{1/2}}(E) \mapsto \mathcal{C}[\mathcal{U}_{B_{1/2}}(E)] = \hat{\mathcal{C}}\mathcal{U}_{B_{1/2}}(-E)^*\hat{\mathcal{C}}^{-1} \quad (\text{A12})$$

where $\hat{\mathcal{C}}$ is a unitary matrix with $\hat{\mathcal{C}}^2 = \pm\mathbb{1}$. A quantum graph with a charge conjugation symmetry obeys

$$\mathcal{U}_{B_{1/2}}(E) = \mathcal{C}[\mathcal{U}_{B_{1/2}}(E)^\dagger] = \hat{\mathcal{C}}\mathcal{U}_{B_{1/2}}(-E)^T\hat{\mathcal{C}}^{-1}. \quad (\text{A13})$$

Note that we have not used the momentum k but the energy E as the argument of the evolution map. For the chiral and charge conjugation symmetry classes one should be aware that the momentum is in general not a constant of motion and thus the energy has to be used. For example, in the Bogoliubov–de-Gennes equation an electron and a hole moving in the positive x -direction at energy E are described by the wavefunctions

$$\psi^{\text{electron}}(x) \sim \begin{pmatrix} 1 \\ 0 \end{pmatrix} e^{i\sqrt{\mu+E}x} \quad \text{and} \quad \psi^{\text{hole}}(x) \sim \begin{pmatrix} 0 \\ 1 \end{pmatrix} e^{-i\sqrt{\mu-E}x} \quad (\text{A14})$$

where μ is the Fermi energy. If $\mu \gg E$ one may expand $k_\pm = \sqrt{\mu \pm E} \approx \sqrt{\mu} \pm E/2\sqrt{\mu} = k_F \pm \delta k$. In the limit $\mu/E \rightarrow \infty$ one may thus replace $E \mapsto \delta k$ and the symmetry relations of the evolution map hold for δk .

Appendix B: Some relevant results of random-matrix theory

Random matrices were first applied to physical systems by Wigner and Dyson [187–190] as a model for complex nuclei. Since then, random-matrix theory has had an enormous impact on various areas in physics and is today one of the main tools to describe statistical properties of complex quantum systems. There are many books and reviews on random-matrix theory [185, 203, 206, 207] and its applications in physics. In this appendix we summarize some of relevant results in the context of this review. We will neither discuss the various methods to calculate properties of

random matrices nor give any proof of the presented results, and we will only summarize results on the Gaussian ensembles of Hermitian matrices.

B.1. *Universality and universality classes*

The success of random-matrix theory relies on the fact that many statistical properties of the spectrum and of the wavefunctions for a large class of complex quantum systems are universal (system independent) yet not trivial. When properly scaled, they only depend on some general properties of the system such as time-reversal invariance. In Appendix A we have described the ten symmetry classes of quantum systems which was completely general. Here, we relate these symmetries to the statistical properties of complex quantum systems described by a random Hamiltonian operator.

A *universality class* is a subset of a symmetry class which shares the same statistical properties – or at least some universal correlation functions up to small system dependent deviations. In general there are many universality classes within one symmetry class. Each of them can be described (and defined) by some ensemble of random matrices in the limit of large matrices. Usually there will be a lot of different ensembles that share the same universal statistical properties [250].

We will focus on the so-called *ergodic universality classes* that can be described by Gaussian ensembles of Hermitian matrices in each of the ten symmetry classes which describe strongly chaotic systems or disordered systems in the delocalized regime. For each of the three Wigner–Dyson symmetry classes (A , AI , and AII) and for two of the charge conjugation symmetry classes (C and CI) there is a unique ergodic universality class. In contrast for the other symmetry classes there is an additional parameter. For instance, the symmetry class BD can be realized in an even or in an odd dimensional Hilbert space and this will effect the spectral statistics. In the odd-dimensional case the symmetry fixes one eigenvalue at $E=0$ which changes the statistical properties of the spectrum near $E=0$ while in the even-dimensional case (also denoted as class D) the charge conjugation symmetry does not fix a vanishing eigenvalue. Similarly, a chiral symmetry operator may fix some integer number $\nu = 0, 1, 2$ of eigenvalues $E=0$. The number ν is known as the topological quantum number and is important for applications of random-matrix theory to quantum chromodynamics. We will only present the results for those ergodic universality classes where no eigenvalue $E=0$ is fixed by the symmetry operators \mathcal{P} or \mathcal{C} (thus $\nu=0$ for the chiral classes).

B.2. *The Gaussian ensembles of random-matrix theory*

A Gaussian random-matrix ensemble [185] consists of $N \times N$ Hermitian matrices $H = H^\dagger$ with a Gaussian distribution

$$P(H) dH = e^{-\lambda \operatorname{tr} H^2} dH. \quad (\text{B1})$$

This form is the same for all ergodic universality classes. However the symmetries of the Hamiltonian operator restrict the number of independent matrix elements. The flat measure $dH = N^{-1} dH_{11} d\operatorname{Re}(H_{12}) d\operatorname{Im}(H_{12}) \cdots$ runs over all independent real and imaginary parts of the Hermitian matrix H with the additional symmetry

requirements of the symmetry class. The real parameter $\lambda > 0$ rescales the spectrum of the system and \mathcal{N} is a normalization constant.

If there are no further symmetry restrictions on $H = H^\dagger$ the ensemble is called the **Gaussian unitary ensemble** (GUE). It describes ergodic systems with broken time-reversal invariance in class *A*. Time-reversal invariance with $\mathcal{T}^2 = \mathbb{1}$ (class *AI*) restricts the matrices $H = H^\dagger$ to be real (and hence symmetric) $H = H^* = H^T$. The corresponding ensemble is called the **Gaussian orthogonal ensemble** (GOE).

Time-reversal invariant systems in symmetry class *AIII* are realized only in even dimensional Hilbert spaces due to Kramers' degeneracy. The random Hamiltonian is a $2N \times 2N$ matrix restricted by the symmetry condition

$$\begin{pmatrix} 0 & \mathbb{1}_N \\ -\mathbb{1}_N & 0 \end{pmatrix} H = H^T \begin{pmatrix} 0 & \mathbb{1}_N \\ -\mathbb{1}_N & 0 \end{pmatrix}$$

and the corresponding ensemble is called the **Gaussian symplectic ensemble** (GSE). Note that we have made a special choice for the time-reversal operators \mathcal{T} for the GOE and GSE.

The Gaussian ensembles for the chiral and charge conjugation symmetry classes can easily be constructed from the three Wigner–Dyson ensembles GUE, GOE, and GSE by reducing the number of independent matrix elements further as required. In the chiral case the ensembles have been called **chiral Gaussian unitary ensemble** (chGUE) for class *AIII*, the **chiral Gaussian orthogonal ensemble** (chGOE) for class *BDI*, and the **chiral Gaussian symplectic ensemble** (chGSE) for class *CII*. The Gaussian ensembles for the charge conjugation symmetry classes do not have any established name. We will refer to them as *C-GE*, *CI-GE*, *D-GE*, and *DIII-GE*.

B.3. Spectral statistics for Gaussian random matrices

The mean density of states for a random-matrix ensemble is defined as

$$\langle d(s) \rangle = \frac{1}{g} \langle \text{tr} \delta(s - H) \rangle = \frac{1}{g} \int dH P(H) \text{tr} \delta(s - H) \tag{B2}$$

where $g=2$ in symmetry classes with Kramers' degeneracy (every eigenvalue is counted only once) while $g=1$ in other ensembles. For large matrices in the Wigner–Dyson ensembles the mean density of states is given by Wigner's semicircle [185, 187, 196] law

$$\langle d(s) \rangle_{\text{GUE, GOE, GSE}} = \sqrt{1 - \frac{\pi^2 s^2}{4N^2}} = 1 + \mathcal{O}\left(\frac{s^2}{N^2}\right) \tag{B3}$$

where we have scaled the spectrum such that $\langle d \rangle = 1$ in the centre of the semicircle by an appropriate choice of the scaling parameter λ in the definition (B1). Here N is the size of the matrix ($N \times N$ for GUE and GOE, $2N \times 2N$ for GSE). The result (B3) is exact in the limit $s, N \rightarrow \infty$ where s/N is kept constant. The relevant limit for our purposes is $N \rightarrow \infty$ keeping s constant. In that limit the density of states is flat and the mean level spacing, $\Delta s = \langle d \rangle^{-1} = 1$.

In the presence of chiral or charge conjugation symmetries, there are deviations from Wigner's semicircle law near $s=0$ due to the symmetric spectrum. On the

scale of the mean level spacing the mean densities of states for these ensembles are given by [236, 251–254]

$$\begin{aligned}
 \langle d(s) \rangle_{\text{chGUE}} &= \frac{\pi^2 |s|}{2} (J_0^2(\pi s) + J_1^2(\pi s)) \\
 \langle d(s) \rangle_{\text{chGOE}} &= \langle d(s) \rangle_{\text{chGUE}} + \frac{\pi}{2} J_0(\pi s) \left(1 - \int_0^{\pi|s|} \mathbf{d}\xi J_0(\xi) \right) \\
 \langle d(s) \rangle_{\text{chGSE}} &= \langle d(2s) \rangle_{\text{chGUE}} - \frac{\pi}{2} J_0(2\pi s) \int_0^{2\pi|s|} \mathbf{d}\xi J_0(\xi) \\
 \langle d(s) \rangle_{\text{C-GE}} &= 1 - \frac{\sin 2\pi s}{2\pi s} \\
 \langle d(s) \rangle_{\text{CI-GE}} &= \langle d(s) \rangle_{\text{chGUE}} - \frac{\pi}{2} J_0(\pi s) J_1(\pi|s|) \\
 \langle d(s) \rangle_{\text{D-GE}} &= 1 + \frac{\sin 2\pi s}{2\pi s} \\
 \langle d(s) \rangle_{\text{DIII-GE}} &= \langle d(2s) \rangle_{\text{CI-GE}} + \frac{\pi}{2} J_1(2\pi|s|). \tag{B4}
 \end{aligned}$$

For all seven ensembles the deviation from the flat density of states is pronounced at $s=0$ and decays for $s \gg 1$. The deviations near $s=0$ are universal interference effects that can be seen in complex quantum systems of the corresponding symmetry class. For quantum graphs this is discussed in section 8.5.

The *spectral two-point correlation function* for an ensemble of matrices is defined as

$$\begin{aligned}
 R_2(s; s_0) &= \langle d(s_0 + \frac{s}{2}) d(s_0 - \frac{s}{2}) \rangle - 1 \\
 &= \frac{1}{s^2} \langle \text{tr} \delta(s_0 + \frac{s}{2} - H) \text{tr} \delta(s_0 - \frac{s}{2} - H) \rangle - 1. \tag{B5}
 \end{aligned}$$

For the Wigner–Dyson ensembles they do not depend on the central energy s_0 (in the limit $N \rightarrow \infty$; $s, s_0 = \text{const.}$, as before) and are given by [185, 196]

$$\begin{aligned}
 R_2(s)_{\text{GUE}} &= \delta(s) - \frac{\sin^2 \pi s}{\pi^2 s^2} \\
 R_2(s)_{\text{GOE}} &= R_2(s)_{\text{GUE}} + \frac{(\pi|s| \cos \pi s - \sin \pi|s|)(2 \text{Si}(\pi|s|) - \pi)}{2\pi^2 s^2} \\
 R_2(s)_{\text{GSE}} &= R_2(2s)_{\text{GUE}} + \frac{2\pi|s| \cos 2\pi s - \sin 2\pi|s|}{4\pi^2 s^2} \text{Si}(2\pi|s|). \tag{B6}
 \end{aligned}$$

The Fourier transform

$$K(\tau) = \int_{-\infty}^{\infty} \mathbf{d}s R_2(s) e^{-2\pi i s \tau} \tag{B7}$$

is known as the *spectral form factor*. For the Wigner–Dyson ensembles the form factors are given by

$$\begin{aligned}
 K(\tau)_{\text{GUE}} &= \begin{cases} |\tau| & \text{for } |\tau| \leq 1, \\ 1 & \text{for } |\tau| \geq 1, \end{cases} \\
 K(\tau)_{\text{GOE}} &= \begin{cases} |\tau|(2 - \ln(2|\tau| + 1)) & \text{for } |\tau| \leq 1, \\ 2 - |\tau| \ln \frac{2|\tau| + 1}{2|\tau| - 1} & \text{for } |\tau| \geq 1, \end{cases} \\
 K(\tau)_{\text{GSE}} &= \begin{cases} \frac{|\tau|}{4}(2 - \ln|1 - |\tau||) & \text{for } |\tau| \leq 2, \\ 1 & \text{for } |\tau| \geq 2. \end{cases}
 \end{aligned} \tag{B8}$$

Since we do not discuss second-order correlation functions for systems with chiral or charge conjugation symmetry we will not state further results. Note, however, that all spectral correlation function go over to the correlation functions of the Wigner–Dyson ensembles for energies $s \gg 1$.

Another frequently used statistic that depends on correlation-functions of any order is the *level-spacing distribution*. Ordering the spectrum such that $s_n \leq s_{n+1}$ the level spacings the differences $s_i = s_{i+1} - s_i$ between two subsequent eigenvalues. Their distribution for the Wigner–Dyson ensembles can be approximated very well by the Wigner surmises

$$\begin{aligned}
 P(s)_{\text{GUE}} &= \frac{32s^2}{\pi^2} e^{-\frac{4}{\pi}s^2} \\
 P(s)_{\text{GOE}} &= \frac{\pi s}{2} e^{-\frac{\pi}{4}s^2} \\
 P(s)_{\text{GSE}} &= \frac{2^{18}s^4}{3^6\pi^3} e^{-\frac{64}{9\pi}s^2}
 \end{aligned} \tag{B9}$$

which are exact for 2×2 (GUE, GOE) or 4×4 (GSE) matrices.

References

- [1] L. Pauling, J. Chem. Phys. **4** 673 (1936).
- [2] H. Kuhn, Helvetica Chimica Acta **31** 1441 (1948).
- [3] H. Kuhn, Helvetica Chimica Acta **32** 2247 (1949).
- [4] J.R. Platt, J. Chem. Phys. **17** 484 (1949).
- [5] K. Ruedenberg and C.W. Scherr, J. Chem. Phys. **21** 1565 (1953).
- [6] C.A. Coulson, Proc. Phys. Soc. London A **67** 608 (1954).
- [7] E.W. Montroll, J. Math. Phys. **11** 635 (1970).
- [8] M.J. Richardson and N.L. Balazs, Ann. Phys. **73** 308 (1972).
- [9] S. Alexander, Phys. Rev. B **27** 1541 (1985).
- [10] C. Flesia, R. Johnston, and H. Kunz, Europhys. Lett. **3** 497 (1987).
- [11] R. Mitra and S.W. Lee, *Analytical Techniques in the Theory of Guided Waves* (Macmillan, New York, 1971).
- [12] P.W. Anderson, Phys. Rev. B **23** 4828 (1981).
- [13] B. Shapiro, Phys. Rev. Lett. **48** 823 (1982).
- [14] J.T. Chalker and P.D. Coddington, J. Phys. C **21** 2665 (1988).
- [15] R. Klesse and M. Metzler, Phys. Rev. Lett. **79** 721 (1997).

- [16] R. Klesse, Der Lokalisierungs-, Delokalisierungsübergang im Netzwerkmodell des Quanten-Hall-Effekts PhD Thesis Köln 1996 (AWOS-Verlag, 1996).
- [17] Y. Avishai and J.M. Luck, *Phys. Rev. B* **45** 1074 (1992).
- [18] T. Nakayama, K. Yakubo, and R.L. Orbach, *Rev. Mod. Phys.* **66** 381 (1994).
- [19] Y. Imry, *Introduction to Mesoscopic Systems* (Oxford University Press, New York, 1996).
- [20] D. Kowal, U. Sivan, O. Entin-Wohlman, and Y. Imry, *Phys. Rev. B* **42** 9009 (1990).
- [21] Ch. Texier and G. Montambaux, *Phys. Rev. B* **72** 115327 (2005).
- [22] Ch. Texier and G. Montambaux, *J. Phys. A* **38** 3455 (2005).
- [23] Ch. Texier and G. Montambaux, *Phys. Rev. Lett.* **92** 186801 (2004).
- [24] O. Hul, Sz. Bauch, P. Pakoński, N. Savytskyy, K. Życzkowski, and L. Sirko. *Phys. Rev. E* **69** 056205 (2004).
- [25] Y. Saito, *Electronic J. Differen. Eqns* **2000** No. 31 (2000).
- [26] Y. Saito, *Analysis* **21** 171 (2001).
- [27] J. Rubinstein and M. Schatzman, *Arch. Ration. Mech. Anal.* **160** 271 (2001).
- [28] P. Kuchment and H. Zeng, *J. Math. Anal. Appl.* **258** 671 (2001).
- [29] P. Exner and O. Post, *J. Geom. Phys.* **54** 77 (2005).
- [30] O. Post, *J. Phys. A* **38** 4917 (2005).
- [31] P. Exner and K. Nĕmcová *J. Phys. A* **34** 7783 (2001).
- [32] P. Exner and T. Ichinose, *J. Phys. A* **34** 1439 (2001).
- [33] P. Exner and K. Yoshitomi, *J. Geom. Phys.* **41** 344 (2002).
- [34] P. Exner and K. Nĕmcová, *J. Phys. A* **36** 10173 (2003).
- [35] P. Exner and M. Tater, *Waves in Random Media* **14** S47 (2004).
- [36] P. Exner and S. Kondej, *Rev. Math. Phys.* **16** 559 (2004).
- [37] P. Exner and S. Kondej, *J. Phys. A* **38** 4865 (2005).
- [38] P. Exner, T. Ichinose, and S. Kondej, [quant-ph/0504060](https://arxiv.org/abs/quant-ph/0504060) (2005).
- [39] P. Exner and R.L. Frank, [math.SP/0508525](https://arxiv.org/abs/math.SP/0508525) (2005).
- [40] J.-P. Roth, *Comptes rendus de l'Académie des sciences Paris* **296** 793 (1983).
- [41] J.-P. Roth, in *Théorie du Potentiel*, Proceedings of the Colloque Jacques Deny, Orsay 1983, edited by G. Mokobodzki and D. Pinchon, *Lecture Notes in Mathematics* (Springer, Berlin, 1985).
- [42] J. von Below, *Lin. Alg. Appl.* **71** 309 (1985).
- [43] J. von Below, *Math. Meth. Appl. Sci.* **10** 383 (1988).
- [44] J. von Below, *Parabolic Network Equations* (Universität Tübingen, Tübingen, 1993).
- [45] J.E. Avron, in *Mesoscopic Quantum Physics*, Proceedings of the Les Houches Summer School LXI 1994, edited by E. Akkermans, G. Montambaux, J.L. Pichard and J. Zinn-Justin (North-Holland, Amsterdam, 1995).
- [46] S. Alberverio and K. Pankrashkin, *J. Phys. A* **38** 4859 (2005).
- [47] P. Exner and P. Šeba, *Rep. Math. Phys.* **28** 7 (1989).
- [48] S.P. Novikov, in *The Arnoldfest*, Proceedings of a Conference in Honour V.I. Arnold for His Sixtieth Birthday, edited by E. Bierstone, B. Khesin, A. Khovanskii, and J. Marsden (American Mathematical Society, Providence, 1999).
- [49] P. Exner, *J. Phys. A* **29** 87 (1996).
- [50] P. Exner and R. Gawlista, *Phys. Rev. B* **53** 7275 (1996).
- [51] P. Exner, *Phys. Rev. Lett.* **74** 3503 (1995).
- [52] P. Exner, *Ann. Inst. H. Poincaré* **66** 359 (1997).
- [53] J.E. Avron, P. Exner, and Y. Last, *Phys. Rev. Lett.* **72** 896 (1994).
- [54] R. Carlson, *Trans. Amer. Math. Soc.* **351** 4069 (1999).
- [55] R. Carlson, *Electronic J. Differen. Eqns* **1997** No. 23 (1997).
- [56] R. Carlson, *Electronic J. Differen. Eqns* **1999** No. 6, (1999).
- [57] V. Kostrykin and R. Schrader, *J. Phys. A* **32** 595 (1999).
- [58] V. Kostrykin and R. Schrader, *Fortschritte der Physik* **48** 703 (2000).
- [59] V. Kostrykin and R. Schrader, in *Quantum Graphs and Their Applications*, Proceedings of the Joint Summer Research Conference in the Mathematical Sciences in Snowbird 2005, edited by G. Berkolaiko, R. Carlson, St. Fulling, and P. Kuchment, *Contemporary Mathematics* **415** (American Mathematical Society, Providence, 2006).
- [60] T. Cheon and P. Exner, *J. Phys. A* **37** L329 (2004).

- [61] P. Exner and O. Turek, in *Quantum Graphs and Their Applications*, Proceedings of the Joint Summer Research Conference in the Mathematical Sciences in Snowbird 2005, edited by G. Berkolaiko, R. Carlson, St. Fulling, and P. Kuchment, Contemporary Mathematics **415** (American Mathematical Society, Providence, 2006).
- [62] S.A. Fulling, in *Quantum Graphs and Their Applications*, Proceedings of the Joint Summer Research Conference in the Mathematical Sciences in Snowbird 2005, edited by G. Berkolaiko, R. Carlson, St. Fulling, and P. Kuchment, Contemporary Mathematics **415** (American Mathematical Society, Providence, 2006).
- [63] R. Carlson, *Waves in Random Media* **14** S29 (2004).
- [64] F. Bentosela, P. Duclos, and P. Exner, *Lett. Math. Phys.* **65** 75 (2003).
- [65] L. Friedlander, *Contemp. Math.* **339** 37 (2003).
- [66] V. Kostrykin and R. Schrader, *Waves in Random Media* **14** S75 (2004).
- [67] M. Aizenman, R. Sims, and S. Warzel, *math-ph/0510069* (2005).
- [68] M. Aizenman and S. Warzel, *Moscow Math. J.* **5** 499 (2005).
- [69] M. Aizenman, R. Sims, and S. Warzel, *math-ph/0502006* (2005).
- [70] M. Aizenman, R. Sims, and S. Warzel, *Commun Math. Phys.* **264** 371 (2006).
- [71] M. Solomyak, *Waves in Random Media* **14** S155 (2004).
- [72] R. Carlson, *Electronic J. Differen. Eqns* **2000** No. 71 (2000).
- [73] K. Naimark and M. Solomyak, *Proc. London Math. Soc.* **80** 690 (2000).
- [74] A. Teplyaev, *J. Funct. Anal.* **159** 537 (1998).
- [75] R. Meyers, R.S. Strichartz, and A. Teplyaev, *Pac. J. Math.* **217** 149 (2004).
- [76] T. Shirai, *Trans. Amer. Math. Soc.* **352** 115 (2000).
- [77] F. Barra and P. Gaspard, *Phys. Rev. E* **65** 016205 (2002).
- [78] P. Exner and E. Seresova, *J. Phys. A* **27** 8269 (1994).
- [79] P. Exner, *Lett. Math. Phys.* **38** 313 (1996).
- [80] P. Exner, *Found. Phys.* **27** 171 (1997).
- [81] N.I. Gerasimenko and B.S. Pavlov, *Theor. Math. Phys.* **74** 230 (1988).
- [82] V. Kostrykin and R. Schrader, *J. Math. Phys.* **42** 1563 (2001).
- [83] Ch. Texier and G. Montambaux, *J. Phys. A* **34** 10307 (2001).
- [84] Ch. Texier, *J. Phys. A* **35** 3389 (2002).
- [85] J. von Below, *Alg. Appl.* **21** 692 (1989).
- [86] A. Comtet, J. Desbois, and S.N. Majumdar, *J. Phys. A* **35** L687 (2002).
- [87] J. Desbois, *J. Phys. A* **33** L63 (2000).
- [88] J. Desbois, *J. Phys. A* **35** L673 (2002).
- [89] T. Dittrich, B. Mehlig, H. Schanz, U. Smilansky, P. Pollner, and G. Vattay, *Phys. Rev. E* **59** 6541 (1999).
- [90] S. Severini and G. Tanner, *J. Phys. A* **37** 6675 (2004).
- [91] V. Kostrykin and R. Schrader, *math.CO/0404467* (2004).
- [92] P. Exner, P. Hejčik, and P. Šeba, *Rep. Math. Phys.* **57** 445 (2006).
- [93] J. von Below, in *Partial Differential Equations on Multistructures*, edited by M. Dekker, *Lecture Notes in Pure and Applied Mathematics* **219** (New York, 2001).
- [94] F. Ali Mehmeti, *Integral Eqns Operator Theory* **9** 753 (1986).
- [95] D. M. Cvetković M. Doob, and H. Sachs, *Spectra of Graphs* (Academic Press, New York, 1980).
- [96] S. Nicaise, *Bull. Sc. Math. 2^e Série* **111** 401 (1987).
- [97] B. Gutkin and U. Smilansky, *J. Phys. A* **34** 6061 (2001).
- [98] V. Kostrykin and R. Schrader, *math-ph/0603010* (2006).
- [99] P. Kurasov and M. Novaczyk, *J. Phys. A* **38** 4910 (2005).
- [100] P. Kurasov and F. Stenberg, *J. Phys. A* **35** 101 (2002).
- [101] V. Pivovarchik, *SIAM J. Math. Anal.* **31** 801 (2001).
- [102] M. Harmer, *J. Phys. A* **38** 4875 (2005).
- [103] M. Harmer, *ANZIAM J.* **44** 161 (2002).
- [104] N.I. Gerasimenko, *Theor. Math. Phys.* **75** 460 (1988).
- [105] L. Friedlander, *Annales de l'Institut Fourier* **55** 199 (2005).
- [106] U. Smilansky, *Waves in Random Media* **14** S143 (2004).
- [107] M. Solomyak, *Waves in Random Media* **14** S173 (2004).

- [108] W.D. Evans and M. Solomyak, *J. Phys. A* **38** 4611 (2005).
- [109] W.D. Evans and M. Solomyak, *J. Phys. A* **38** 7661 (2005).
- [110] P. Kuchment, *Waves in Random Media* **12** R1 (2003).
- [111] P. Kuchment, *Waves in Random Media* **14** S107 (2004).
- [112] P. Kuchment, *J. Phys. A* **38** 4887 (2005).
- [113] P. Kuchment (Guest Editor), Special Section: *Quantum Graphs Waves in Random Media* **14** S1 (2005).
- [114] G. Dell'Antonio, P. Exner, and V. Gejler (Guest Editors) Special Issue: *Singular Interactions in Quantum Mechanics: Solvable Models* *J. Phys. A* **38** Number 22 (2005); Section *Quantum Graphs: Usual, Fat, and Leaky* p. 4859.
- [115] G. Berkolaiko, R. Carlson, S. Fulling, and P. Kuchment (Editors), *Quantum Graphs and Their Applications*, Proceedings of the Joint Summer Research Conference in the Mathematical Sciences in Snowbird 2005, *Contemporary Mathematics* **415** (American Mathematical Society, Providence, 2006).
- [116] T. Kottos and U. Smilansky, *Phys. Rev. Lett.* **79** 4794 (1997).
- [117] T. Kottos and U. Smilansky, *Annals of Physics* **274** 76 (1998).
- [118] M.C. Gutzwiller, *J. Math. Phys.* **12** 343 (1971).
- [119] M.C. Gutzwiller, *Chaos in Classical and Quantum Mechanics* (Springer, New York, 1990).
- [120] B. Winn, The Laplacian on a graph and quantum chaology, PhD thesis, University of Bristol (2003).
- [121] A. Comtet, J. Desbois, and Ch. Texier, *J. Phys. A* **38** R341 (2005).
- [122] F. Barra and P. Gaspard, *J. Stat. Phys.* **101** 283 (2000).
- [123] G. Berkolaiko and J.P. Keating, *J. Phys. A* **32** 7827 (1999).
- [124] G. Berkolaiko, H. Schanz, and R.S. Whitney, *J. Phys. A* **36** 8373 (2003).
- [125] G. Berkolaiko, *Waves in Random Media* **14** S7 (2004).
- [126] G. Berkolaiko, Quantum star graphs and related systems, PhD thesis, University of Bristol (2000).
- [127] G. Berkolaiko, E.B. Bogomolny, and J.P. Keating, *J. Phys. A* **34** 335 (2001).
- [128] G. Berkolaiko, H. Schanz, and R.S. Whitney, *Phys. Rev. Lett.* **82** 104101 (2002).
- [129] J. Bolte and J. Harrison, *J. Phys. A* **36** 2747 (2003).
- [130] J. Bolte and J. Harrison, *J. Phys. A* **36** L433 (2003).
- [131] T. Kottos and H. Schanz, *Physica E* **9** 523 (2001).
- [132] P. Pakoński, K. Życzkowski, and M. Kuś, *J. Phys. A* **34** 9303 (2001).
- [133] P. Pakoński, G. Tanner, and K. Życzkowski, *J. Stat. Phys.* **111** 1331 (2003).
- [134] H. Schanz and U. Smilansky, *Phil. Mag. B* **80** 1999 (2000).
- [135] H. Schanz and U. Smilansky, *Electronic J. Combin.* **8** R16 (2001).
- [136] G. Tanner, *J. Phys. A* **33** 3567 (2000).
- [137] G. Tanner, *J. Phys. A* **34** 8485 (2001).
- [138] G. Tanner, *J. Phys. A* **35** 5985 (2002).
- [139] S. Gnutzmann and B. Seif, *Phys. Rev. E* **69** 056219 (2004).
- [140] S. Gnutzmann and B. Seif, *Phys. Rev. E* **69** 056220 (2004).
- [141] S. Gnutzmann and A. Altland, *Phys. Rev. Lett.* **93** 194101 (2004).
- [142] S. Gnutzmann and A. Altland, *Phys. Rev. E* **72** 056215 (2005).
- [143] D. Bercioux, M. Governale, V. Cataudella, and V. Marigliano Ramaglia, *Phys. Rev. Lett.* **93** 056802 (2004).
- [144] L. Kaplan, *Phys. Rev. E* **64** 036225 (2001).
- [145] H. Schanz and U. Smilansky, *Phys. Rev. Lett.* **84** 1427 (2000).
- [146] S. Gnutzmann, U. Smilansky, and J. Weber, *Waves in Random Media* **14** S61 (2004).
- [147] J.P. Keating, J. Marklof, and B. Winn, *Commun. Math. Phys.* **241** 421 (2003).
- [148] H. Schanz and T. Kottos, *Phys. Rev. Lett.* **90** 234101 (2003).
- [149] G. Berkolaiko, J.P. Keating, and B. Winn, *Phys. Rev. Lett.* **91** 134103 (2003).
- [150] G. Berkolaiko, J.P. Keating, and B. Winn, *Commun. Math. Phys.* **250** 259 (2004).
- [151] T. Kottos and U. Smilansky, *Phys. Rev. Lett.* **85** 968 (2000).
- [152] T. Kottos and U. Smilansky, *J. Phys. A* **36** 3501 (2003).
- [153] H. Schanz, M. Puhlmann, and T. Geisel, *Phys. Rev. Lett.* **91** 134101 (2003).

- [154] D. Cohen, T. Kottos, and H. Schanz, *J. Phys. A* **264** 11755 (2006).
- [155] M. Puhlmann, H. Schanz, T. Kottos, and T. Geisel, *Europhys. Lett.* **69** 313 (2005).
- [156] T. Kottos and H. Schanz, *Waves in Random Media* **14** S91 (2004).
- [157] T. Kottos, *J. Phys. A* **3** 10761 (2005).
- [158] S. Müller, S. Heusler, P. Braun, F. Haake, and A. Altland, *Phys. Rev. Lett.* **93** 014103 (2004).
- [159] S. Müller, S. Heusler, P. Braun, F. Haake, and A. Altland, *Phys. Rev. E* **72** 046207 (2005).
- [160] K. Richter and M. Sieber, *Phys. Rev. Lett.* **89** 206801 (2002).
- [161] M. Sieber and K. Richter, *Phys. Scr. T* **90** 128 (2001).
- [162] M. Sieber, *J. Phys. A* **35** L613 (2002).
- [163] Yu. Dabaghian and R. Blümel, *Phys. Rev. E* **68** 055201(R) (2003).
- [164] R. Blümel, Y. Dabaghian, and R.V. Jensen, *Phys. Rev. E* **65** 046222 (2002).
- [165] R. Blümel, Y. Dabaghian, and R.V. Jensen, *Phys. Rev. Lett.* **88** 044101 (2002).
- [166] A.G.M. Schmidt, B.K. Cheng, and M.G.E da Luz, *J. Phys. A* **36** L545 (2003).
- [167] M. Sieber, H. Primack, U. Smilansky, I. Ussishkin, and H. Schanz, *J. Phys. A* **28** 5041 (1995).
- [168] F. Barra and P. Gaspard, *Phys. Rev. E* **63** 066215 (2001).
- [169] I. Bengtsson, Å. Ericsson, M. Kuś, W. Tadej, and K. Życzkowski, *Commun. Math. Phys.* **259** 307 (2005).
- [170] K. Życzkowski, M. Kuś, W. Słomczyński, and H.-J. Sommers, *J. Phys. A* **36** 3425 (2003).
- [171] G. Berkolaiko, *J. Phys. A* **34** L319 (2001).
- [172] P. Gaspard, *Chaos, Scattering, and Statistical Mechanics* (Cambridge University Press, Cambridge, 1998).
- [173] P. Cvitanović, R. Artuso, R. Mainieri, G. Tanner, and G. Vattay, *Chaos: Classical and Quantum* ChaosBook.org (Niels Bohr Institute, Copenhagen, 2005). Online publication only available at ChaosBook.org
- [174] Ya.G. Sinai, *Russian Math. Surveys* **27** 21 (1972).
- [175] R. Bowen, *Equilibrium States and the Ergodic Theory of Anosov Diffeomorphisms*, Lecture Notes in Mathematics **470** (Springer, Berlin, 1975).
- [176] D. Ruelle, *Amer. J. Math.* **98** 619 (1976).
- [177] J.H. Hannay and A.M. Ozorio de Almeida, *J. Phys. A* **17** 3429 (1984).
- [178] L. Friedlander, *Israel Journal of Mathematics* **146** 149 (2005).
- [179] M. Kac, *American Mathematical Monthly* **73** 1 (1966).
- [180] T. Shapira and U. Smilansky, in *Nonlinear Dynamics and Fundamental Interactions*, Proceedings of the Nato Advanced Research Workshop, Tashkent 2004, edited by F. Khanna and D. Matrasulov (Springer, Berlin, 2005).
- [181] E. Akkermans, A. Comtet, J. Desbois, G. Montambaux, and Ch. Texier, *Ann. Phys.* **284** 10 (2000).
- [182] J.P. Keating and M.V. Berry, *J. Phys. A* **20** L1139 (1987).
- [183] M.V. Berry and J.P. Keating, *J. Phys. A* **23** 4839 (1990).
- [184] M. Kac, *Am. J. Math.* **62** 122 (1940).
- [185] M.L. Mehta, *Random Matrices*, 3rd edn (Academic Press, New York, 1991).
- [186] R.U. Haq, A. Pandey, and O. Bohigas, *Phys. Rev. Lett.* **48** 1086 (1982).
- [187] E. Wigner, *Ann. Math.* **67** 325 (1958).
- [188] F.J. Dyson, *J. Math. Phys.* **3** 140 (1962).
- [189] F.J. Dyson, *J. Math. Phys.* **3** 157 (1962).
- [190] F.J. Dyson, *J. Math. Phys.* **3** 166 (1962).
- [191] M.R. Zirnbauer, *J. Math. Phys.* **37** 4986 (1996).
- [192] M. V. Berry and M. Tabor, *Proc. R. Soc. London A* **356** 375 (1977).
- [193] O. Bohigas, M.-J. Giannoni, and C. Schmit, *Phys. Rev. Lett.* **52** 1 (1984).
- [194] M.V. Berry, *Ann. Phys. (New York)* **131** 163 (1981).
- [195] G. Casati, F. Valz-Gris, and I. Guarneri, *Lettere al Nuovo Cimento* **28** 279 (1980).
- [196] F. Haake, *Quantum Signatures of Chaos*, 2nd edn (Springer, Berlin, 2000).
- [197] H.-J. Stöckmann, *Quantum Chaos: An Introduction* (Cambridge University Press, Cambridge, 1999).

- [198] A.M. Ozorio de Almeida, *Hamiltonian Systems: Chaos and Quantization* (Cambridge University Press, Cambridge, 1990).
- [199] M.V. Berry, in *Chaos and Quantum Physics*, Les Houches Session LII 1989, edited by M.-J. Giannoni, A. Voros, and J. Zinn-Justin (North-Holland, Amsterdam, 1991).
- [200] J.P. Keating, *Nonlinearity* **4** 309 (1991).
- [201] E.B. Bogomolny, B. Georgeot, M.-J. Giannoni, and C. Schmit, *Phys. Rep.* **291** 219 (1997).
- [202] J. Zakrzewski, K. Dupret, and D. Delande, *Phys. Rev. Lett.* **74** 522 (1995).
- [203] T. Guhr, A. Müller-Groeling, and H.A. Weidenmüller, *Phys. Rep.* **299** 189 (1998).
- [204] Y. Fyodorov, *Introduction to Random Matrix Theory: Gaussian Unitary Ensembles and Beyond*, Lectures at the Isaac Newton Institute Summer School (Cambridge, Cambridge, 2004).
- [205] J.J.M. Verbaarschot, H.A. Weidenmüller, and M.R. Zirnbauer, *Phys. Rep.* **129** 367 (1985).
- [206] C.W.J. Beenakker, *Rev. Mod. Phys.* **69** 731 (1997).
- [207] P. Brouwer, On the random-matrix theory of quantum transport, PhD thesis, University of Leiden (1997).
- [208] K. Efetov, *Supersymmetry in Disorder and Chaos* (Cambridge University Press, Cambridge, 1997).
- [209] A.D. Mirlin, *Phys. Rep.* **326** 259 (2000).
- [210] P. Braun, S. Gnutzmann, F. Haake, M. Kuś, and K. Życzkowski, *Found. Phys.* **31** 613 (2001).
- [211] Ph. Pechukas *Phys. Rev. Lett.* **51** 943 (1983).
- [212] T. Yukawa, *Phys. Rev. Lett.* **54** 1883 (1985).
- [213] N. Argaman, F.M. Dittes, E. Doron, J.P. Keating, A.Yu. Kitaev, M. Sieber, and U. Smilansky, *Phys. Rev. Lett.* **71** 4326 (1993).
- [214] M.V. Berry, *Proc. R. Soc. Lond. A* **400** 229 (1985).
- [215] E.B. Bogomolny and J.P. Keating, *Phys. Rev. Lett.* **77** 1472 (1996).
- [216] D. Cohen, H. Primack, and U. Smilansky, *Ann. Phys. (New York)* **264** 108 (1998).
- [217] U. Smilansky and B. Verdene, *J. Phys. A* **36** 3525 (2003).
- [218] I.L. Aleiner and A.I. Larkin, *Phys. Rev. B* **54** 14423 (1996).
- [219] I.L. Aleiner and A.I. Larkin, *Phys. Rev. E* **55** R1243 (1997).
- [220] I.L. Aleiner and A.L. Larkin, *Chaos, Solitons Fractals* **8** 1179 (1997).
- [221] S. Heusler, S. Müller, P. Braun, and F. Haake, *J. Phys. A* **37** L31 (2004).
- [222] S. Müller, *Eur. Phys. J. B* **34** 305 (2003).
- [223] M. Turek, D. Spehner, S. Müller, and K. Richter, *Phys. Rev. E* **71** 016210 (2005).
- [224] M. Turek and K. Richter, *J. Phys. A* **36** L455 (2003).
- [225] D. Spehner, *J. Phys. A* **36** 7269 (2003).
- [226] O. Agam, B.L. Altshuler, and A.V. Andreev, *Phys. Rev. Lett.* **75** 4389 (1995).
- [227] O. Agam, A.V. Andreev, and B.D. Simons, *Chaos, Solitons Fractals* **8** 1099 (1997).
- [228] A.V. Andreev and B. Altshuler, *Phys. Rev. Lett.* **75** 902 (1995).
- [229] B.A. Muzykantskii and D.E. Khmel'nitskii, *JETP Lett.* **62** 76 (1995).
- [230] J. Müller and A. Altland, *J. Phys. A* **38** 3097 (2005).
- [231] T. Dittrich and U. Smilansky, *Nonlinearity* **4** 85 (1991).
- [232] R. Scharf, B. Dietz, M. Kuś, F. Haake, and M.V. Berry, *Europhys. Lett.* **5** 383 (1988).
- [233] J.J.M. Verbaarschot and I. Zahed, *Phys. Rev. Lett.* **70** 3852 (1993).
- [234] J.J.M. Verbaarschot, *Phys. Rev. Lett.* **72** 2531 (1994).
- [235] A. Altland and M.R. Zirnbauer, *Phys. Rev. Lett.* **76** 3420 (1996).
- [236] A. Altland and M.R. Zirnbauer, *Phys. Rev. B* **55** 1142 (1997).
- [237] A.F. Andreev, *Sov. Phys. JETP* **19** 1228 (1964).
- [238] C.W.J. Beenakker, *Lecture Notes in Physics* **667** 131 (2005).
- [239] J.A. Melsen, P.W. Brouwer, K.M. Frahm, and C.W.J. Beenakker, *Europhys. Lett.* **35** 7 (1996).
- [240] A. Altland, B.D. Simons, and D. Taras-Semchuk, *Adv. Phys.* **49** 321 (2000).
- [241] D. Taras-Semchuk and A. Altland, *Phys. Rev. B* **64** 014512 (2001).

- [242] M.C. Goorden, Superconductivity in nanostructures: Andreev billiards and Josephson junction qubits, PhD thesis, University of Leiden (2005).
- [243] S. Gnuzmann, B. Seif, F. von Oppen, and M.R. Zirnbauer, Phys. Rev. E **67** 046225 (2003).
- [244] A.D. Mirlin, in *New Directions in Quantum Chaos*, Proceedings of the international School of Physics 'Enrico Fermi', Course CXLIII, edited by G. Casati, I. Guarneri, and U. Smilansky (IOS Press, Amsterdam, 2000).
- [245] Y.V. Fyodorov, in *Mesoscopic Quantum Physics*, Proceedings of the Les Houches Summer School LXI 1994, edited by E. Akkermans, G. Montambaux, J.L. Pichard and J. Zinn-Justin (North-Holland, Amsterdam, 1995).
- [246] M.R. Zirnbauer, J. Phys. A **29** 7113 (1996).
- [247] M.R. Zirnbauer, in *Proceedings of the 13th International Congress of Mathematical Physics*, edited by D. DeWit, A.J. Bracken, M.D. Gould, and P.A. Pearce (International Press, Cambridge, 1998).
- [248] M.R. Zirnbauer, in *Supersymmetry and Trace Formulae: Chaos and Disorder*, edited by I.V. Lerner, J.P. Keating, and D.É. Khmelnitskii (Kluwer/Plenum, New York, 1993).
- [249] A. Altland, B.D. Simons, and M.R. Zirnbauer, Phys. Rep. **359** 283 (2002).
- [250] G. Hackenbroich and H.A. Weidenmüller, Phys. Rev. Lett. **76** 110 (1996).
- [251] P.J. Forrester, Nucl. Phys. B **402** 709 (1993).
- [252] J. Verbaarschot, Nucl. Phys. B **426** 559 (1994).
- [253] T. Nagao and K. Slevin, J. Math. Phys. **34** 2317 (1993).
- [254] D.A. Ivanov, J. Math. Phys. **43** 126 (2002).
- [255] J. Brüning, V. Geysler, K. Pankrashkin, to be published in Comm. Math. Phys (math-ph/0511057).
- [256] K. Pankrashkin, Lett. Math. Phys. **77** 139 (2006).
- [257] K. Pankrashkin, math-ph/0607034.
- [258] C. Cattaneo, Monatsh. Math **124** 215 (1997).